Evidence-Based Complementary and Alternative Medicine

Plant-Derived Compounds as Novel Anticancer Agents

Lead Guest Editor: Shuli Yang
Guest Editors: Shoib Baba and Zhenzhen Jin

Plant-Derived Compounds as Novel Anticancer Agents

Evidence-Based Complementary and Alternative Medicine

Plant-Derived Compounds as Novel Anticancer Agents

Lead Guest Editor: Shuli Yang
Guest Editors: Shoib Baba and Zhenzhen Jin

Contents

The Prognostic Value of AT-Rich Interaction Domain (ARID) Family Members in Patients with Hepatocellular Carcinoma
Siyi Li, Zhulin Wu, Qiuyue Li, Qiting Liang, Hengli Zhou, Yafei Shi, Rong Zhang, and Huafeng Pan
Research Article (16 pages), Article ID 1150390, Volume 2022 (2022)

Study on the Diagnostic Value of Contrast-Enhanced Ultrasound and Magnetic Resonance Imaging in Prostate Cancer
Xinnian Pang, Jianhua Zhang, Lvcou Chen, Yang Yuan, and Dong Xu
Research Article (6 pages), Article ID 7983530, Volume 2022 (2022)

Hindawi
Evidence-Based Complementary and Alternative Medicine
Volume 2023, Article ID 9764181, 1 page
https://doi.org/10.1155/2023/9764181

Retraction

Retracted: Application Value of Metagenomics Next-Generation Sequencing (mNGS) in Detection of Mucormycosis after Chemotherapy in Childhood Acute Leukemia

Evidence-Based Complementary and Alternative Medicine

Received 1 August 2023; Accepted 1 August 2023; Published 2 August 2023

This article has been retracted by Hindawi following an investigation undertaken by the publisher [1]. This investigation has uncovered evidence of one or more of the following indicators of systematic manipulation of the publication process:

(1) Discrepancies in scope
(2) Discrepancies in the description of the research reported
(3) Discrepancies between the availability of data and the research described
(4) Inappropriate citations
(5) Incoherent, meaningless and/or irrelevant content included in the article
(6) Peer-review manipulation

The presence of these indicators undermines our confidence in the integrity of the article's content and we cannot, therefore, vouch for its reliability. Please note that this notice is intended solely to alert readers that the content of this article is unreliable. We have not investigated whether authors were aware of or involved in the systematic manipulation of the publication process.

In addition, our investigation has also shown that one or more of the following human-subject reporting requirements has not been met in this article: ethical approval by an Institutional Review Board (IRB) committee or equivalent, patient/participant consent to participate, and/or agreement to publish patient/participant details (where relevant).

Wiley and Hindawi regrets that the usual quality checks did not identify these issues before publication and have since put additional measures in place to safeguard research integrity.

We wish to credit our own Research Integrity and Research Publishing teams and anonymous and named external researchers and research integrity experts for contributing to this investigation.

The corresponding author, as the representative of all authors, has been given the opportunity to register their agreement or disagreement to this retraction. We have kept a record of any response received.

References

[1] W. Li, H. Zhu, L. Wen, M. Quan, and L. Wang, "Application Value of Metagenomics Next-Generation Sequencing (mNGS) in Detection of Mucormycosis after Chemotherapy in Childhood Acute Leukemia," *Evidence-Based Complementary and Alternative Medicine*, vol. 2022, Article ID 7366432, 5 pages, 2022.

Hindawi
Evidence-Based Complementary and Alternative Medicine
Volume 2023, Article ID 6715978, 6 pages
https://doi.org/10.1155/2023/6715978

Research Article

Role of Huangqin Decoction in Intestinal Homeostasis and Colon Carcinogenesis Based on "SREBP1 Cholesterol Metabolism Treg Cell Differentiation"

Junde Zhou,[1] Nannan Lu,[2] Xinxin Lv,[3] Xin Wang,[3] Jing Li,[3] and Lixia Ke[3]

[1]*Ward 3 of General Surgery, The Second Affiliated Hospital of Harbin Medical University, No. 246 Xuefu Road, Nangang District, Harbin 150001, China*
[2]*Department of Pathology, Bei'an First People's Hospital, No. 222, Longjiang Road, Bei'an 164099, China*
[3]*Department of Oncology, Beidahuang Industry Group General Hospital, No. 235, Hashuang Road, Nangang District, Harbin 150001, China*

Correspondence should be addressed to Jing Li; kexiongshi523@163.com and Lixia Ke; lixiake@stu.ahu.edu.cn

Received 14 July 2022; Revised 30 July 2022; Accepted 10 August 2022; Published 1 June 2023

Academic Editor: Shuli Yang

Objective. To explore the role of Huangqin Decoction in intestinal homeostasis maintenance and colon carcinogenesis based on "sterol regulatory element binding protein-1c (SREBP-1)-cholesterol metabolism regulatory T cell (Treg) differentiation." *Methods*. It was decided to utilize a total of 50 healthy Wistar rats for the study, 20 of which were chosen at random to serve as controls, and 30 of which were used to create an intestinal homeostasis imbalance model. It was determined whether or not the modeling was successful by killing 10 rats from each of the two groups. The remaining 10 rats in the normal group were then employed as the control group for the experiment. The random number table method was used to split the rats into two groups: the Huangqin Decoction ($n = 10$) and the Natural Recovery ($n = 10$) groups. For seven days, participants in the Huangqin Decoction group received the herb, whereas those in the natural healing group received normal saline. The relative density of SREBP1, the levels of cholesterol ester (CE), free cholesterol (FC), total cholesterol (TC), and Treg cells were detected and compared. *Results*. When compared to the control group, the relative density of SREBP1 increased significantly before administration in the Huangqin Decoction group and the natural recovery group, but decreased significantly after administration, with statistical significance ($P < 0.05$) in the Huangqin Decoction group and the natural recovery group; the Huangqin Decoction group and natural recovery group had significantly higher levels of CE, FC, and TC than the control group before to administration, and these levels increased significantly after administration. CE, FC, and TC levels in Huangqin Decoction and natural recovery groups were much lower than those in natural recovery groups, and the difference was statistically significant ($P < 0.05$), according to the results; Prior to administration, Treg cell levels in Huangqin Decoction group and the natural recovery group were significantly higher, and Treg cell levels in the Huangqin Decoction group and natural recovery group were significantly lower after administration; the decrease in the Huangqin Decoction group was significantly greater than that in natural recovery group. $P < 0.05$ indicated that the difference was significant. *Conclusion*. Using Huangqin Decoction, one may efficiently regulate SREBP1, cholesterol metabolism, and Treg cell development, all of which play an important role in maintaining intestinal stability and minimizing the incidence of colon cancer.

1. Introduction

Intestinal homeostasis is a dynamic equilibrium state formed by the interaction of metabolites, nutrition, intestinal environment, and the host, which is affected by many factors such as eating habits, lifestyle, and environment [1]. As well as keeping the body's regular physiological functions in check, intestinal homeostasis is critical for preventing harmful microbe colonization, controlling immune system activity, and enhancing digestion and nutritional absorption

[2]. Rheumatoid arthritis, central nervous system disorders, cardiovascular system diseases, endocrine system diseases, and digestive system diseases, including colon cancer, can all be caused by an imbalance [3]. Huangqin Decoction, from the Treatise on Febrile Diseases, has a variety of traditional Chinese medicine effects such as clearing away heat, neutralizing and relieving pain. It has a protective effect on the gastrointestinal tract and is commonly used to treat illnesses of the digestive system. In recent years, some scholars have pointed out that recent studies have found that Huangqin Decoction can not only reduce the death caused by chemotherapy in colon cancer model mice but also has preventive and therapeutic effects on colon cancer associated with colitis [4], and also plays an essential role in maintaining body homeostasis [5]. In addition, some studies have shown that sterol regulatory element-binding protein-1c (SREBP-1), cholesterol metabolism, and regulatory T cell (Treg) differentiation play an essential role in maintaining intestinal homeostasis [6–8]. However, few studies have explored the role of Huangqin Decoction in maintaining intestinal homeostasis and reducing colon cancer based on this aspect, which deserves further study. In order to better understand the role of Huangqin Decoction in maintaining intestinal homeostasis and preventing colon cancer, this study will investigate the "SREBP1-cholesterol metabolism-Treg cell differentiation" link between Huangqin Decoction and colon cancer.

2. Material and Methods

2.1. Selection and Grouping of Experimental Animals. 50 clean-grade healthy Wistar rats (Beijing Vitonlihua Experimental Animal Co., Ltd., certificate number: SCXK 20060009) weighing 180 g to 220 g, 4 weeks old, and half male and half female, were selected [9].

2.2. Preparation of Huangqin Decoction. There are 12 significant dates in the Huangqin Decoction (1 big date weighs about 4 G) according to the proportion of Huangqin 9 g, Shaoyao 6 g, Liquorice 6 g, and it has a dosage of about 70 g [10]. The total amount of Huangqin Decoction is about 140 g, which is decocted according to the traditional Chinese medicine into a liquid medicine containing 1 g/ML of crude drug, and the residue is filtered with gauze and a 200 mesh nylon filter with a 0.22 μm filter to remove bacteria in the clean table and kept at 4°C for later use.

2.3. Modeling, Grouping, and Administration. Lincomycin (Zhejiang Tianrui Pharmaceutical Co., Ltd., Standard Chinese Medicine H33022237) was administered to 20 Wistar rats from a total of 50 rats; the remaining 30 rats were given 0.3 g/mL lincomycin per day, a mouse model of intestinal homeostasis imbalance was established by 0.3 ml once and twice a day, in contrast, the control group received the same volume of sterile water [11]. To see if the modeling was successful, endotoxin, acetic acid, enterobacteriaceae, enterococcus, lactobacillus, and bifidobacterium were identified in the blood of 10 rats from each group after four days. Remaining normal-group rats were employed as controls, while the remaining 20 normal-group rats were divided into two groups: the Huangqin Decoction group (10 rats) and the natural recovery groups (ten rats). According to the random number table, the Huangqin Decoction group was given 0.3 ml Huangqin Decoction for gastric perfusion treatment, and the natural recovery group was given the same amount of saline for gastric perfusion treatment, 2 times a day for 7 days.

2.4. Detection Methods

2.4.1. Detection of SREBP1 Expression by Western Blotting. Three groups of intestinal mucosal cells were collected before and 7 days after administration, and the cells were lysed with three decontamination lysates (Shanghai Kanglang Biotechnology Co., Ltd.), the precipitate was removed by centrifugation at 5000 r/min, and the protein content was measured using the BCA kit (Shanghai Yanxi Biotechnology Co., Ltd.), with the above sample buffer (Shanghai ABX Shanghai Biotechnology Co., Ltd.), the protein concentration of each group was adjusted to the same, and the gel was processed under 10% SDS-Polyacrylamide, after 2 hours of electrophoresis (120 V gel, 80 V gel), it was electrotransferred (100 MA, 4°C, 3 H) to the polyvinylidene fluoride (PDVF) membrane and dyed with Lichunhong (Hebei Pengyu Biotechnology Co., Ltd.), then the effect of the protein transfer was observed and the standard position of the protein molecular weight was determined. Rabbit anti-mouse SREBP1 was incubated at 37°C for 2 hours at a ratio of 1 : 1000 after being closed for 1 hour with 5% fat-free milk TBST (Shanghai Xuanke Biotechnology Co., Ltd.), then TBST was washed three times, and a 1 : 2,000 scale was added to the Horseradish peroxidase labeled sheep anti-rabbit II (Santa Cruz, USA). Following 0.5 hours of incubation at 37°C and three TBST washes, the samples were developed and fixed using a fluorescence detection kit (Shanghai Yanqi Biotechnology Co., Ltd.). The results were analyzed with an image analyzer (Shanghai Instrument & Electric Instrument Co., Ltd.).

2.4.2. Cholesterol Test. Three sets of intestinal mucosal cells were collected before and after delivery; the cells were lysed with triple decontamination lysate, and the precipitates were removed by centrifugation at 5000 r/min. The buffer solution was used to get the protein concentration in each group down to 1.0 g/L, and then the medium was discarded. The lytic cells were frozen and thawed 3 times using PBS buffer solution (Semmerphisil Technology Co., Ltd.) and 500 μL 0.1 mol/l sodium hydroxide solution (Zhengzhou Yongkun Environmental Protection Technology Co., Ltd.). After quantifying the protein content with the BCA reagent, the protein was precipitated with 7.2% trichloroacetic acid. The supernatant was centrifuged at 800 × g for 10 min. Taking stigmasterol as the internal standard and making the standard curve, the supernatant of 100 μL was added to 200 μL 8.9 mol/L potassium hydroxide, total cholesterol (TC) was obtained by hydrolysis of cholesteryl ester (CE), and free cholesterol (FC) was obtained by adding 200 μL

1 mol/l sodium hydroxide. The samples were mixed separately with the internal standard solution and then extracted with anhydrous ethanol (Yucheng haowei Chemical Co., Ltd.) and N-hexane (Shandong Weiming Chemical Co., Ltd.), 1.5 chromium trioxide, and vacuum drying. The samples were dissolved by 80 μL Yiqing (Shandong Hongcheng Chemical Co., Ltd.) and 20 μL isopropanol (Wuxi Dongneng Chemical Technology Co., Ltd.) through the high-performance liquid chromatography (Shanghai Wufeng Scientific Instruments Co., Ltd.) on the sample. C18 column (Shanghai Weixi Biological Technology Co., Ltd.) was used for the detection. UV light at 250 nm, flow rate of 1 ml/min, column temperature of 4°C, TC was quantified by peak area and calibrated by an internal standard, mg/G cell protein. CE = TC-FC.

2.4.3. Treg Cell Test. After drawing 2 mL of anticoagulant blood from each group, the erythrocytic-lysate solution (Hangzhou Haoxin Biotechnology Co., Ltd.) was added, and the mixture was uniformly mixed before being incubated for 15 minutes at room temperature, the rat anti-human FITC-CD4 antibody (Shanghai Bangjing Industrial Co., Ltd.) was added with 1 × 105 cells/L after washing twice with PBS buffer. The cells were then rinsed with PBS buffer and treated for 30 minutes at 4°C with rabbit anti-human PE-CD25 antibody (Shanghai Wanjiang Biotechnology Co., Ltd.) and rat anti-human Foxp3-PE-Cy5 antibody (Beijing Boao Pike Biotechnology Co., Ltd.), followed by Flow cytometry cells and CD4CD25FOXP3 + cells. Finally, cell quest V 3.2 the proportion of Treg cells in the total CD4 + T lymphocyte was analyzed.

2.5. Observational Index. ① Compare the relative density of SREBP1 before and after administration in each group; ② Compare CE, FC and TC levels in each group before and after administration; and ③ Compare Treg cell levels in each group before and after administration.

2.6. Statistical Methods. In the statistical study, SPSS 18.0 was utilized, and the mean ± standard deviation ($\pm s$) was employed to represent the data, T was used to test, N or% was used to express the data, X2 was used to test. Using the F value, the difference between the two groups was tested, and $P < 0.05$ was utilized to signify significance.

3. Outcome

3.1. Comparison of SREBP1 Relative Density before and after Administration in Each Group. There was a significant difference ($P < 0.05$) in the relative density of SREBP1 between the Huangqin Decoction and natural recovery groups and the control group before delivery, and after administration, SREBP1 concentrations were considerably lower in the Huangqin Decoction group than in the natural recovery group. Table 1 shows that the Huangqin Decoction group's decline range was considerably greater than that of the natural recovery group ($P < 0.05$) Figures 1, 2, 3, 13.

3.2. Comparison of CE, FC, and TC Levels before and after Administration in Each Group. Before administration, the levels of CE, FC, and TC in Huangqin Decoction group and natural recovery group were significantly higher than those in control group ($P < 0.05$), and the levels of CE, FC, and TC in Huangqin Decoction group and natural recovery group were significantly lower after administration, the decrease range of Huangqin Decoction group was significantly greater than that of natural recovery group ($P < 0.05$), see Table 2.

3.3. Comparison of Treg Cell Levels before and after Administration in Each Group. In the Huangqin Decoction and natural recovery groups, the Treg cell level was considerably greater before administration ($P < 0.05$) than that in the control group, and after administration, the Treg cell level was significantly reduced in the Huangqin Decoction and natural recovery groups, According to Table 3, there was a significant difference between the Huangqin Decoction and the natural recovery groups ($P < 0.05$).

4. Discussion

The role of intestinal homeostasis in the vital activities of the body has received increasing attention in clinical practice; there are significant differences in the composition of intestinal microflora between colorectal cancer patients and noncolorectal cancer patients, implying that homeostasis is closely related to the occurrence of colon cancer. Because of the high density of intestinal flora in the colon, when it is out of balance, it can cause the incidence and development of colon disease. Intestinal homeostasis imbalance can result in intestinal mucosal immune function imbalance, the decrease of intestinal short-chain fatty acid, the metabolic disorder of intestinal bile acid, the increase of susceptibility to carcinogens and the proliferation of colonic epithelium. In addition, bile acids can produce carcinogenic metabolites under the action of intestinal microflora, which promote the development of colon cancer. Huangqin Decoction group rigorous, with Huangqin qingre detoxification, peony astringent and ying pain, adjuvant medicine licorice, so that the Chinese date and in the first, four drugs combined, play Qingre dysentery, slow pain relief effect. Pharmacological studies show that Huangqin Decoction has obvious antibacterial, anti-inflammatory, spasmolytic, analgesic, antipyretic, enhancing immunity, sedative and other effects. It has essential implications for maintaining intestinal homeostasis [12]. Aside from this, the effect of Huangqin Decoction in the preservation of intestinal homeostasis and the development of colon cancer on the basis of "SREBP1-cholesterol metabolism-Treg cell differentiation" has not yet been investigated.

SREBP1 is composed of DNA binding subunits and regulatory subunits, located in the endoplasmic reticulum, which is an essential regulatory protein for cholesterol metabolism and membrane binding transcription factors in cells [13]. Abnormal blood lipids can cause upregulation of SREBP1, however, Tongmai Jiangzhuo decoction

Table 1: Comparison of SREBP1 relative density before and after administration in each group ($\pm s$).

Time	Control group ($n = 10$)	Huangqin Decoction group ($n = 10$)	Natural recovery group ($n = 10$)	F/t value	P value
Premeditation	0.18 ± 0.03	1.15 ± 0.12	1.19 ± 0.13	6.524	0.017
Postmedication	0.15 ± 0.09	$0.33 \pm 0.04^*$	$0.84 \pm 0.06^*$	5.473	0.032

Note: *indicates the comparison between the same groups before and after administration, $^*P < 0.05$.

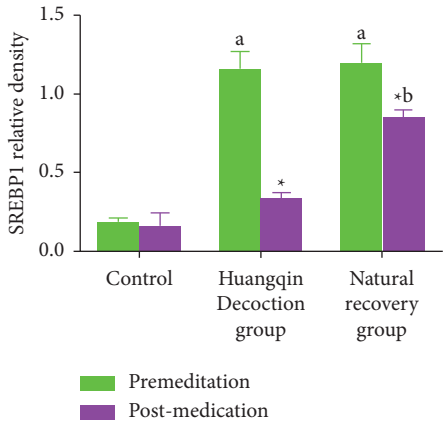

Figure 1: Comparison of SREBP1 relative density before and after administration in each group.

(containing Bupleurum Root 15 g, radix scutellariae 9 g, radix et rhizoma Rhei 6 g, radix paeoniae alba 9 g, jujube 9 g, Pinellia ternata 9 g) could effectively downregulate the expression of SREBP1, before administration, the relative density of SREBP1 in Huangqin Decoction group and natural recovery group was higher than that in the control group [14, 15]. After administration, the relative density of SREBP1 in the Huangqin Decoction group was lower than that in the control group and the SREBP1 was upregulated in the group of Huangqin Decoction and upregulated in the group of Huangqintang, which is significant for maintaining intestinal homeostasis and reducing the risk of colon cancer. Metabolic abnormality is an essential feature of intestinal homeostasis imbalance and tumor cells, which is characterized by hyperactive cholesterol oxidation, alteration of related metabolic enzymes, and enhancement of tumor signaling pathways [16]. SREBP1, a key transcription factor regulating lipid metabolism, regulates gene expression of key enzymes in fatty acid and cholesterol synthesis and plays a regulatory role in lipid regeneration. The expression and activity of SREBP1 in normal cells and tissues are low. SREBP1 can be activated in hard egg tumors and promote the expression of genes downstream of SREBP1. SREBP1 can not only accelerate the synthesis of cholesterol and fatty acids; moreover, it can also affect the metabolism of amino acid, glucose and lipid of tumor cells through various signal pathways, providing certain material and energy for tumor cell metastasis and proliferation [17]. Baicalin, Paeoniflorin, and other effective components in Huangqin Decoction can not only effectively interfere with the immune response of the body but also regulate the intestinal microorganisms [18]. It has been suggested that Huangqin Decoction can increase tumor cell necrosis, promote monocyte to M1 transformation and regulate microenvironment; as a result, preventing colon cancer by maintaining intestinal homeostasis is extremely important.

Studies by Moriya et al. [19] show that the TC level of colorectal cancer is significantly increased after the occurrence of colorectal cancer, which is closely related to the tumor stage, the ability of proliferation, and the degree of invasion. Both the Huangqin Decoction and natural recovery groups had significantly increased levels of CE, FC, and TC compared to the control group. After administration, the levels of CE, FC, and TC in the two groups decreased. Huangqin Decoction, on the other hand, decreased more, which was in line with the results of Ding Xiaorui and izhenwei, who found that it had a similar effect, indicating that the imbalance of intestinal homeostasis could cause abnormal metabolism of cholesterol and that Scutellaria baicalensis can correct its metabolic disorder. As tumor invasion progresses, cholesterol's role in cancer formation and progression becomes increasingly important., the higher the stage of tumor and the stronger the ability of cell division and proliferation, the more cholesterol is required. In order to maintain intestinal homeostasis and prevent the incidence of colon cancer, the glycosides in Huangqin Decoction have favorable effects on decreasing blood lipid and blood pressure.

The results of Moriya et al. [19] showed that the level of Treg in colon cancer patients with intestinal obstruction increased, but after effective treatment, the level of Treg decreased effectively. Fan et al. [20] showed that Huangqin Decoction could regulate the level of Treg in the body and regulate the homeostasis of intestinal immunity, treg cell level decreased in the two groups after administration, but the decrease was more obvious in the Huangqin Decoction group than in the natural recovery group, which was consistent with the results of Du et al. and Zhao et al. the Huangqin Decoction group could effectively regulate the differentiation of Treg cells [21, 22]. Treg, as an immune cell, can inhibit the differentiation of immunocompetent cells by direct action between cells. The activity of numerous inflammatory substances can also hinder the immune response against tumors, baicalein, Baicalin, and Paeonia lactiflora pall in the Huangqin Decoction can effectively regulate the immune system, therefore, anti-inflammatory properties of Huangqin Decoction help preserve intestinal homeostasis and minimize colon cancer risk [23, 24].

To summarize, Huangqin Decoction has a high clinical reference value for maintaining intestinal homeostasis and reducing colon cancer risk through regulation of SREBP1, cholesterol metabolism, and Treg cell development in the body.

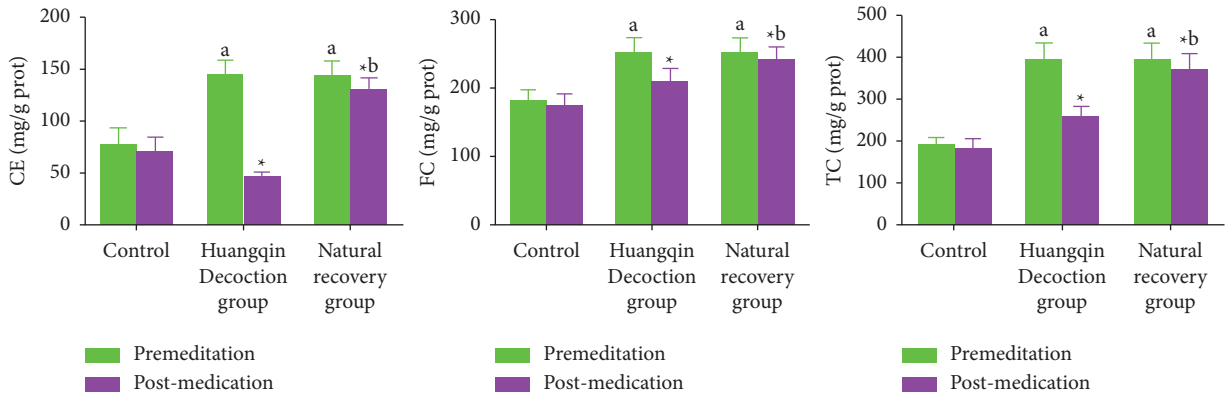

Figure 2: Comparison of CE, FC, and TC levels before and after administration in each group.

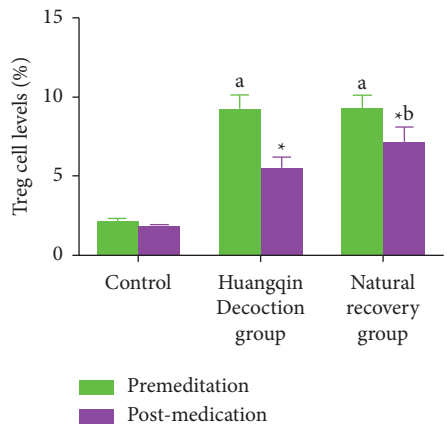

Figure 3: Comparison of Treg cell levels before and after administration in each group.

Table 2: Comparison of CE, FC, and TC levels before and after administration in each group (mg/g prot, $\pm s$).

Measurements		Control group ($n = 10$)	Huangqin Decoction group ($n = 10$)	Natural recovery group ($n = 10$)	F/t value	P value
CE	Premedication	77.02 ± 16.26	143.40 ± 15.01	142.68 ± 15.27	18.026	0.000
	Postmedication	69.98 ± 14.96	45.28 ± 5.50*	130.23 ± 11.23*	7.633	0.002
FC	Premedication	181.32 ± 16.20	250.91 ± 23.16	251.10 ± 23.15	8.431	0.000
	Postmedication	173.62 ± 18.93	210.21 ± 19.52*	240.17 ± 21.31*	7.018	0.010
TC	Premedication	188.23 ± 21.61	393.16 ± 40.25	393.31 ± 40.13	9.142	0.000
	Postmedication	180.36 ± 23.69	255.84 ± 26.02*	370.33 ± 38.98*	7.809	0.000

Note: *indicates the comparison between the same groups before and after administration, $^{*}P < 0.05$.

Table 3: Comparison of Treg cell levels before and after administration in each group (%, $\pm s$).

Time	Control group ($n = 10$)	Huangqin Decoction group ($n = 10$)	Natural recovery group ($n = 10$)	F/t value	P value
Premeditation	2.09 ± 0.27	9.15 ± 1.00	9.21 ± 0.92	6.518	0.020
Postmedication	1.78 ± 0.16	5.45 ± 0.75*	7.11 ± 1.00*	5.162	0.039

Note: *indicates the comparison between the same groups before and after administration, $^{*}P < 0.05$;

Data Availability

The data used to support the findings of this study are available from the corresponding author upon request.

Disclosure

Junde Zhou and Nannan Lu are Co-first authors.

Conflicts of Interest

The authors declare that they have no conflicts of interest.

Authors' Contributions

Junde Zhou and Nannan Lu are contributed equally to this work.

Acknowledgments

This work was supported by the Harbin Medical University.

References

[1] E. E. Alexeev, J. M. Lanis, D. J. Kao et al., "Microbiota-derived indole metabolites promote human and murine intestinal homeostasis through regulation of interleukin-10 receptor," *American Journal Of Pathology*, vol. 188, no. 5, pp. 1183–1194, 2018.

[2] M. Olivares, A. M. Neyrinck, S. A. Potgens et al., "The DPP-4 inhibitor vildagliptin impacts the gut microbiota and prevents disruption of intestinal homeostasis induced by a Western diet in mice," *Diabetologia*, vol. 61, no. 8, pp. 1838–1848, 2018.

[3] G. S. Wan, M. L. Xie, H. J. Yu, and H. Chen, "Intestinal dysbacteriosis activates tumor-associated macrophages to promote epithelial-mesenchymal transition of colorectal cancer," *Innate Immunity*, vol. 24, no. 8, pp. 480–489, 2018.

[4] G. Chen, Y. Yang, C. Hu et al., "Protective effects of Huangqin Decoction against ulcerative colitis and associated cancer in mice," *Oncotarget*, vol. 7, no. 38, pp. 61643–61655, 2016.

[5] Y. X. Zhang, Y. Y. Gu, Y. H. Chen et al., "Dingxin recipe IV attenuates atherosclerosis by regulating lipid metabolism through LXR-α/SREBP1 pathway and modulating the gut microbiota in ApoE -/- mice fed with HFD," *Journal of Ethnopharmacology*, vol. 266, no. 1, pp. 113436–121136, 2021.

[6] Y. Jiang and L. Fan, "The effect of Poria cocos ethanol extract on the intestinal barrier function and intestinal microbiota in mice with breast cancer," *Journal of Ethnopharmacology*, vol. 266, Article ID 113456, 2021.

[7] X. L. Jiang, X. Y. Gu, X. X. Zhou et al., "Intestinal dysbacteriosis mediates the reference memory deficit induced by anaesthesia/surgery in aged mice," *Brain, Behavior, and Immunity*, vol. 80, pp. 605–615, 2019.

[8] M. Leonard and B. Williams, "Usage of social media twitter in the intervention of diabetes mellitus," *Science Progress and Research*, vol. 1, no. 3, pp. 236–242, 2021.

[9] W. S. Garrett, "The gut microbiota and colon cancer," *Science*, vol. 364, no. 6446, pp. 1133–1135, 2019.

[10] M. Molska and J. Reguła, "Potential mechanisms of probiotics action in the prevention and treatment of colorectal cancer," *Nutrients*, vol. 11, no. 10, p. 2453, 2019.

[11] D. S. Che, A. Seidu, and W. Cai, "Effects of Huangqin Decoction fiber on growth performance, nutrient digestibility, microbial composition, VFA production, gut pH, and immunity of weaned pigs," *Microbiologyopen*, vol. 8, no. 5, pp. 712–714, 2019.

[12] Y. H. Xu, X. Y. Tan, Y. C. Xu, T. Zhao, L. H. Zhang, and Z. Luo, "Novel insights for SREBP-1 as a key transcription factor in regulating lipogenesis in a freshwater teleost, grass carp Ctenopharyngodon idella," *British Journal of Nutrition*, vol. 122, no. 11, pp. 1201–1211, 2019.

[13] H. F. Xu, J. Luo, G. Z. Ma et al., "Acyl-CoA synthetase short-chain family member 2 (ACSS2) is regulated by SREBP-1 and plays a role in fatty acid synthesis in caprine mammary epithelial cells," *Journal of Cellular Physiology*, vol. 233, no. 2, pp. 1005–1016, 2018.

[14] Y. X. Pan, M. Q. Zhuo, D. D. Li, Y. H. Xu, K. Wu, and Z. Luo, "SREBP-1 and LXRα pathways mediated Cu-induced hepatic lipid metabolism in zebrafish Danio rerio," *Chemosphere*, vol. 215, no. 3, pp. 370–379, 2019.

[15] Y. Zou, J. Lin, W. Li et al., "Huangqin-tang ameliorates dextran sodium sulphate-induced colitis by regulating intestinal epithelial cell homeostasis, inflammation and immune response," *Scientific Reports*, vol. 6, no. 1, pp. 39299–99, 2016.

[16] X. Zhang, X. W. Zhao, D. B. Liu et al., "Lipid levels in serum and cancerous tissues of colorectal cancer patients," *World Journal of Gastroenterology*, vol. 20, no. 26, pp. 8646–8652, 2014.

[17] Z. Yuan, L. Yang, X. Zhang, P. Ji, Y. Hua, and Y. Wei, "Mechanism of Huang-lian-Jie-du decoction and its effective fraction in alleviating acute ulcerative colitis in mice: regulating arachidonic acid metabolism and glycerophospholipid metabolism," *Journal of Ethnopharmacology*, vol. 259, Article ID 112872, 2020.

[18] J. Zhao, X. H. Zhang, T. Gao et al., "SIK2 enhances synthesis of fatty acid and cholesterol in ovarian cancer cells and tumor growth through PI3K/Akt signaling pathway," *Cell Death & Disease*, vol. 11, no. 1, pp. 25–27, 2020.

[19] Y. Moriya, Y. Koyama, K. Hojo, and R. Tsunematsu, "Continuous intravenous administration of 1-(2-tetrahydrofuryl)-5-fluorouracil [FT] by intravenous hyperalimentation (IVH)--stability of FT in IVH solution and tumor levels of 5-fluorouracil (5-FU)," *Japanese Journal of Clinical Oncology*, vol. 13, no. 1, pp. 31–35, 1983.

[20] X. L. Fan, Q. X. Zeng, X. Li et al., "Induced pluripotent stem cell-derived mesenchymal stem cells activate quiescent T cells and elevate regulatory T cell response via NF-κB in allergic rhinitis patients," *Stem Cell Research & Therapy*, vol. 9, no. 1, pp. 170–172, 2018.

[21] Y. M. Du, Y. X. Zhuansun, R. Chen, L. Lin, Y. Lin, and J. Li, "Mesenchymal stem cell exosomes promote immunosuppression of regulatory T cells in asthma," *Experimental Cell Research*, vol. 363, no. 1, pp. 114–120, 2018.

[22] T. Zhao, H. Tang, L. Xie et al., "Scutellaria baicalensis Georgi. (Lamiaceae): a review of its traditional uses, botany, phytochemistry, pharmacology and toxicology," *Journal of Pharmacy and Pharmacology*, vol. 71, no. 9, pp. 1353–1369, 2019.

[23] M. X. Li, M. Y. Li, J. X. Lei et al., "Huangqin decoction ameliorates DSS-induced ulcerative colitis: role of gut microbiota and amino acid metabolism, mTOR pathway and intestinal epithelial barrier," *Phytomedicine*, vol. 100, Article ID 154052, 2022.

[24] W. Lam, Z. Jiang, F. Guan et al., "PHY906 (KD018), an adjuvant based on a 1800-year-old Chinese medicine, enhanced the anti-tumor activity of Sorafenib by changing the tumor microenvironment," *Scientific Reports*, vol. 5, no. 1, p. 9384, 2015.

Hindawi
Evidence-Based Complementary and Alternative Medicine
Volume 2023, Article ID 2176371, 8 pages
https://doi.org/10.1155/2023/2176371

Research Article

An Evaluation of Fluorouracil plus Paclitaxel and Oxiliplatin as a First-Line Treatment for Advanced Gastric Squamous Cell Carcinoma

Jie Qin,[1] Yingpeng Shi,[2] Xueli Zheng,[3] Ya Lan,[4] Mingxin Zhang,[1] and Mi Liu[1]

[1]*Department of Gastroenterology, The First Affiliated Hospital of Xi'an Medical University, Xi'an 710077, Shaanxi, China*
[2]*Department of General Practice, The First Affiliated Hospital of Xi'an Medical University, Xi'an 710077, Shaanxi, China*
[3]*Cataract Refractive Center, Xianyang First People's Hospital, Xianyang 712000, Shaanxi, China*
[4]*Department of Gastroenterology, Shangluo Central Hospital, Shangluo 726000, Shaanxi, China*

Correspondence should be addressed to Mi Liu; liumi@xyfy.net.cn

Received 4 August 2022; Revised 15 August 2022; Accepted 17 August 2022; Published 6 April 2023

Academic Editor: Shoib Baba

Objective. To investigate the efficacy of fluorouracil (FU) combined with paclitaxel (PTX) and oxaliplatin (OXA) as the first-line treatment for advanced gastric signet ring cell carcinoma (SRCC) and its influence on human epidermal growth factor receptor 2 (HER-2) expression. *Methods*. We collected one hundred and sixty-eight patients with advanced gastric SRCC, including 87 patients treated with FU combined with PTX and OXA as the study group (SG) and 81 patients treated with FU combined with OXA as the control group (CG). We compared indicators such as efficacy and adverse reactions after treatment between the two groups and also detected serum HER-2 expression pre- and post-treatment. *Results*. The incidence of adverse reactions differed insignificantly between SG and CG ($P > 0.05$). SG presented a notably higher objective response rate (ORR) and disease control rate (DCR) than that of CG ($P < 0.05$). After treatment, the serum HER-2 expression level of patients in both groups decreased significantly ($P < 0.05$), and that in SG was significantly declined compared to CG ($P < 0.05$). HER-2 was negatively correlated with the efficacy of both SG and CG. The 1-year survival rate in SG (29.89%) was significantly higher than that in CG (16.05%) ($P < 0.05$). The median OS and PFS were higher in DG than that in CG ($P < 0.05$). *Conclusion*. FU combined with PTX and OXA can effectively improve the efficacy of first-line treatment for advanced gastric SRCC while reducing HER-2 expression, without increasing the adverse reaction rate. This treatment is worthy of clinical promotion.

1. Introduction

Gastric cancer (GC) is the fifth most frequently diagnosed cancer worldwide and the third leading cause of cancer-related death [1, 2]. It is also the second-largest cancer-related death cause and the second most common invasive cancer in China, with approximately 500,000 people dying of GC in 2015 [3]. Although the overall incidence of GC has declined in recent decades, the incidence of gastric signet ring cell carcinoma (SRCC) is still increasing [4]. Gastric SRCC is mainly composed of scattered malignant cells containing cytoplasmic mucin, which accounts for more than 50% of the tumor [5], and is diagnosed as an adenocarcinoma based on the microscopic characteristics defined by the World Health Organization (WHO) [6]. Studies have shown that gastric SRCC and non-SRCC are considered to be unique biological entities originating from different carcinogens [7].

Most patients with gastric SRCC generally enter the hospital in the late stage due to nonspecific symptoms [8]. As the histological manifestation of gastric SRCC is characterized by poor adhesion and tends to invade through submucosal and subserosal pathways, the prognosis of advanced gastric SRCC is dreadful [9]. The treatment of patients with advanced gastric SRCC is similar to that of patients with other subtypes of GC [10], so it is necessary to develop and establish a variety of clinical treatment strategies to improve patient outcomes. Human epidermal

growth factor receptor 2 (HER-2), a member of the HER family, is directly involved in the pathogenesis and progression of various human cancers [11, 12]. It is therefore often considered a bad prognostic factor [13, 14]. With the revolutionary influence of anti-HER-2 therapy in breast cancer patients [15], HER-2 and its blocking effect have been widely evaluated in other tumor types [16, 17]. The use of HER-2 inhibitor in GC has yielded favorable results and can be a prognostic factor in this disease [18]. FU is vital in the treatment of various cancers [19], and 5-FU has been identified as one of the standard first-line chemotherapy drugs for locally advanced or metastatic GC [20]. The combination of 5-FU and TRAIL had a greater inhibitory effect on the proliferation of gastric cancer cells than TRAIL alone. 5-FU significantly enhanced TRAIL-induced gastric cancer cell apoptosis. A new therapeutic strategy has been proposed to enhance the antitumor effect induced by 5-FU in GC cells resistant to 5-FU by TXN [21].

According to the Chicago consensus on peritoneal metastasis in 2020, PTX and OXA can be considered as the first-line chemotherapy for gastric cancer patients with peritoneal metastasis. In this study, we collected one hundred and sixty-eight patients with advanced gastric SRCC, including 87 patients treated with FU combined with PTX and OXA as the study group (SG) and 81 patients treated with FU combined with OXA as the control group (CG). Then, we tested indicators such as efficacy, adverse reactions, and HER-2 expression in two groups of patients under different treatment schemes to explore the therapeutic effect of fluorouracil (FU) combined with paclitaxel (PTX) and oxaliplatin (OXA) on advanced gastric SRCC and its influence on HER-2 expression.

2. Materials and Methods

2.1. General Information. One hundred and sixty-eight patients with advanced gastric SRCC in our hospital were collected as the research participants. Among them, 87 patients treated with FU combined with PTX and OXA were selected as the study group (SG), including 54 males and 33 females, with an average age of (69.37 ± 3.58) years. Eighty-one patients treated with FU combined with OXA were selected as the control group (CG), including 49 males and 32 females, with an average age of (70.28 ± 3.67) years.

2.2. Inclusion Criteria. Patients who were accompanied by family members and diagnosed with gastric SRCC by imaging and pathology were included, with TNM stage IIIb-IV, measurable lesions, Karnofsky performance status (KPS) score > 70, and complete clinicopathological data. All the patients had not received chemotherapy or other antitumor treatment within the last month, and the blood routine, liver and kidney function, and electrocardiogram were all normal before treatment.

2.3. Exclusion Criteria. Patients with an expected survival time of fewer than 3 months, previous history of mental illness and family history of mental illness, history of autoimmune deficiency, history of severe organ disease, and history of drug dependence were excluded. As well as those patients who cannot cooperate with the examination due to aphasia, irritability, confusion, and communication disorder. The experimental process was described to the patients and their families in advance, and this study was ratified by the Ethics Committee of our hospital, with the written informed consent obtained from the patients and their families.

2.4. Treatment of Patients. Patients in CG were given OXA 90 mg/m^2 and 0.1 g calcium levofolinate intravenously for 3 h on the first day. On the second day, 0.1 g calcium levofolinate was given intravenously, followed by 48 h of intravenous infusion of FU 2000 mg/m^2. One treatment cycle lasted for 15 days.

For patients in the SG, PTX 130 mg/m^2 and 0.1 g leucovorin were given intravenously for 3 h on the first day, and dexamethasone was given twice at 5 mg/time, which was intravenously dripped 10 h and 30 min before PTX administration for pretreatment. On the second day, OXA (90 mg/m^2) and folinate (0.1 g) were given intravenously for 3 h, followed by 48 h of intravenous infusion of FU 2000 mg/m^2. The treatment took 15 days as a cycle.

Before chemotherapy, 5-HT3 receptor antagonists were routinely administered to prevent vomiting, and proton pump inhibitors were given to protect gastric mucosa. Patients should avoid exposure to ice-cold substances during medication. All patients received treatment for ≥2 cycles, and continued treatment for 2 cycles if the condition did not improve.

Before treatment and after two cycles of treatment, 5 ml of fasting venous blood was collected and loaded into an anticoagulant tube for 60 min (20–25°C). Thereafter, the samples were centrifuged at 1369.55xp and 4°C for 15 minutes with a centrifuge (Sichuan Shuke Instrument, Chengdu, China, TG 112), and then it was put into the −70°C cryogenic refrigerator for reserve. Serum HER-2 (Human HER-2 ELISA kit, Shanghai Yanhui biotechnology, PTGCN) level was detected by enzyme-linked immunosorbent assay (ELISA) strictly following the manufacturer's protocol.

2.5. Outcome Measures. The adverse reactions of two groups of patients during treatment were counted. After every 2 cycles of treatment, the therapeutic effects, which were divided into complete response (CR), partial response (PR), stable disease (SD), and progressive disease (PD), were recorded in the two groups. Objective response rate (ORR) = number of (CR + PR) cases/total number of cases, and disease control rate (DCR) = number of (CR + PR + SD) cases/total number of cases. Serum HER-2 levels were compared before and after 2 cycles of treatment, and the correlation between HER-2 and the curative effect of advanced gastric SRCC was analyzed. The patients were followed up for one year, and the 1-year survival rate, total survival time (OS, the time from drug use to death or the last follow-up), and progression-free survival time (PFS, the time from drug use to disease progression or death) of the two groups were compared statistically.

Table 1: Comparison of general data between the two groups $(x \pm s)/(n(\%))$.

	Study group ($n = 87$)	Control group ($n = 81$)	t/X^2	P
Age (years old)	69.37 ± 3.58	70.28 ± 3.67	1.62	0.11
BMI (kg/m^2)	22.08 ± 2.04	22.24 ± 2.12	0.50	0.62
Gender			0.04	0.83
Male	54 (62.07)	49 (60.49)	—	—
Female	33 (37.93)	32 (39.51)	—	—
Drinking history			0.00	0.99
Yes	59 (67.82)	55 (67.90)	—	—
No	28 (32.18)	26 (32.10)	—	—
Smoking history			0.07	0.79
Yes	53 (60.92)	51 (62.96)	—	—
No	34 (39.08)	30 (37.04)	—	—
III_b	15 (17.24)	12 (14.81)	0.18	0.67
IV	72 (82.76)	69 (85.19)	—	—
Initial treatment	32 (36.78)	28 (34.57)	0.09	0.76
Retreatment	55 (63.22)	53 (65.43)	—	—

2.6. Statistical Methods. The results of this study were statistically analyzed by SPSS20.0 (IBM Corp, Armonk, NY, USA), and graphs were drawn with GraphPad Prism 7 (GraphPad Software Co., Ltd., San Diego, USA). Represented by $n(\%)$, the counting data between groups were compared by Chi-square test. The measured data were expressed by $(x \pm s)$, and the comparison between groups was made by t-test. Spearman's correlation coefficient was responsible for correlation analysis. $P < 0.05$ indicates that the difference was statistically significant.

3. Results

3.1. General Information. General information such as age, body mass index (BMI), smoking history, and drinking history of patients in the two groups were collected, as shown in Table 1. The average age in the study group was 69.37 ± 3.58 and 70.28 ± 3.67 in the control group. The BMI (kg/m^2) in the study group and in the control group was 22.08 ± 2.04 and 22.24 ± 2.12, respectively. No significant difference was present in general information between SG and CG ($P > 0.05$).

3.2. Comparison of Adverse Reactions between the Two Groups. See Figure 1 for the incidence of adverse reactions (fatigue, nausea and vomiting, leukopenia, etc.) between the two groups. The incidence of nausea and vomiting, diarrhea, and peripheral sensory adverse reactions were higher in study groups than in control groups. The myelosuppression and fatigue were lower in study groups than in control groups. There was no significant difference in the incidence of adverse reactions between SG (41.38%) and CG (44.44%) ($P > 0.05$), and both groups recovered after symptomatic treatment without chemotherapy-related death.

3.3. Comparison of Clinical Efficacy between the Two Groups. The curative effects of the two groups after treatment were compared, as shown in Figure 2. The number of people with PR and SD were higher than the control groups, while the SD was lower than in control groups. SG presented notably higher ORR and DCR (33.33%, 81.61%) than that of CG (18.52%, 65.43%) ($P < 0.05$).

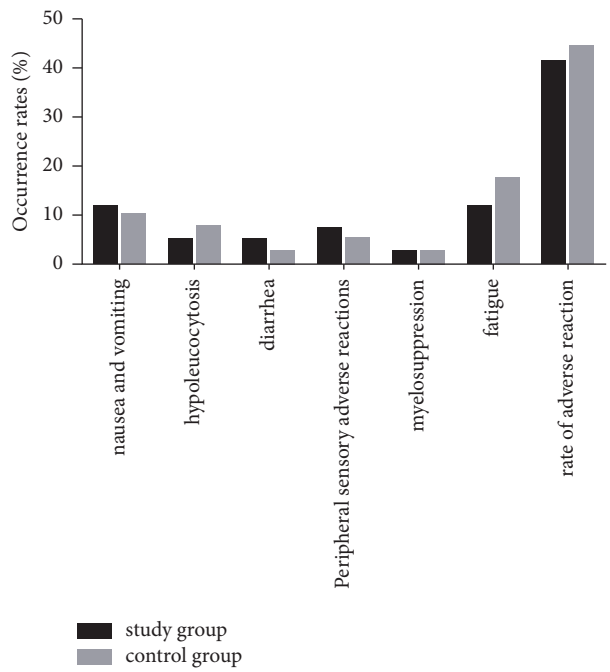

Figure 1: Comparison of adverse reactions between the two groups, with no significant difference.

3.4. Comparison of Serum HER-2 between the Two Groups Pre- and Post-Treatment. Serum HER-2 levels pre- and post-treatment were compared between the two groups, as shown in Figure 2. The serum HER-2 level did not differ remarkably between SG and CG before treatment ($P > 0.05$), but after treatment, it reduced evidently in both groups ($P < 0.05$), and the decrease was more significant in SG than in CG ($P < 0.05$).

There was no significant difference in HER-2 between the two groups before treatment, but it decreased significantly in both groups after treatment, and the HER-2 level

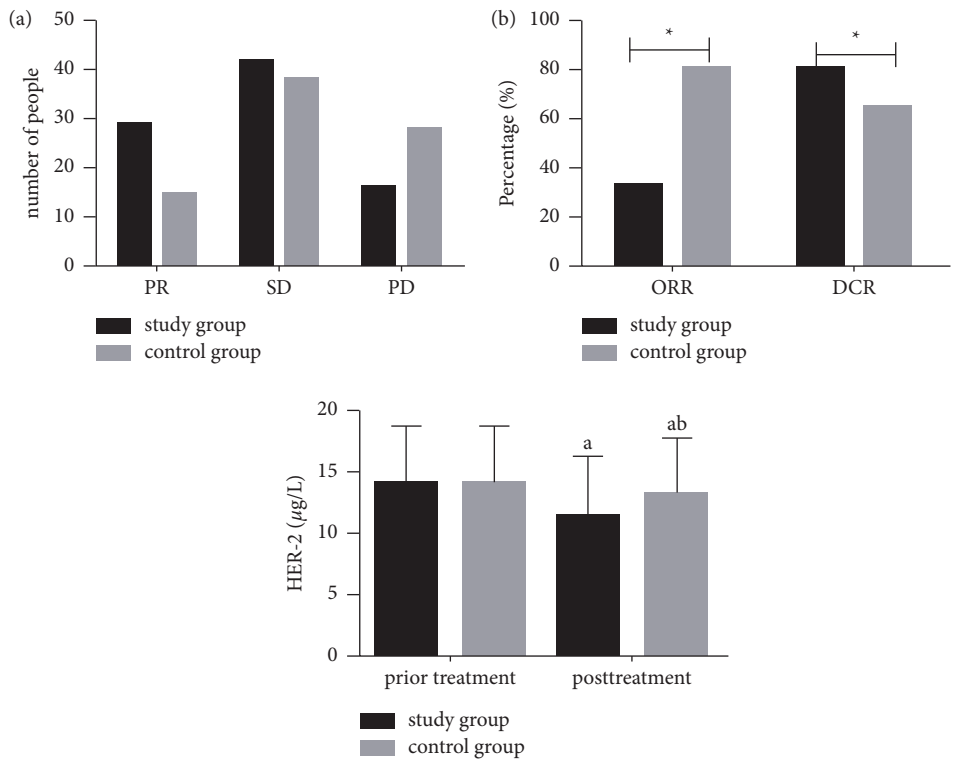

Figure 2: Comparison of serum HER-2 expression level between the two groups before and after treatment.

was significantly lower in the study group than that in the control group.

Note: *a* indicates $P < 0.05$ compared within the same group before and after treatment; *b* indicates $P < 0.05$ compared with the study group after treatment.

3.5. Correlation between HER-2 and Curative Effect in the Two Groups. See Figure 3 for the correlation between HER-2 and the curative effect of advanced 0020030 gastric SRCC. HER-2 had a significant negative correlation with the curative effect in both SG and CG ($r = -0.45$, $r = -0.52$, $p < 0.05$).

3.6. Comparison of Survival between the Two Groups. Statistics are made on the 1-year survival rate of patients in two groups, as shown in Figure 4. All the 168 patients were successfully followed up. The 1-year survival rate of SG (29.89%) was significantly higher than 16.05% of CG ($P < 0.05$).

3.7. Comparison of Median OS and PFS between the Two Groups. Median OS and PFS of the two groups were compared, as shown in Figure 5. The median OS and PFS in SG were higher compared to CG ($P < 0.05$).

4. Discussion

Gastric SRCC accounts for 4%–17% of all types of GC [22]. In the United States, gastric SRCC has an incidence of 0.094/100000 and a 5-year survival rate of 82.8%, and tumor stage and size are independent predictors of lymph node metastasis [23]. All the enrolled patients were followed up for 1 year, and the 1-year survival rate of patients was noticeably higher in SG than in CG, indicating that the treatment regimen used in SG can effectively improve the survival rate of patients with advanced gastric SRCC. Some reports have demonstrated that compared with the standard cisplatin plus FU regimen, PTX plus FU does not statistically prolong OS in patients with locally advanced esophageal squamous cell carcinoma [24]. Studies have shown that the survival rates of gastric SRCC in different periods are varying, and the five-year overall survival rates of early and late SRCC are 0.830 and 0.164, respectively [25]. Currently, chemotherapy is a primary means of clinical treatment for advanced GC [26].

FU is vital in the treatment of various cancers [19], and 5-FU has been identified as one of the standard first-line chemotherapy drugs for locally advanced or metastatic GC [20]. A new therapeutic strategy has been proposed to enhance the antitumor effect induced by 5-FU in GC cells resistant to 5-FU by TXN [21]. Some studies have also suggested that gastrectomy combined with OXA +5-FU has a definite therapeutic effect on GC, which can achieve a better short-term clinical therapeutic effect [27]. In Japan, oral FU plus cisplatin is the standard treatment for advanced GC, while PTX is an option. Clinically developed for breast cancer, nonsmall cell lung cancer and pancreatic cancer, PTX has also been clinically applied for the treatment of GC in Japan, and the results of the second-stage study have been published, indicating that this combination therapy is well tolerated and has yielded antitumor efficacy in patients with

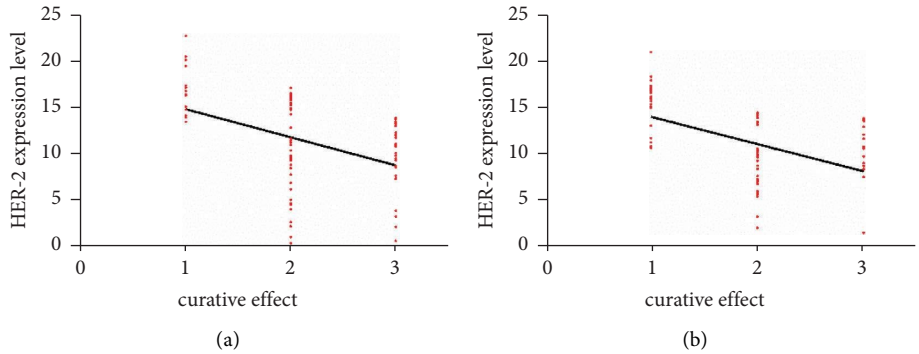

Figure 3: Correlation between HER-2 and curative effect of advanced gastric signet-ring cell carcinoma. (a) HER-2 was significantly negatively correlated with curative effect in the study group. (b) HER-2 was negatively correlated with the efficacy in the control group. Note: 1 indicates low PD, 2 indicates SD, and 3 indicates PR.

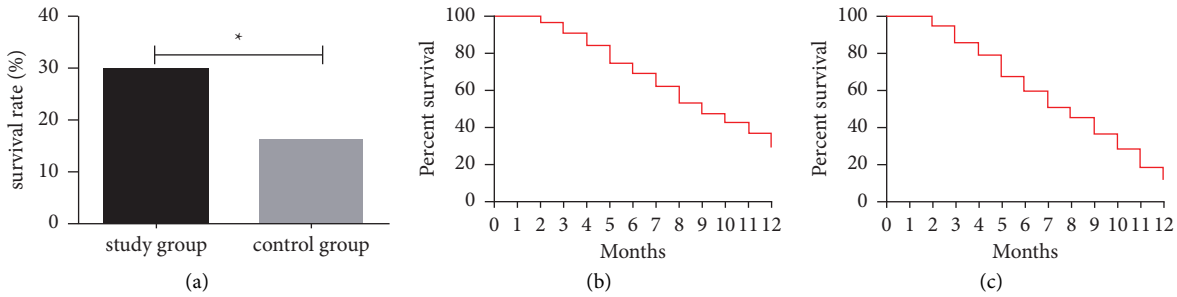

Figure 4: Comparison of 1-year survival rate between the two groups. (a) The 1-year survival rate of patients in the study group was significantly higher than that in the control group. (b) The 1-year overall survival rate of patients in the study group was 29.89%. (c) The 1-year overall survival rate of patients in the control group was 16.05%. Note: *indicates $P < 0.05$ compared between the two groups.

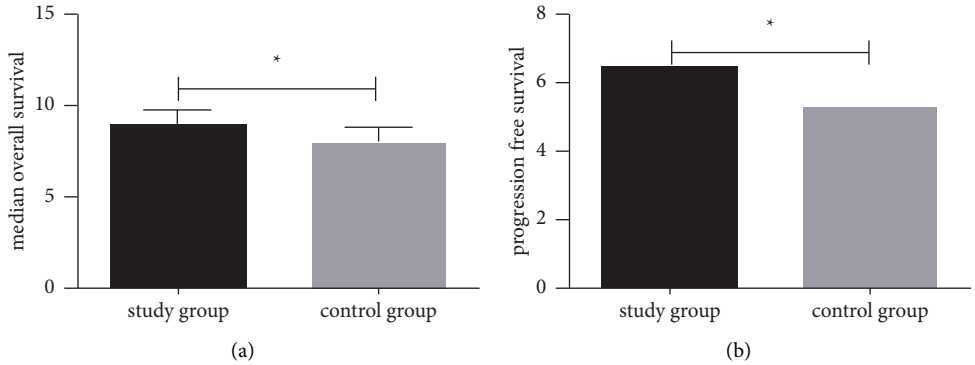

Figure 5: Comparison of median OS and PFS between the two groups. (a) The median OS in the study group was significantly higher than that in the control group. (b) The median PFS in the study group was significantly higher than that in the control group. Note: *indicates $P < 0.05$ compared between the two groups.

advanced GC [28], while OXA is one of the most extensively used chemotherapeutic agents in the treatment of various cancers including GC. However, due to its toxicity and drug resistance, its therapeutic indicator is narrow. It is necessary to develop new therapies to enhance efficacy and reduce toxicity [29]. Therefore, the purpose of this study was to explore the efficacy of FU combined with PTX and OXA in the treatment of advanced gastric SRCC.

Adverse reactions of chemotherapy mainly include gastrointestinal reactions, myelosuppression, and neurotoxic reactions. Implementation of family was advised to support the patients, and patients are supported by nutrition management intervention, which is helpful for patients to overcome the adverse reactions, such as nausea and vomiting [30]. Although there was no marked difference, the incidence of adverse reactions in the SG was still lower than

that in the CG, which indicated that the treatment regimen applied in the SG could more effectively alleviate the pain and was more conducive to the successful completion of treatment for patients. Studies have shown that PTX combined with 5-FU is well tolerated and effective in the treatment of advanced GC [31]. Also, it is shown that chemotherapy based on FU and Kanglaite injection can enormously improve the clinical efficacy of patients with advanced gastrointestinal malignancies and reduce adverse reactions [32]. Therefore, this study further compared the efficacy of the two groups of patients after treatment, and found that the number of cases with ORR and DCR in SG was significantly higher than those in CG. A study [33] included 61 patients with gastric SRCC and found that there was 1 case of CR, 36 cases of PR, 15 cases of SD, and 9 cases of PD after treatment with docetaxel combined with cisplatin and FU, which was similar to this study, indicating that FU combined with PTX and OXA could profoundly improve the curative effect of advanced gastric SRCC. In the treatment of GC patients, the detection of HER2 expression has become a routine [34]. Human epidermal growth factor receptor 2 (HER-2), a member of the HER family, is directly involved in the pathogenesis and progression of various human cancers. It is therefore often considered as a bad prognostic factor. With the revolutionary influence of anti-HER-2 therapy in breast cancer patients, HER-2 and its blocking effect have been widely evaluated in other tumor types. The use of HER-2 inhibitor in GC has yielded favorable results and can be a prognostic factor in this disease. This study analyzed the correlation between HER-2 and the curative effect of advanced gastric SRCC, and concluded that HER-2 was significantly negatively correlated with the curative effect in both SG and CG, in other words, HER-2 increased with the decrease of the efficacy, indicating that HER2 could be used to judge the curative effect of advanced gastric SRCC. It was also found that serum HER-2 differed insignificantly between the two groups before treatment, but it decreased significantly in both groups after treatment, indicating that the two chemotherapy methods were effective for advanced gastric SRCC. Whereas, the HER-2 in SG was significantly lower than that in CG, suggesting that the treatment regimen of the SG could reduce HER-2 more effectively and improve the curative effect on advanced gastric SRCC. Gastric SRCC is mainly composed of scattered malignant cells containing cytoplasmic mucin, which accounts for more than 50% of the tumor, and is diagnosed as an adenocarcinoma based on the microscopic characteristics defined by the World Health Organization (WHO). Studies have shown that gastric SRCC and non-SRCC are considered to be unique biological entities originating from different carcinogens. Gastric cancer is one of the leading causes of cancer-related death worldwide. Many patients have inoperable disease at diagnosis or have recurrent disease after resection with curative intent. Literature has identified that the 5-year cumulative survival rate of gastric SRCC is 0.49, while the 5-year overall survival rate is 0.16, with 17.4% complications [25]. This is similar to the 1-year survival rate of patients in the CG in this study. Other reports have revealed that the addition of docetaxel to cisplatin and 5-FU regimen can profoundly improve the progression time and OS of untreated advanced GC patients with a median PFS of 7.2 months. Similar findings were obtained in the current study. The median OS and PFS of patients in SG treated with FU combined with PTX and OXA were higher than those in CG treated with OXA combined with 5-FU. This further indicated that the treatment plan used in SG can effectively improve the survival rate of patients with advanced gastric SRCC.

In this article, the curative effect, adverse reactions, and HER-2 of two groups of patients under different treatment schemes were tested to explore the curative effect of FU combined with PTX and OXA on advanced gastric SRCC and its influence on the expression level of HER-2, hoping to provide a theoretical basis for the treatment of advanced gastric SRCC. However, there are still some limitations in this study. The experimental subjects are limited, and the specific role of HER-2 in advanced gastric SRCC and the way in which the differential expression of HER-2 is caused are not clear. First-line treatment of FU combined with PTX and OXA can effectively improve the efficacy of first-line treatment for advanced gastric SRCC while enormously reducing HER-2 expression without increasing the adverse reaction rate [35].

5. Conclusion

Gastric cancer is one of the leading causes of cancer-related death worldwide. Many patients have inoperable disease at diagnosis or have recurrent disease after resection with curative intent. In this study, we tested the curative effect, adverse reactions, and HER-2 of two groups of patients under different treatment schemes to explore the curative effect of FU combined with PTX and OXA on advanced gastric SRCC and its influence on the expression level of HER-2. We hoped to provide a theoretical basis for the treatment of advanced gastric SRCC. However, there are still some limitations. The experimental subjects are limited, and the specific role of HER-2 in advanced gastric SRCC and the way in which the differential expression of HER-2 is caused are not clear. It is hoped that the research content will be improved continuously in the future research to provide more scientific reference for clinical treatment.

The novelty of this study was to show that FU combined with PTX and OXA can effectively improve the efficacy of first-line treatment for advanced gastric SRCC, without increasing the adverse reaction rate. This treatment is worthy of clinical promotion. However, there are also limitations of this study. The underlying mechanism was not so clear and which molecular that act with HER-2 was not clarified. Further studies are needed to study how HER-2 regulates the prognosis of gastric cancer.

Data Availability

The datasets used and/or analyzed during this study are available from the corresponding author on reasonable request.

Conflicts of Interest

The authors declare that they have no conflicts of interest.

References

[1] F. Bray, J. Ferlay, I. Soerjomataram, R. L. Siegel, L. A. Torre, and A. Jemal, "Global cancer statistics 2018: GLOBOCAN estimates of incidence and mortality worldwide for 36 cancers in 185 countries," *CA: A Cancer Journal for Clinicians*, vol. 68, no. 6, pp. 394–424, 2018.

[2] J. Ferlay, M. Colombet, I. Soerjomataram et al., "Estimating the global cancer incidence and mortality in 2018: GLOBOCAN sources and methods," *International Journal of Cancer*, vol. 144, no. 8, pp. 1941–1953, 2019.

[3] W. Chen, R. Zheng, P. D. Baade et al., "Cancer statistics in China, 2015," *CA: A Cancer Journal for Clinicians*, vol. 66, no. 2, pp. 115–132, 2016.

[4] Z. M. Bamboat, L. H. Tang, E. Vinuela et al., "Stage-stratified prognosis of signet ring cell histology in patients undergoing curative resection for gastric adenocarcinoma," *Annals of Surgical Oncology*, vol. 21, no. 5, pp. 1678–1685, 2014.

[5] H. J. Chon, W. J. Hyung, C. Kim et al., "Differential prognostic implications of gastric signet ring cell carcinoma: stage adjusted analysis from a single high-volume center in asia," *Annals of Surgery*, vol. 265, no. 5, pp. 946–953, 2017.

[6] I. D. Nagtegaal, R. D. Odze, D. Klimstra et al., "The 2019 WHO classification of tumours of the digestive system," *Histopathology*, vol. 76, no. 2, pp. 182–188, 2020.

[7] Y. C. Kao, W. L. Fang, R. F. Wang et al., "Clinicopathological differences in signet ring cell adenocarcinoma between early and advanced gastric cancer," *Gastric Cancer*, vol. 22, no. 2, pp. 255–263, 2019.

[8] S. Pernot, T. Voron, G. Perkins, C. Lagorce-Pages, A. Berger, and J. Taieb, "Signet-ring cell carcinoma of the stomach: impact on prognosis and specific therapeutic challenge," *World Journal of Gastroenterology*, vol. 21, no. 40, pp. 11428–11438, 2015.

[9] S. H. Lee, S. R. Jee, J. H. Kim, and S. Y. Seol, "Intramucosal gastric cancer: the rate of lymph node metastasis in signet ring cell carcinoma is as low as that in well-differentiated adenocarcinoma," *European Journal of Gastroenterology and Hepatology*, vol. 27, no. 2, pp. 170–174, 2015.

[10] Y. Li, F. H. Ma, L. Y. Xue, and Y. T. Tian, "Neoadjuvant chemotherapy vs. upfront surgery for gastric signet ring cell carcinoma: a retrospective, propensity score-matched study," *World Journal of Gastroenterology*, vol. 26, no. 8, pp. 818–827, 2020.

[11] F. Sanguedolce, A. Cormio, P. Massenio et al., "Altered expression of HER-2 and the mismatch repair genes MLH1 and MSH2 predicts the outcome of T1 high-grade bladder cancer," *Journal of Cancer Research and Clinical Oncology*, vol. 144, no. 4, pp. 637–644, 2018.

[12] C. Yapijakis, M. Adamopoulou, K. Tasiouka, C. Voumvourakis, and G. Stranjalis, "Mutation screening of her-2, N-ras and Nf1 genes in brain tumor biopsies," *Anticancer Research*, vol. 36, no. 9, pp. 4607–4612, 2016.

[13] E. Di Oto, A. A. Brandes, M. C. Cucchi, and M. P. Foschini, "Prognostic impact of HER-2 Subclonal Amplification in breast cancer," *Virchows Archiv*, vol. 471, no. 3, pp. 313–319, 2017.

[14] M. K. Gheybi, A. Baradaran, M. R. Mohajeri, A. Ostovar, P. Hajalikhani, and S. Farrokhi, "Validity of immunohistochemistry method in predicting HER-2 gene status and association of clinicopathological variables with it in invasive breast cancer patients," *Acta Pathologica, Microbiologica et Immunologica Scandinavica*, vol. 124, no. 5, pp. 365–371, 2016.

[15] L. H. Li, B. Xiao, A. Muhetaer, and Z. H. Sun, "[Differences in circRNA expression profiles between HER-2-positive breast cancer cells and normal mammary epithelial cells]," *Zhonghua Zhongliu Zazhi*, vol. 41, no. 5, pp. 331–337, 2019.

[16] X. T. Zhang, Z. Zhang, Y. N. Xin, X. Z. Ma, and S. Y. Xuan, "Impairment of growth of gastric carcinoma by miR-133-mediated Her-2 inhibition," *Tumor Biology*, vol. 36, no. 11, pp. 8925–8930, 2015.

[17] X. Lin and Y. Wang, "Re-expression of microRNA-4319 inhibits growth of prostate cancer via Her-2 suppression," *Clinical and Translational Oncology*, vol. 20, no. 11, pp. 1400–1407, 2018.

[18] V. Fanotto, E. Ongaro, K. Rihawi et al., "HER-2 inhibition in gastric and colorectal cancers: tangible achievements, novel acquisitions and future perspectives," *Oncotarget*, vol. 7, no. 42, pp. 69060–69074, 2016.

[19] D. Ilem-Ozdemir, E. Atlihan-Gundogdu, M. Ekinci et al., "Radiolabeling and in vitro evaluation of a new 5-fluorouracil derivative with cell culture studies," *Journal of Labelled Compounds and Radiopharmaceuticals*, vol. 62, no. 13, pp. 874–884, 2019.

[20] L. Zhang, Y. Xing, Q. Gao, X. Sun, D. Zhang, and G. Cao, "Combination of NRP1-mediated iRGD with 5-fluorouracil suppresses proliferation, migration and invasion of gastric cancer cells," *Biomedicine and Pharmacotherapy*, vol. 93, pp. 1136–1143, 2017.

[21] G. Y. Xu and X. J. Tang, "Troxerutin (TXN) potentiated 5-Fluorouracil (5-Fu) treatment of human gastric cancer through suppressing STAT3/NF-κB and Bcl-2 signaling pathways," *Biomedicine and Pharmacotherapy*, vol. 92, pp. 95–107, 2017.

[22] K. Murai, K. Takizawa, T. Shimoda et al., "Effect of double-layer structure in intramucosal gastric signet-ring cell carcinoma on lymph node metastasis: a retrospective, single-center study," *Gastric Cancer*, vol. 22, no. 4, pp. 751–758, 2019.

[23] S. K. Pokala, C. Zhang, Z. Chen et al., "Incidence, survival, and predictors of lymph node involvement in early-stage gastric signet ring cell carcinoma in the US," *Journal of Gastrointestinal Surgery*, vol. 22, no. 4, pp. 569–577, 2018.

[24] Y. Chen, J. Ye, Z. Zhu et al., "Comparing paclitaxel plus fluorouracil versus cisplatin plus fluorouracil in chemoradiotherapy for locally advanced esophageal squamous cell cancer: a randomized, multicenter, phase III clinical trial," *Journal of Clinical Oncology*, vol. 37, no. 20, pp. 1695–1703, 2019.

[25] I. M. Arer, H. Yabanoglu, A. Akdur, N. Akkapulu, and M. Kus, "Total versus subtotal gastrectomy for signet ring cell carcinoma of the stomach," *J Coll Physicians Surg Pak*, vol. 27, no. 10, pp. 616–620, 2017.

[26] H. Chai, C. Sun, J. Liu, H. Sheng, R. Zhao, and Z. Feng, "The relationship between ZEB1-AS1 expression and the prognosis of patients with advanced gastric cancer receiving chemotherapy," *Technology in Cancer Research and Treatment*, vol. 18, Article ID 153303381984906, 2019.

[27] K. Yan, K. Wu, L. Yan, L. Liang, and Y. Yuan, "Efficacy of postoperative intraperitoneal hyperthermic perfusion chemotherapy with oxaliplatin + 5-Fluorouracil in the treatment of gastric cancer patients with peritoneal carcinomatosis," *J BUON*, vol. 24, no. 4, pp. 1587–1594, 2019.

[28] N. Nakayama, K. Ishido, K. Chin et al., "A phase I study of S-1 in combination with nab-paclitaxel in patients with unresectable or recurrent gastric cancer," *Gastric Cancer*, vol. 20, no. 2, pp. 350–357, 2017.

[29] P. Zhang, L. Shi, T. Zhang et al., "Piperlongumine potentiates the antitumor efficacy of oxaliplatin through ROS induction in gastric cancer cells," *Cellular Oncology*, vol. 42, no. 6, pp. 847–860, 2019.

[30] H. Xie, Q. Lu, H. Wang, X. Zhu, and Z. Guan, "Two postoperative chemotherapies for gastric cancer: FOLFOX4 vs. TPF," *Oncology Letters*, vol. 17, no. 1, pp. 933–936, 2019.

[31] B. Yang, C. Shi, X. Lin, X. Wang, and Q. Chen, "Retrospective study on efficacy of a paclitaxel combined with a leucovorin and fluorouracil regimen for advanced gastric cancer," *Tumori Journal*, vol. 105, no. 6, pp. 509–515, 2019.

[32] Q. Song, J. Zhang, Q. Wu, G. Li, and E. L. H. Leung, "Kanglaite injection plus fluorouracil-based chemotherapy on the reduction of adverse effects and improvement of clinical effectiveness in patients with advanced malignant tumors of the digestive tract: a meta-analysis of 20 RCTs following the PRISMA guidelines," *Medicine (Baltimore)*, vol. 99, no. 17, Article ID e19480, 2020.

[33] Y. Bozkaya, G. U. Erdem, N. Y. Ozdemir et al., "Advanced signet-ring cell carcinoma of the stomach: clinicopathological characteristics of patients and efficacy of the modified docetaxel, cisplatin, and fluorouracil regimen," *Journal of Cancer Research and Therapeutics*, vol. 14, no. 10, pp. S742–S747, 2018.

[34] R. Chen, X. Zhou, J. Liu, and G. Huang, "Relationship between 18F-fdg PET/CT findings and HER2 expression in gastric cancer," *Journal of Nuclear Medicine*, vol. 57, no. 7, pp. 1040–1044, 2016.

[35] E. Van Cutsem, X. Sagaert, B. Topal, K. Haustermans, and H. Prenen, "Gastric cancer," *The Lancet*, vol. 388, no. 10060, pp. 2654–2664, 2016.

Hindawi
Evidence-Based Complementary and Alternative Medicine
Volume 2023, Article ID 1266778, 5 pages
https://doi.org/10.1155/2023/1266778

Research Article

Clinical Study of 3DCRT Combined with SBRT in the Treatment of Patients with EGFR Mutation Oligometastatic Non-Small Cell Lung Cancer

Deng Wang,[1] Yingbang Wan,[1] and Lihua Wang[2]

[1]*Ezhou Central Hospital (Respiratory and Critical Care Unit), Ezhou, Hubei 436000, China*
[2]*Department of Respiratory Endology, People's Hospital of Dongxihu District, Wuhan, Hubei 430040, China*

Correspondence should be addressed to Lihua Wang; 201904217238@stu.zjsru.edu.cn

Received 30 June 2022; Revised 27 July 2022; Accepted 8 August 2022; Published 16 February 2023

Academic Editor: Shuli Yang

Background. Lung cancer is one of the malignant tumors with the highest morbidity and mortality in my country and the world. Among them, non-small-cell lung cancer (NSCLC) accounts for about 80%. For patients who are diagnosed with NSCLC and have epidermal growth factor receptor, EGFR gene-sensitive mutations The treatment is particularly important. *Aims*. To investigate the efficacy and prognosis of 3DCRT combined with local SBRT in patients with EGFR mutation oligometastatic NSCLC. *Materials and Methods*. Eighty patients with EGFR mutation oligometastatic NSCLC were selected by random remainder grouping method. 3DCRT combined with SBRT is effective and safer in patients with EGFR-mutant oligometastatic NSCLC, and significantly improves the patient's immune and tumor marker levels. It has a certain reference value in the clinical treatment of EGFR-mutant oligometastatic NSCLC.

1. Introduction

Lung cancer is the malignant tumor that causes the most deaths in the world. Most patients are already in stages III to IV when they see a doctor and cannot be removed by radical surgery [1]. For locally advanced nonresectable NSCLC, the main treatment currently recommended is still a combination of chemotherapy and radiotherapy. In particular, radiotherapy plays an extremely important role in the treatment of these patients [2]. Patients with peripheral locally advanced lung cancer, in addition to the primary lung tumors, are also accompanied by mediastinal lymph node metastasis. Therefore, the scope of radiotherapy covers mostly the primary lung and the area of mediastinal lymph node metastasis. The irradiation area is often larger. Great [3]. When formulating a radiotherapy plan, it is necessary to consider that normal organs are not exposed to excessively high doses, but also to ensure that the tumor receives a radical dose, which is a major problem in clinical practice [4]. Due to its special dosimetry advantages, the high dose of the irradiated target area, and the low dose of surrounding normal tissues, SBRT's status as a radical treatment in patients with early lung cancer has been confirmed by many studies, and it is recommended for the early stage of intolerable surgery. Patients with lung cancer [5].

Based on this, our department has explored the effect of 3DCRT combined with local SBRT consolidation therapy on the efficacy and prognosis of EGFR-mutant oligometastatic NSCLC. The current research results are reported as follows.

2. Material and Methods

2.1. Exclusion Criteria. Inclusion criteria were as follows: (i) diagnostic criteria for EGFR mutation oligometastatic NSCLC [6]; (ii) pathological diagnosis of NSCLC and positive EGFR driver gene mutation. The Eastern Cooperative Oncology Group (ECOG) score [7]: 0–2, acquired drug resistance after first and second-generation EGFR-TKI treatment and expected survival time ≥3 months; local treatments (such as surgical resection,

radiotherapy, microwave ablation, radiofrequency ablation, seed implantation, argon, and helium knife) were received for the progressive lesions. The T790M gene mutation test result was negative before local treatment, and it reappeared after local treatment. The disease progresses and the treatment plan is changed.

Exclusion criteria were as follows: (i) patients whose EGFR-TKI resistance and the original EGFR-TKI combined with local treatment cannot be evaluated by imaging, and who have a recurrence of recurring cancer (except intraepithelial carcinoma) within 5 years; (ii) there are three types of patients, namely, pregnancy, ineffective contraception, and lactation.

2.2. Nursing Intervention Methods. The control group was given 3DCRT, namely.

2.2.1. Radiotherapy Positioning. Lie on your back, put your arms around your elbows in front of your forehead, with the phantom fixed. After wearing the phantom, a C-enhanced scan was performed, with a thickness of 5 mm, and the scan range was from the hyoid bone to the lower pole of the kidney. SBRT is positioned three days before the end of 3DCRT, and the position is the same as that of 3DCRT. Lie on your back, put your arms around your elbows in front of your forehead, with the phantom fixed. CT scanning method: after the phantom is put on, an enhanced CT scan is performed, with a thickness of 5 mm, and the scanning range is from the hyoid bone to the lower pole of the kidney.

2.2.2. Delineation of Tumor Target Areas and Organs at Risk. The target area of 3DCRT is delineated, GTV, and lung lesions are delineated when the chest CT window width is 1600HU and the window level is −600HU, and the mediastinal lesions are delineated when the chest CT window width is 400HU and the window level is 20HU. CTV, pulmonary lesions are GTV externally placed 6–8 mm; mediastinal lesions are the areas where metastatic lymph nodes are located, such as 4R area metastasis including the entire 4R area, or mediastinal lesions GTV externally placed 5 mm. PTV is CTV externally placed respiratory movement + positioning The error and respiratory movement are measured by the patient under a simulated positioning machine. The positioning error varies from 5 to 7 mm in each direction. The target area of SBRT is delineated, the lesion seen in the lung window by GTV, and the PTV is 0.5 cm of GTV. The delineation of organs at risk, including the spinal cord, normal lung tissue, trachea, esophagus, heart, and important nerves (such as the brachial plexus).

2.2.3. Formulation of Radiotherapy Plan. 3DCRT plan 3–5 field technology, requires a 95% isodose curve to surround 95% of PV, the divided dose is 2 Gy/time, 5 times/week, the total dose of 46–50 Gy, requires both lungs V20 < 25%, V30 < 18%, MLD < 18 Gy, and maximum spinal cord dose ≤40 Gy.

The treatment group implemented 3DCRT combined with SBRT, that is., the patient lies supine on a carbon fiber positioning bed, with both hands elbows lifted on top of the head, the position adopts a vacuum negative pressure bag fixing device, and the three-dimensional laser light determines the coordinates of the reference point and marks it on the skin. The marking point should be as close as possible to lesions. First, observe the movement trajectory of the tumor in the fluoroscopy mode of the simulated machine, and then in the state of free breathing, spiral-enhanced CT scans continuously with a layer spacing of 3mm. The scan range is from the entrance of the thorax to the bottom of the lung, including the whole lung and the lesion up and down 10–15 cm. The scan is completed then the data is transferred to the Philips Pinnacle9 treatment planning system workstation. After a senior physician with more than 7 years of radiotherapy experience performs the delineation and three-dimensional reconstruction of the target area and important organs, a physicist with more than 3 years of work experience sets up the field and makes a radiotherapy plan. Refer to the chest CT or PET-CT results before radiotherapy, and according to the definition requirements of ICRU No. 50 and No. 62 reports, the tumor lesions can be seen as gross tumor areas (GTV) in the treatment planning system according to the lung window imaging standards, and the GTV is expanded by 5mm to form a clinical target area (CTV), the planned target volume (PTV) is determined according to the range of tumor movement with breathing under fluoroscopy, positioning error, and the dose relationship of adjacent lesions. Generally, the PTV is formed by 3–5 mm of CTV. The target area was delineated in the Pinnacles9 radiotherapy planning system, using linear accelerator 6MV-X-rays with 6–12 coplanar fields and isocentric irradiation. The treatment plan was PTV45–60 Gy, divided by 5–10 times, and the bioequivalent dose (BED) was 70.5–120.0 Gy, once a day, 5 times a week. Use the dose volume histogram and isodose line chart of the treatment planning system to comprehensively evaluate all plans. The prescribed dose is required to meet more than 95% PV, and the 90% isodose line completely covers the target area. All planned dose limits for major blood vessels, large air ducts, ribs, spinal cord, chest wall, and other organs at risk refer to the United States Radio Oncology Cooperative Group (RTOG) No. 0236 agreement. Incoming the X-ray simulator control system to reset the patient, observe whether the irradiation field range meets the requirements of the treatment plan under fluoroscopy, otherwise reposition, and make a plan. If the plan is satisfactory, then perform calibration on the simulated CT to measure whether the distance from the tumor center to the front, back, left, and right body surfaces is consistent with the treatment plan system. When the reset and alignment are satisfied, the accelerator will be verified, and the electronic field imaging device will be verified at 0 degrees and 90 degrees, respectively. Radiotherapy is performed when the image matching error does not exceed 1mm, and the clinical requirements are fully met. Each treatment strict reset and position verification were carried out according to the above requirements before.

Table 1: Comparison of general information between the two groups [n, ($\overline{x}$, $\pm$ s)].

Group	Gender (male/female)	Average age (age)	Tumor diameter (cm)	Pathological type		
				Squamous cell carcinoma	Adenocarcinoma	Squamous adenocarcinoma
Control group (40)	28/12	36.63 ± 8.32	13.31 ± 1.67	10	22	8
Treatment group (40)	29/11	36.62 ± 8.31	13.33 ± 1.25	11	23	6
χ^2/t	0.061	0.007	0.074	0.065	0.051	0.346
P	0.805	0.995	0.941	0.799	0.822	0.556

2.3. Observation Indicators. Beckman CytoFLEX flow cytometer detects CD4+, CD3+, and CD4+/CD8+. The curative effect judgment standard is based on the solid tumor curative effect evaluation standard RECIST to evaluate the short-term curative effect: the total diameter of the measurable target lesions increased by 20% and exceeded the minimum total observed (beyond the baseline, if the total decrease was not observed during treatment), and the minimum absolute value increased by 5 mm. Disease control rate (DCR) = (CR + PR + SD) the number of cases/total number of cases × 100%.

3. Results

3.1. Comparison of General Information. The general data of the two groups of patients, such as gender, average age, tumor diameter, and pathological type were not significantly different by *t*-test and chi-square test ($P > 0.05$). See Table 1.

4. Discussion

The dose of radiation therapy for locally advanced NSCLC is still being explored. As early as 40 years ago, Dr. Fletcher proposed that in radiotherapy, a dose of 50 Gy is required to eliminate subclinical lesions, a radiation dose of 60 Gy is required to eliminate small lesions visible on the image, and a radiation dose of 75 Gy is required to eliminate a 3 cm tumor. Larger tumors require 80 to 90 Gy of radiation therapy dose. Some retrospective and nonrandomized prospective research data also indicate that the higher the dose, the better the treatment effect. When treating NSCLC, increasing the dose may lead to a longer survival time. Therefore, how can we ensure that normal tissues are not affected by comparison? Under the premise of high-dose irradiation, increasing the dose of the tumor area as much as possible and improving the local control rate have become the main goals of radiotherapy for locally advanced NSCLC [8]. In clinical practice, many scholars have studied the application of SBRT in lung cancer. For NSCLC who cannot or are unwilling to undergo surgery due to medical diseases, compared with conventional radiotherapy, the local control rate of SBRT is significantly higher than that of conventional radiotherapy [9]. In the application of lung cancer, compared with conventional radiotherapy, SBRT is significantly higher than conventional radiotherapy in terms of local control rate for NSCLC who are unable or unwilling to undergo surgery due to medical diseases. It is for the above reasons that this study, aimed at patients with peripheral locally advanced NSCLC, first irradiated peripheral lung lesions and mediastinal lymph node area with 46–60 Gy using 3DCRT technology, and then repositioned, using SBRT radiotherapy for lung lesions to further increase the dose so that the equivalent biological dose of the tumor reaches 72 Gy–86 Gy, while the radiation dose to the lungs is significantly reduced [10].

In this study, two cases were selected for the comparison of the whole CRT plan and the 3DCRT + SBRT plan. It was found that the 3DCRT + SBRT irradiation method was used under the premise that the primary tumor received a radical dose (equivalent biological dose BED) of 66 Gy~72 Gy. The V20, V30, and MLD of both lungs are lower than that of 3DCRT, which means that the probability of severe radiation pneumonia is reduced. Research reports in recent years have shown that radiation-induced lung injury is a dose-limiting factor for lung radiotherapy [11]. Under the premise of ensuring that the dangerous organs are not excessive, the BED of the primary tumor using the 3DCRT + SBRT irradiation mode is higher, which can reach 72Cy. In some cases with small lung lesions in this group, when the volume of B00ST is less than $50cm^3$, the lung BED of this lesion can reach about 80 Gy [12]. The following results we finally observed: (1) The use of 3DCRT + SBRT radiotherapy has fewer radiotherapy-related adverse reactions. Only one patient developed grade III acute radiation pneumonia. The cause was considered to be related to the induction of upper respiratory tract infection in the late stage of radiotherapy. In other patients, no serious radiation pneumonia was found, and no serious esophagus, heart, and tracheal reactions were found during radiotherapy [13]. (2) The local control rate is high. The local control rate within one year is 95.7%. The patients with recurrence in the field are due to excessive mediastinal lymph nodes. The dose of 3DCRT cannot control the mediastinal lymph nodes well, and because the BED of lung lesions is higher, no local recurrence was found [14].

Of course, there are still some shortcomings in this study. SBRT can only be applied to peripheral NSCLC. Due to the influence of normal organs such as heart, large blood vessels, and trachea, it is difficult to operate the peripheral tumor of mediastinal lymph nodes. The therapeutic dose can only be given by 3DCRT. Due to the presence of dangerous organs such as the spinal cord, the dose of mediastinal lymph nodes can only be given at a dose of about 60 Gy. Therefore, a small number of patients have the recurrent laryngeal nerve and superior vena cava compression due to mediastinal lymph node recurrence, and serious later symptoms affect the quality of life. Therefore, it is necessary to study a more reasonable dose of 3DCRT combined with SBRT for the control of mediastinal lesions.

5. Conclusion

In summary, 3DCRT combined with SBRT for patients with EGFR-mutant oligometastatic NSCLC has a better curative effect and is safer, and significantly improves the patient's immune and tumor marker levels.

Data Availability

The experimental data used to support the findings of this study are available from the corresponding author upon request.

Additional Points

The implementation of a whole process informationized health management model combined with cardiac rehabilitation intervention for elderly patients with coronary

heart disease after PCI can improve the quality of life and exercise endurance, and at the same time improve the patient's self-care ability. Design and peer review process.

Conflicts of Interest

The authors declare that they have no conflicts of interest.

Authors' Contributions

All the authors have seen and approved the manuscript.

Acknowledgments

This work was supported by Guangzhou Municipal Health and Technology Project (20191A011036).

References

[1] S. S. Lee and Y. K. Cheah, "The interplay between MicroRNAs and cellular components of tumour microenvironment (TME) on non-small-cell lung cancer (NSCLC) progression," *Journal of Immunology Research*, vol. 2019, Article ID 3046379, 13 pages, 2019.

[2] E. N. Imyanitov, A. G. Iyevleva, and E. V. Levchenko, "Molecular testing and targeted therapy for non-small cell lung cancer: current status and perspectives," *Critical Reviews in Oncology*, vol. 157, Article ID 103194, 2021.

[3] Y. K. Chae, S. Chang, T. Ko et al., "Epithelial-mesenchymal transition (EMT) signature is inversely associated with T-cell infiltration in non-small cell lung cancer (NSCLC)," *Scientific Reports*, vol. 8, no. 1, p. 2918, 2018.

[4] X. Xie, W. Zhang, and H. Wang, "Dynamic adaptive residual network for liver CT image segmentation," *Computers & Electrical Engineering*, vol. 91, 2021.

[5] K. L. Zeng, C. L. Tseng, H. Soliman, Y. Weiss, A. Sahgal, and S. Myrehaug, "Stereotactic body radiotherapy (SBRT) for oligometastatic spine metastases: an overview," *Frontiers Oncology*, vol. 9, p. 337, 2019.

[6] Chinese Medical Association, "Chinese medical association Oncology branch, Chinese medical association journal press. Chinese medical association lung cancer clinical diagnosis and treatment guidelines (2018 edition)," *Chinese Journal of Oncology*, vol. 40, no. 12, pp. 935–964, 2018.

[7] E. Boran, G. Ramantani, N. Krayenbühl et al., "High-density ECoG improves the detection of high frequency oscillations that predict seizure outcome," *Clinical Neurophysiology*, vol. 130, no. 10, pp. 1882–1888, 2019.

[8] X. Xie, X. Pan, W. Zhang, and J. An, "A context hierarchical integrated network for medical image segmentation," *Computers & Electrical Engineering*, vol. 101, Article ID 108029, 2022.

[9] V. R. Adorno Febles, S. Blacksburg, J. A. Haas, and D. R. Wise, "Translating the immunobiology of SBRT to novel therapeutic combinations for advanced prostate cancer," *Frontiers Oncology*, vol. 10, p. 830, 2020.

[10] J. Peng, A. K. Lalani, and A. Swaminath, "Cytoreductive stereotactic body radiotherapy (SBRT) and combination SBRT with immune checkpoint inhibitors in metastatic renal cell carcinoma," *Can Urol Assoc J*, vol. 15, no. 8, pp. 281–286, 2021.

[11] N. Besson, V. Pernin, S. Zefkili, and Y. M. Kirova, "Evolution of radiation techniques in the treatment of mediastinal lymphoma: from 3D conformal radiotherapy (3DCRT) to intensity-modulated RT (IMRT) using helical tomotherapy (HT): a single-centre experience and review of the literature," *British Journal of Radiology*, vol. 89, no. 1059, Article ID 20150409, 2016.

[12] S. N. Chen, P. Ramachandran, and P. Deb, "Dosimetric comparative study of 3DCRT, IMRT, VMAT, Ecomp, and Hybrid techniques for breast radiation therapy," *Radiation Oncology Journal*, vol. 38, no. 4, pp. 270–281, 2020.

[13] A. Solanki, S. H. Kombathula, S. Manna et al., "Adjuvant irradiation in carcinoma breast patients: comparison of 3DCRT and semi-automated complex VMAT hypofractionated plans," *Gulf Journal of Oncology*, vol. 1, no. 34, pp. 58–64, 2020.

[14] E. C. Fields, R. Rabinovitch, N. E. Ryan, M. Miften, and D. C. Westerly, "A detailed evaluation of TomoDirect 3DCRT planning for whole-breast radiation therapy," *Medical Dosimetry*, vol. 38, no. 4, pp. 401–406, 2013.

Hindawi
Evidence-Based Complementary and Alternative Medicine
Volume 2023, Article ID 7530725, 5 pages
https://doi.org/10.1155/2023/7530725

Research Article

Esculentoside A Inhibits Proliferation, Colony Formation, Migration, and Invasion of Human Colorectal Cancer Cells

Maha Abdullah Momenah,[1] Layla Awad Almutairi,[1] Haifa Ali Alqhtani,[1] Fatimah A. Al-Saeed,[2] Khalid M. Al Syaad,[3,4] Sadeq K. Alhag,[5] Mohammed A. Al-qahtani,[2] Zaki Hussain Hakami,[6] Jewel Mallick,[7] and Ahmed Ezzat Ahmed[8,9,10]

[1]*Department of Biology, College of Science, Princess Nourah bint Abdulrahman University, P.O. Box 84428, Riyadh 11671, Saudi Arabia*
[2]*Department of Biology, College of Science, King Khalid University, Abha 61413, Saudi Arabia*
[3]*Biology Department, Faculty of Science, King Khalid University, P.O. Box 9004, Abha 61413, Saudi Arabia*
[4]*Director of the Research Center, Faculty of Science, King Khalid University, P.O. Box 9004, Abha 61413, Saudi Arabia*
[5]*Biology Department, College of Science and Arts, King Khalid University, Muhayl Asser, Saudi Arabia*
[6]*Department of Medical Laboratory Technology, Faculty of Applied Medical Sciences, Jazan University, Jazan, Saudi Arabia*
[7]*Department of Pharmacy, BGC Trust University Bangladesh, Chittagong 4381, Bangladesh*
[8]*Department of Biology, College of Science, King Khalid University, P.O. Box 9004, Abha 61413, Saudi Arabia*
[9]*Prince Sultan Bin-Abdul-Aziz Center for Environment and Tourism Studies and Researches, King Khalid University, P.O. Box 960, Abha 61421, Saudi Arabia*
[10]*Department of Theriogenology, Faculty of Veterinary Medicine, South Valley University, Qena 83523, Egypt*

Correspondence should be addressed to Jewel Mallick; jewel@bgctub.ac.bd

Received 12 July 2022; Revised 10 August 2022; Accepted 16 August 2022; Published 10 February 2023

Academic Editor: Shuli Yang

Esculentosides include a group of plant-derived compounds with tremendous pharmacological potential. The antiproliferative effects of esculentoside A against different colorectal cancer cells were evaluated. We found that the proliferation of all the colorectal cancer cells was halted by esculentoside A. The IC_{50} of esculentoside A ranged from 16 to 24 μM against different colorectal cancer cells. Investigation of the underlying molecular mechanism revealed that esculentoside A caused an increase in the colorectal cancer cells at the G1 phase of the cell cycle, indicative of G0/G1 cell cycle arrest. The percentage of G1 cells increased from 22.68% in control to 54.23% at 16 μM esculentoside A. We also found that the colony formation of HT-29 cells was inhibited by 59% at 24 μM esculentoside A. Finally, effects of esculentoside A on the motility of HT-29 colorectal cancer cells were investigated, and it was found that esculentoside A caused a significant decline in HT-29 colorectal cancer cell migration and invasion. The migration and invasion of esculentoside A-treated HT-29 cells were 45% and 51% higher, respectively, than those of untreated cells. Summing up, these results suggest that esculentoside A exhibits antiproliferative effects against human colorectal cancer cells.

1. Introduction

Esculentosides constitute a large and diverse group of oleanene-type saponins with a wide array of pharmacological properties [1]. They are generally isolated from plant species belonging to the family *Phytolaccaceae*. Plant species such as *Phytolacca esculenta* and *Phytolacca americana* are important sources of esculentosides [2, 3]. They have been shown to have diverse bioactivities, which include antimicrobial, anti-inflammatory, and anticancer properties, to name a few

[1–3]. Esculentoside A is an important saponin that has been shown to suppress the growth of several cancer types. Liu et al. showed that esculentoside A halts the growth of human breast cancer cells by inducing apoptotic cell death [4]. They showed that esculentoside A exhibits this property *b* by blocking the IL-6/STAT3 signaling [4]. However, esculentoside A has been evaluated for its anticancer properties against human colorectal cancer cells (CCC). Annually, colorectal cancer has been reported to cause around 0.8 million deaths and is currently one of the most predominant cancer types in both men and women [5]. It has been predicted that the burden of colon cancer will keep on increasing if there is no development in early detection and if no effective interventions for advanced staged colorectal cancer are made [6]. At present, routine colonoscopy and subsequent surgical resection of the tumors are the primary innervational options available for colorectal cancer patients. The chemotherapeutic drugs have many side effects, and the disease often relapses, making it very difficult to manage [7]. Accordingly, research efforts are being put into detecting the disease at an early stage and developing potential chemotherapeutic agents for the management of colorectal cancer. Herein, we evaluated the growth inhibitory effects of esculentoside A against human colorectal cancer cells. It was revealed that esculentoside A halted the growth of cancer cells and inhibited their colony formation and metastasis. We believe that this investigation will play an important role in establishing esculentoside A as a lead molecule for colorectal cancer.

2. Materials and Methods

2.1. Cell Lines and Culturing. CCC lines (HCT-116, HT-29, and SW620) were bought from ATCC and cultured in DMEM with 10% fetal bovine serum, 1% streptomycin/penicillin at 37°C, with 5% CO_2.

2.2. Cell Viability Assay. Cell counting kit-8 assay was used to evaluate the viability of colorectal cancer cells (HCT-116, HT-29, and SW620). At the density of cells (2×10^4 cells per well), the cells were put in 96-well plates and administered with varied dosages of esculentoside A. Subsequently, 10 μL CCK-8 solution was supplemented to the cells, which were then incubated for 1 h at 37°C. After this, the optical density was determined at 450 nm using an ELISA plate reader.

2.3. Colony Formation Assay. In the case of the colony-forming assay, the culturing of HT-29 cells was done.

10 mL of culturing medium with 5000 cells per dish. Then, culturing of the cells was done for 2 weeks. After the colonies became visible, they fixed them using crystal violet for 15 min and photographed them.

2.4. Cell Cycle Analysis. HT-29 cells were subjected to fixation with 70% ethanol at 4°C for 12 h. Afterwards, a 100 μL suspension was treated with 50 μg propidium iodide (PI) at 4°C for 35 min. Lastly, cell cycle phase distribution was estimated by using a flow cytometer. 15,000 cells/sample were taken and analysed by BD FACSuite software version 1.0.

2.5. Transwell Assay. Migration and invasion of cells were estimated using Transwell chambers (BD Biosciences) with either Matrigel coating or without it for cell invasion and migration, respectively. HT-29 cells were put into the upper chambers. Nonetheless, lower chambers were filled with 10% FBS-containing medium. Cells were then incubated for 24 h and passed via membranes that were stained with 0.1% crystal violet (Sangon Biotech).

2.6. Statistical Analysis. Experimental procedures were done in triplicate. Data are presented as mean ± standard deviation (SD). For statistical analysis, Student's *t*-test with $P < 0.05$ was used.

3. Results

3.1. Esculentoside A Inhibits Proliferation of Colorectal Cancer Cells. Effects of esculentoside A (Figure 1(a)) on the proliferation of HT-29, HCT-116, and SW620 cell lines by the CCK-8 assay showed that esculentoside A triggered growth inhibitory effects on all three colorectal cancer cell lines (Figure 1(b)). These growth inhibitory effects of esculentoside A were found to be dose-dependent. The IC_{50} of esculentoside A ranged between 16 and 24 μM. The lowest IC_{50} of 16 μM was observed against the HT-29 cell line. As a result, this cell line was used for next experiments.

3.2. Esculentoside A Induces Cell Cycle Arrest of Colorectal Cancer Cells. Effects of Esculentoside A were assessed on HT-29 cells' distribution in phases of the cell cycle. We found that the esculentoside A of HT-29 cells triggered their accumulation at the G1 phase of the cell cycle. The percentage of the G1 phase cells was enhanced from 22.68% to 54.23% at 16 μM dosage of esculentoside A (Figure 2). These findings are indicative of G0/G1 cell cycle arrest.

3.3. Esculentoside A Inhibits Colony Formation of Colorectal Cancer Cells. The effects of esculentoside on the colony forming property of HT-29 cells were also examined. HT-29 cells were administrated with different dosages of esculentoside A and subsequently incubated at 37°C for 14 days. We found that esculentoside A diminished the colony forming property of HT-29 cells. At 16 μM esculentoside A concentration, the colony formation was inhibited by 59% compared to the untreated HT-29 cells (Figure 3).

3.4. Esculentoside A Inhibits Migration and Invasion of Colorectal Cancer Cells. Effects of esculentoside A on HT-29 cells migration and invasion were evaluated by the transwell assay. The results showed that the migration and invasion of esculentoside A-treated HT-29 cells were diminished in a dose-dependent manner. The migration and invasion of esculentoside A-treated HT-29 cells were 45% and 51% higher, respectively, than those of untreated cells (Figures 4(a) and 4(b)).

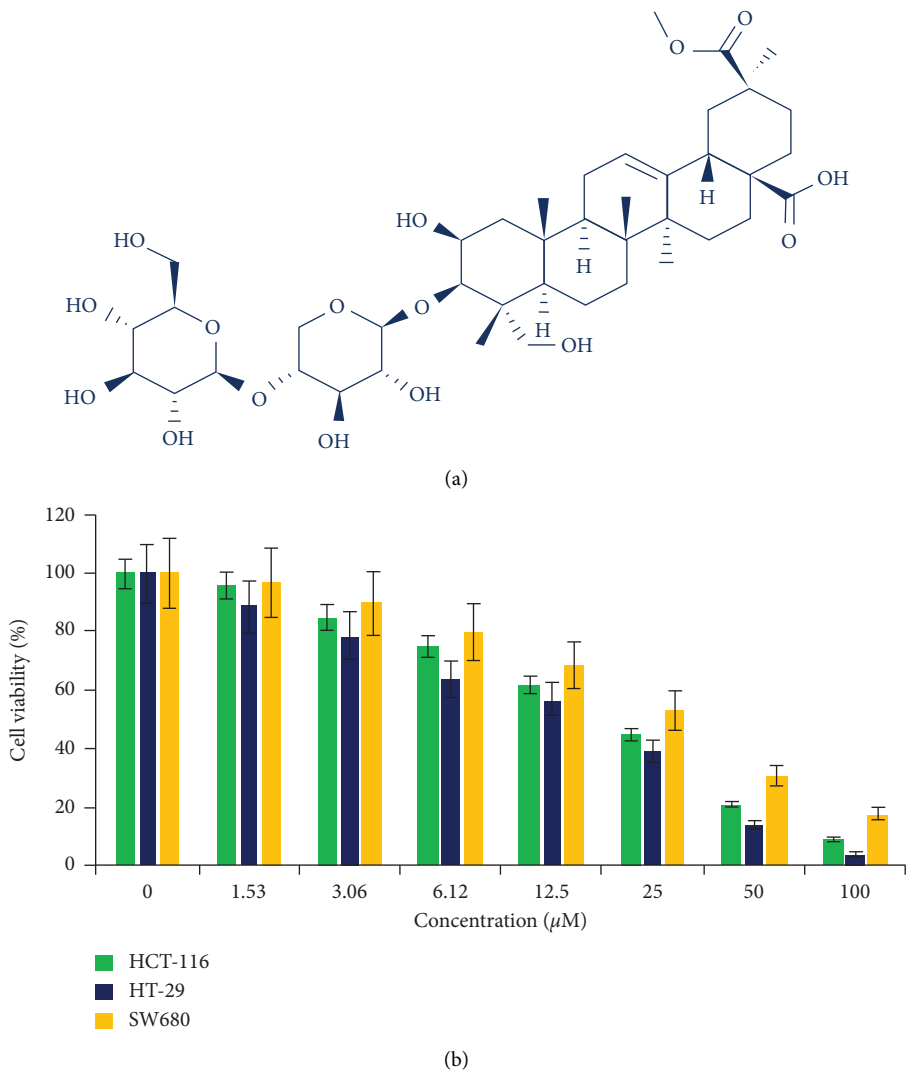

Figure 1: Esculentoside A exerts antiproliferative effects on colorectal cancer cells. (a) Esculentoside A structure. (b) Effect of esculentoside A on the viability of colorectal cancer cells. Experiments were done in triplicate.

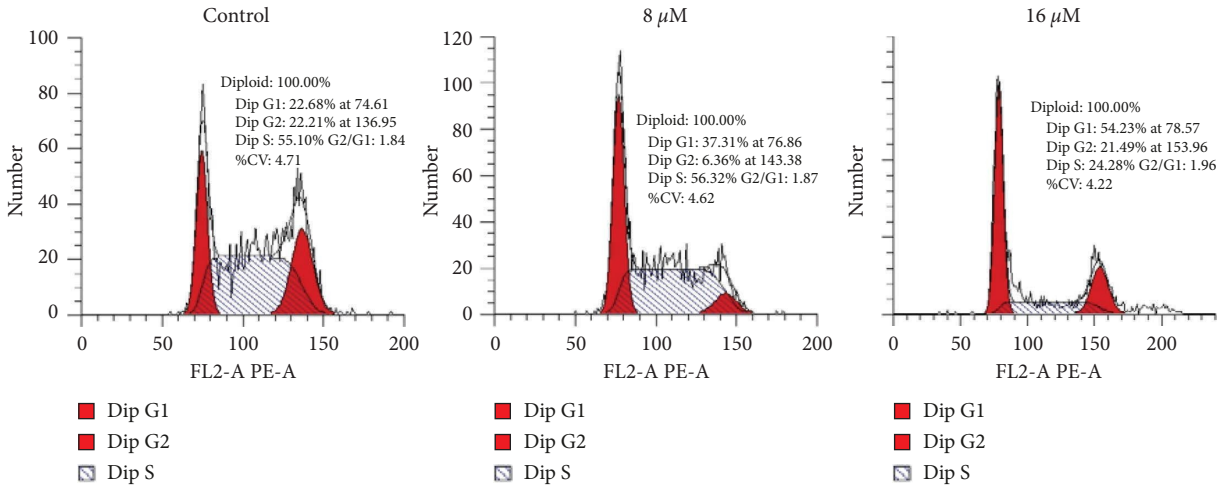

Figure 2: Esculentoside A induces cell arrest of colorectal cancer cells. Flow cytometry showing HT-29 cells distribution at various phases of cell cycle. The experiments were carried out in triplicate.

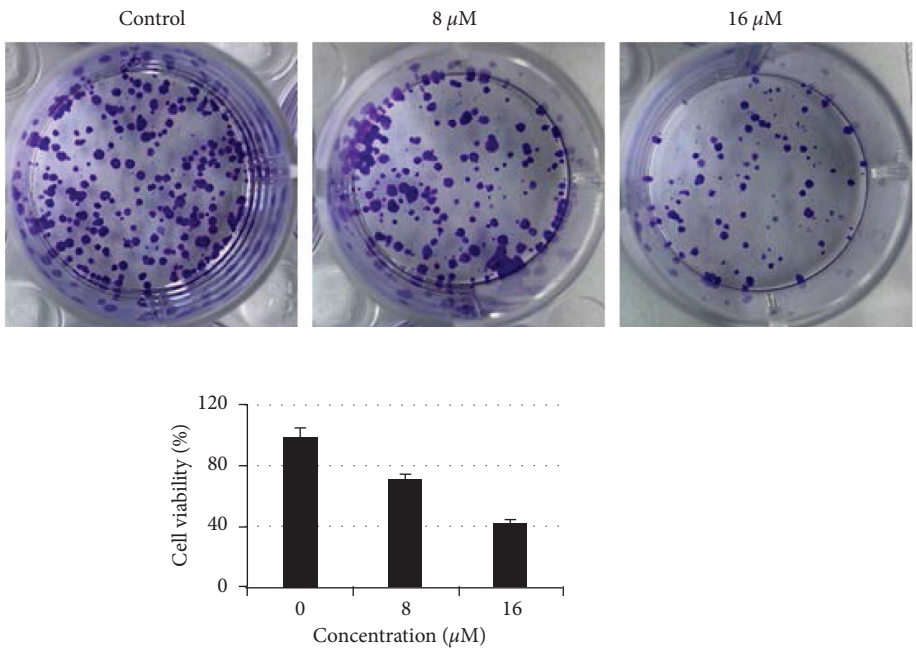

Figure 3: Esculentoside A inhibits formation of colorectal cancer cell colonies. Colony formation assay showing the effect of various concentrations of esculentoside A on the colony formation potential of HT-29 cells. Experiments were repeated thrice.

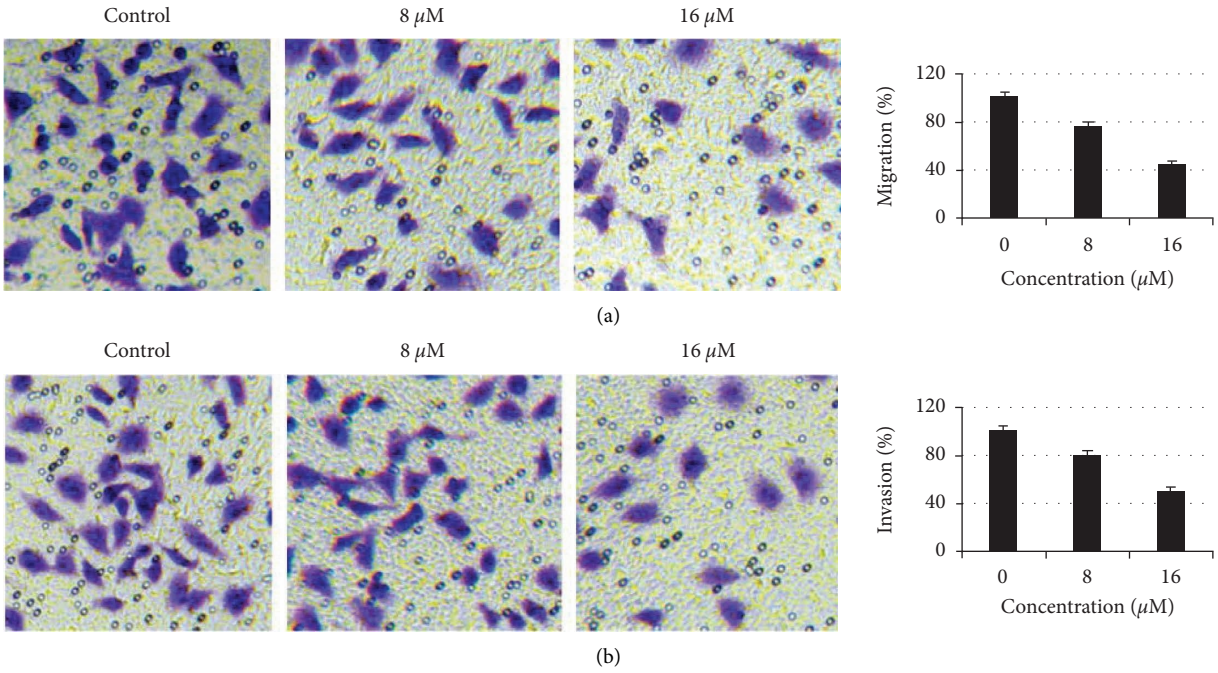

Figure 4: Esculentoside A inhibits colorectal cancer cell migration and invasion. The transwell assay showing the effect of different doses of esculentoside A on (a) migration and (b) invasion of HT-29 cells. Experiments were performed in triplicate.

4. Discussion

Colorectal cancer is a devastating disease, causing a huge number of human mortalities across the world every year [8]. A lot of research efforts are put in from different corners of the world to decrease the incidence of colorectal cancer. However, due to the lack of reliable procedures for early detection and efficient chemotherapeutic agents without adverse effects, the management of colorectal cancer has become a mammoth task [9]. Researchers are looking for anticancer drugs from plant sources, as many previously used anticancer drugs have also come from plants [10]. Many plants are edible by nature, and it is believed that anticancer agents from such plants may prove to be nontoxic

and safe [11–13]. In this study, a plant-derived saponin, esculentoside A, was evaluated for its antiproliferative effect against human colorectal cancer cells. Esculentoside A suppressed the growth of all the colorectal cancer cells. Liu et al. showed that esculentoside A targets the IL-6/STAT3 cascade to halt the growth of breast cancer cells [4]. Many related compounds, such as esculentoside H, have been shown to block the NF-kB signaling cascade and suppress CCC proliferation. Cell cycle analysis showed that esculentoside A arrests the cells at the G0/G1 phase [14]. Several saponins have previously been shown to induce cell cycle arrest; for example, Pennogenyl saponins triggered cell cycle arrest in hepatocellular carcinoma cells [15]. Previously, migration and invasion of colon cancer cells were inhibited by esculentoside H [14]. In this study, the effects of esculentoside A on the migration and invasion of colorectal cancer cells were evaluated. Interestingly, the migration and invasion of colorectal cancer cells were blocked by esculentoside A treatment, indicative of its antimetastatic potential [16–18].

5. Conclusion

Esculentosides are plant-derived compounds that have tremendous pharmacological applications. The present investigation showed that esculentoside was able to suppress the proliferation and colony formation of colorectal cancer cells via G0/G1 cell cycle arrest. Furthermore, esculentoside A also reduced the movement and invasion of human colorectal cancer cells. Therefore, esculentoside A may prove to be a potential lead molecule for colorectal cancer chemotherapy. However, in vivo studies are required for further confirmation.

Data Availability

All data used to support the findings of this study are included within the article.

Conflicts of Interest

The authors declare that they have no conflicts of interest.

Acknowledgments

\This research was supported by Princess Nourah bint Abdulrahman University Researchers Supporting Project number (PNURSP2023R224), Princess Nourah bint Abdulrahman University, Riyadh, Saudi Arabia.

References

[1] C. Bailly and G. Vergoten, "Esculentosides: insights into the potential health benefits, mechanisms of action and molecular targets," *Phytomedicine*, vol. 79, Article ID 153343, 2020.

[2] H. Yu, L. Gong, X. Wang et al., "Rabbit conjunctivae edema and release of NO, TNF-α, and IL-1β from macrophages induced by fractions and esculentosides isolated from Phytolacca americana," *Pharmaceutical Biology*, vol. 54, no. 1, pp. 98–104, 2016.

[3] W. Gong, Z. Jiang, P. Sun et al., "Synthesis of novel derivatives of esculentoside A and its aglycone phytolaccagenin, and evaluation of their haemolytic activity and inhibition of lipopolysaccharide induced nitric oxide production," *Chemistry and Biodiversity*, vol. 8, no. 10, pp. 1833–1852, 2011.

[4] C. Liu, L. Dong, Z. Sun et al., "Esculentoside A suppresses breast cancer stem cell growth through stemness attenuation and apoptosis induction by blocking IL 6/STAT3 signaling pathway," *Phytotherapy Research*, vol. 32, no. 11, pp. 2299–2311, 2018.

[5] R. L. Siegel, K. D. Miller, A. Goding Sauer et al., "Colorectal cancer statistics, 2020," *CA: A Cancer Journal for Clinicians*, vol. 70, no. 3, pp. 145–164, 2020.

[6] N. Hafez and S. Gettinger, "Oligometastatic disease and local therapies: a medical oncology perspective," *The Cancer Journal*, vol. 26, no. 2, pp. 144–148, 2020.

[7] J. Y. Douillard, S. Siena, J. Cassidy et al., "Final results from PRIME: randomized phase III study of panitumumab with FOLFOX4 for first-line treatment of metastatic colorectal cancer," *Annals of Oncology*, vol. 25, no. 7, pp. 1346–1355, 2014.

[8] M. M. Center, A. Jemal, R. A. Smith, and E. Ward, "Worldwide variations in colorectal cancer," *CA: A Cancer Journal for Clinicians*, vol. 59, no. 6, pp. 366–378, 2009.

[9] E. R. Fearon, "Molecular genetics of colorectal cancer," *Annual Review of Pathology: Mechanisms of Disease*, vol. 6, no. 1, pp. 479–507, 2011.

[10] J. M. Pezzuto, "Plant-derived anticancer agents," *Biochemical Pharmacology*, vol. 53, no. 2, pp. 121–133, 1997.

[11] J. Iqbal, B. A. Abbasi, T. Mahmood et al., "Plant-derived anticancer agents: a green anticancer approach," *Asian Pacific Journal of Tropical Biomedicine*, vol. 7, no. 12, pp. 1129–1150, 2017.

[12] G. M. Cragg and D. J. Newman, "Plants as a source of anticancer agents," *Journal of Ethnopharmacology*, vol. 100, no. 1-2, pp. 72–79, 2005.

[13] U. Shah, R. Shah, S. Acharya, and N. Acharya, "Novel anticancer agents from plant sources," *Chinese Journal of Natural Medicines*, vol. 11, no. 1, pp. 16–23, 2014.

[14] S. H. Ha, K. M. Kwon, J. Y. Park et al., "Esculentoside H inhibits colon cancer cell migration and growth through suppression of MMP 9 gene expression via NF kB signaling pathway," *Journal of Cellular Biochemistry*, vol. 120, no. 6, pp. 9810–9819, 2019.

[15] F. Y. Long, Y. S. Chen, L. Zhang et al., "Pennogenyl saponins induce cell cycle arrest and apoptosis in human hepatocellular carcinoma HepG2 cells," *Journal of Ethnopharmacology*, vol. 162, pp. 112–120, 2015.

[16] S. Mitra, M. S. Lami, A. Ghosh et al., "Hormonal therapy for gynecological cancers: how far has science progressed toward clinical applications?" *Cancers*, vol. 14, no. 3, p. 759, 2022.

[17] M. M. Rahman, F. Islam, S. Afsana Mim et al., "Multifunctional therapeutic approach of nanomedicines against inflammation in cancer and aging," *Journal of Nanomaterials*, vol. 2022, Article ID 4217529, 19 pages, 2022.

[18] M. R. Islam, F. Islam, M. H. Nafady et al., "Natural small molecules in breast cancer treatment: understandings from a therapeutic viewpoint," *Molecules*, vol. 27, no. 7, p. 2165, 2022.

Hindawi
Evidence-Based Complementary and Alternative Medicine
Volume 2023, Article ID 4025734, 10 pages
https://doi.org/10.1155/2023/4025734

Research Article

Garlic Extract Participates in the Proliferation and Apoptosis of Nonsmall Cell Lung Cancer Cells Via Endoplasmic Reticulum Stress Pathway

Deguang Pan,[1] **Mingjun Zheng**,[2] **Jin Liu**,[3] **Ze Sun**,[1] **and Xiulian Shi**[4]

[1]*Department of Cardiothoracic Surgery, Chun'an County People's Hospital, Hangzhou, Zhejiang, China*
[2]*Department of Orthopedics, Chun'an County People's Hospital, Hangzhou, Zhejiang, China*
[3]*Department of Emergency, Chun'an County People's Hospital, Hangzhou, Zhejiang, China*
[4]*Department of Medical Education, Chun'an County People's Hospital, Hangzhou, Zhejiang, China*

Correspondence should be addressed to Xiulian Shi; shixiulian2021@163.com

Received 12 August 2022; Revised 19 September 2022; Accepted 24 November 2022; Published 6 February 2023

Academic Editor: Shuli Yang

Objective. To investigate the effect of garlic extract (GE) on the proliferation and apoptosis of cell lines A549 and H1299 in lung cancer (LC). *Methods*. A549 and H1299 cells with well-developed logarithmic growth were added with GE at a concentration of 0 μg/ml, 25 μg/ml, 50 μg/M, 75 μg/ml, and 100 μg/ml, respectively. The inhibition of A549 cell proliferation was detected using CCK-8 after cultured for 24 h, 48 h, and 72 h. The apoptosis of A549 cells was analyzed via flow cytometry (FCM) after 24 h of cultivation. In vitro migration of A549 and H1299 cells was determined by cell wound scratch assay after 0 h and 24 h culture. The caspase-3 and caspase-9 protein expression levels in A549 and H1299 cells were evaluated through western blot after 24 h of cultivation. *Results*. Colony formation and EdU assays revealed that Z-ajoene could inhibit cell viability and cell proliferation in NSCLC cells. After 24 h culture, there was no significant difference in the proliferation rate of A549 and H1299 cells with different GE concentrations ($P > 0.05$). A remarkable proliferation rate difference emerged between A549 and H1299 cells with different GE concentrations after 48 and 72 hours of cultivation. The proliferation rate of A549 and H1299 cells in the experiment group was significantly lower than that in the control group. With an elevated level of GE concentration, the proliferation rate of A549 and H1299 cells decreased ($P < 0.05$) while the apoptotic rate increased continuously. *Conclusion*. GE could exert toxic effects on A549 and H1299 cells, inhibit cell proliferation, promote apoptosis, and attenuate cell migration. Meanwhile, it might induce apoptosis of A549 and H1299 cells through the caspase signal pathway, which is positively correlated with the mass action concentration and is expected to be a new drug for LC treatment.

1. Introduction

Lung cancer remains the most common malignancy and the leading cause of cancer-related death worldwide over the past decades [1], and nonsmall cell lung cancer (NSCLC) accounts for over 80% of all lung cancer diagnoses [2, 3]. Despite the advances in management and diagnostics for NSCLC, the overall survival (OS) of NSCLC patients has not been significantly improved, with the 5-year OS rate of less than 20% [4–6]. Drug resistances, undesirable side effects of chemotherapy, and high metastatic rates are significant obstacles to successful treatment of NSCLC [7] as well as insufficient efforts in disease prevention and early diagnosis and integrated therapies for early remission, though enormous, which does not support a reduced survival rate [8]. It is still imperative to develop more effective drugs and more sensitive diagnostics for timely prevention and intervention to improve NSCLC survival.

ER is the main site for protein synthesis and folding in cells, and is responsible for other basic cellular activities, including intracellular protein maturation and translocation [9]. ER stress (ERS) is initiated when ER homeostasis disturbance results in unfolded/misfolded protein accumulation in the ER lumen. In this process, ERS triggers a series of

accommodative mechanisms, known as the unfolded protein response (UPR), including attenuation of translation, elevated expressions of ER chaperones and associated proteins, and degradation of unfolded/misfolded proteins by a quality-control system [10]. However, once the restoration of ER function fails, apoptotic signalings will be induced by ERS [11, 12].

Garlic (*Allium sativum* L., *Amaryllidaceae*) is one of the oldest known spices and a widely used flavoring agent that has been well utilized to treat numerous ailments over thousands of years and is also considered one of the most powerful chemopreventive and anticancer foods (20). Potential therapeutic properties, such as antithrombotic [13], lipid-lowering [14], anti-oxidative [15], and anti-hypercholesterolemia activities [16], have been studied. In the present study, we reported the effects of Z-ajoene (Z-4, 5, 9-trithiadodeca- 1, 6, 11-triene 9-oxide) (Figure 1(a)) found in crushed garlic on NSCLC cell behaviors and ERS. The anti-inflammatory [17], anti-oxidant, [18], and antifatty liver activities of ajoene, a mixture of E– and Z-isomers, have been previously reported [19–21].

2. Materials and Methods

2.1. Ajoene Extract and Z-Ajoene from Garlic. Garlic (2 kg) was bought in the Korean retail market, divided into three parts, put into three different plastic buckets, and soaked in different concentrations of alcohol solution to extract the corresponding ingredients. Next, after incubating at room temperature for 1 hour, it was extracted with ethyl acetate (at 60°C for 8 hours). The ethyl acetate extract was evaporated in vacuo to make ajoene extract for *in vitro* experiments. The observed content of Z-ajoene determined by high-performance liquid chromatography (HPLC) was 11.1% (w/w), which was subsequently isolated and purified by repeated column chromatography. As described previously, z-ajoene extract with a purity greater than 98% was obtained [22].

2.2. Cell Culture, Treatment, and Transfection. Human NSCLC A549 and H1299 cell lines were obtained from the American Type Culture Collection (ATCC, Manassas, VA, USA). The cells were cultured in RPMI-1640 medium supplemented with 10% FBS in a humidified environment after resuscitation, and the medium was replaced with a fresh medium every other day. The cells were divided into five groups: control, Z-ajoene, Z-ajoene + DLG1-specific shRNA (sh-DLG1), Z-ajoene + YAP-specific shRNA (sh-YAP), and Z-ajoene + sh-DLG1 + sh-YAP. Those in the four treatment groups were incubated with Z-ajoene for 72 h at 37°C. Three treatment groups were transfected with sh-DLG1 and/or sh-YAP using Lipofectamine 3000 reagent (Life Technologies, Carlsbad, CA, USA) to knock down DLG1 and/or YAP. The cells transfected with sh-RNA-NC were used as negative controls (GenePharma, Guangzhou, China). The target sequences for sh-DLG1 and sh-YAP are 5′-AGC GAU GGU CCA UTC UUG CAA-3′ and 5′-GGG UCT UGC AUT UGC ACU ATT-3′, respectively.

2.3. Cell Counting Kit-8 Assay. Cell viability of each group was detected using the CCK-8 assay (Beyotime, Beijing, China). The cells at an appropriate concentration were inoculated in 96-well plates and treated accordingly. CCK-8 solution was added to each well, followed by two h of incubation in the dark. The optical density was measured at 450 nm.

2.4. Colony Formation Assay. Cells (1,000 cells/well) were seeded in a 6-well plate and incubated for two weeks. Clones were fixed with methanol, stained with 0.1% crystal violet for four h at room temperature, and counted under a light microscope (Olympus, Tokyo, Japan).

2.5. 5-Ethynyl-2′-Deoxyuridine (EdU) Assay. Cell proliferation was measured using an EdU assay. A total of 2×10^5 cells were transferred into 24-well plates and allowed to adhere overnight. After transfection, the cells were incubated with 100 μL EdU for two h, fixed with 4% paraformaldehyde for 30 min, and stained using a Cell-LightTM EdU Apollo®488 In Vitro Imaging kit (Guangzhou RiboBio Co., Ltd.) according to the manufacturer's instructions.

2.6. Cell Apoptosis Assay. Flow cytometry was conducted to detect cell apoptosis. The cells (1×10^6 cells/well) were seeded in 6-well plates. They were harvested after 24 h of treatment and stained with an annexin-V fluorescein isothiocyanate (FITC) and propidium iodide (PI) apoptosis detection kit (Invitrogen, USA) to detect cell apoptosis using a FACScalibur flow cytometer (BD Biosciences, CA, USA).

2.7. Quantitative Real-Time PCR. Total RNA from cell samples was extracted using the TRIpure isolation reagent (Invitrogen, USA), and reverse transcription was performed using a PrimeScript RT kit (TaKaRa, Japan). After the master mix was prepared, DLG1 and YAP mRNA expression levels were detected using a real-time PCR assay with SYBR green, normalized to internal control ACTB.

2.8. Western Blot Analysis. Total proteins in tissues or cells were cleaved with RIPA lysate buffer (Beyotime Inc., China), including benzosulfonyl fluoride (Beyotime Inc., China) and protease inhibitor cocktail (Beyotime Inc., China). SDS-PAGE was conducted to isolate 20 mg of protein and transfer it to the PVDF membrane (Millipore Inc., USA, No. sc-27655). The membrane was incubated overnight with the primary antibody monoclonal Bax antibody (1 : 1000, cat. no. YZ-29450 N), monoclonal cleaved caspase three antibodies (1 : 1000, cat. no. YZ-29450 N), monoclonal Cleaved caspase three antibodies (1 : 1000, cat. no. YZ-29450 N), and monoclonal Bcl-2 antibody (1 : 500, cat. no. YZ-12059U) purchased from Santa Cruz Biotechnology, Inc., Dallas, TX, USA, and monoclonal caspase-3 antibody (1 : 500, cat. no. ab19030Z) at four °C, and then incubated with HRP-conjugated secondary antibody (1 : 1000, Santa Cruz Inc., China, No. FLD4894-BK). Anti-GAPDH antibody (1 : 1000,

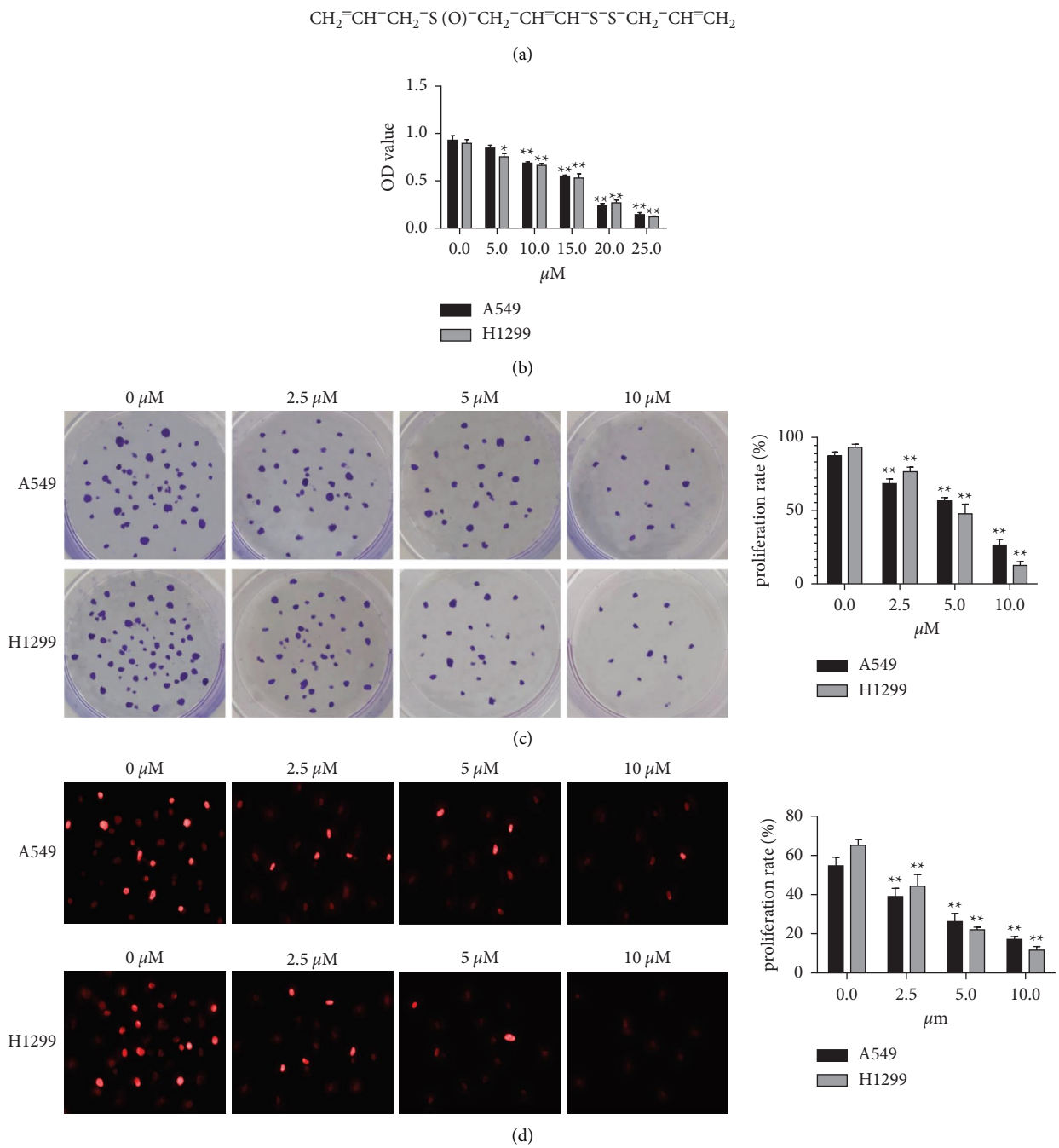

Figure 1: Z-Ajoene inhibits cell viability and cell proliferation in NSCLC cells. (a) Z-ajoene in garlic extracts. (b) A549 and H1299 cells were treated with Z-ajoene for 72 h and subjected to the CCK-8 assay. (c and d) Colony formation and EdU assays revealed suppressed cell proliferation in A549 and H1299 cells.

Santa Cruz Inc., China, No. FLD4546-JM) was performed as an internal control. Prints were measured using the ECL substrate (Beyotime Inc., China).

2.9. Statistical Analysis. All experiments were performed independently, in triplicate. Quantitative variables were presented as the mean ± standard deviation (SD) from three independent experiments. As appropriate, the statistics were performed using the Student's *t*-test or one-way ANOVA in SPSS (version 17.0). A P value of <0.05 was considered statistically significant.

3. Results

3.1. Z-Ajoene Inhibits Cell Viability and Cell Proliferation in NSCLC Cells. We evaluated its cytotoxicity and how it affected behaviors of NSCLC A549 and H1299 cells after 72 h

of Z-ajoene treatment using the CCK-8 assay. A significant dose-dependent (0–25 μM) decrease in cell viability was observed in cells treated with Z-ajoene (Figure 1(b)), together with dose-dependent (0–10 μM) inhibition of cell proliferation in colony formation and cell proliferation (Figures 1(c) and 1(d)).

3.2. Z-Ajoene Stimulates ERS in NSCLC Cells. Since Z-ajoene inhibited cell proliferation in NSCLC cells, we assessed whether Z-ajoene was involved in the ER stress pathway in NSCLC cells, and protein expressions of the pathway coSeminars in Interventional Radiologyponents were determined. The results showed pronouncedly increased expressions of binding protein (BiP) and protein kinase R-like endoplasmic reticulum kinase (PERK) after the Z-ajoene treatment (Figure 2(a)), as expected, which prompted us to detect the downstream UPR targets of PERK, activating transcription factor 4 (ATF4) and homologous protein (CHOP). ATF4 and CHOP proteins were significantly elevated with the Z-ajoene treatment compared to the control group. Z-ajoene was also very effective in inducing their expressions at the mRNA levels (Figure 2(b)).

3.3. Z-Ajoene Induces NSCLC Cell Apoptosis. Flow cytometry was performed to explore the effects of Z-ajoene on cell apoptosis in A549 and H1299 cells. Tumor cell apoptosis was markedly enhanced dose-dependently by the Z-ajoene treatment compared to that achieved in the control group (Figure 3(a)). The Western blot of several essential apoptosis-associated proteins showed that expressions of pro-apoptotic Bax, cleaved caspase 3, and cleaved caspase 9 expressions significantly increased in cells treated with Z-ajoene with a low expression of the anti-apoptosis protein Bcl-2dose-dependently (Figure 3(b)).

3.4. Z-Ajoene-Induced NSCLC Cell Apoptosis Is Associated with Enhanced ERS. Z-Ajoene has stimulated apoptosis and ERS in NSCLC cells; however, whether there was a potential relationship between them is worthy of further exploration. We added 4-phenylbutyric acid (4-PBA), an ERS inhibitor, to detect whether apoptosis could be rescued. Compared to the Z-ajoene group, a decrease in cell apoptosis was observed in both A549 and H1299 cells cotreated with Z-ajoene and 4-PBA (Figure 4(a)). Similarly, pro-apoptotic Bax, Cleaved caspase 3, and Cleaved caspase nine expressions markedly decreased, and anti-apoptoticBcl-2 was elevated in the Z-ajoene + 4-PBA group versus Z-ajoene-treated controls (Figure 4(b)).

3.5. Z-Ajoene-Induced NSCLC Cell Apoptosis Is Activated by ERS Via DLG1/YAP Signaling Inhibition. Furthermore, we assessed whether Z-ajoene exerted its pro-apoptotic effect on NSCLC cells via the DLG1/YAP pathway, an essential mediator of ERS. The Western blot assay showed that compared to the control group LATS2 and YAP protein expressions were significantly downregulated, and DLG1 levels upregulated dose-dependently in A549 and H1299 cells treated with Z-ajoene (Figure 5(a)).

A549 and H1299 cells were transfected with sh-DLG1 and/or sh-DLG1 with pcDNA YAP before the Z-ajoene treatment, and DLG1 mRNA expression was sharply downregulated in cells transfected with sh-DLG1, and YAP remarkably upregulated in pcDNA YAP-transfected cells (Figure 5(b)). Figure 5(c) shows that the cells treated with Z-ajoene alone showed the strongest apoptosis. A reduced apoptosis rate was detectable in sh-DLG1-transfected cells, whereas the opposite finding was observed in sh-YAP-transfected cells. In cells co-transfected with sh-DLG1 and sh-YAP, the already inhibited apoptosis by sh-DLG1 was robustly reversed. We delineated that DLG1 knockdown remarkably suppressed Bip, PERK, ATF4, and CHOP expressions after the Z-ajoene treatment compared to negative controls, which were subsequently boosted after cotransfection with sh-YAP (Figure 5(d)).

4. Discussion

NSCLC is the most prevalent lung cancer and the primary cause of cancer-associated mortality worldwide [23, 24]. Some studies have proved the efficiency of existing treatments for nonsmall cell lung cancer, but the survival rate of advanced nonsmall cell lung cancer has not improved, which remains virtually unchanged. Therefore, the identification of novel and effective agents for the management of advanced NSCLC is the priority. In the present study, we found that Z-ajoenedose-dependently inhibited cell viability or cytotoxicity and proliferation in NSCLC cells, showing an anti-proliferative effect against NSCLC.

The endoplasmic reticulum (ER) is an intricate organelle vital for cellular function and survival. When ER activity is hindered, the accumulation of unfolded proteins stimulates the transmembrane sensors to initiate the UPR, ultimately restoring ER homeostasis [25]. When the restoration of ER homeostasis or ERS attenuation fails, the UPR of ER activates signalings towards apoptosis. However, little research has been conducted on the specific mechanism of ER homeostasis recovery and focusing on ERS-mediated apoptosis may create new treatment options for cancer patients [26]. For the involvement of ERS in Z-ajoene-mediated apoptosis, our results revealed strong ERS responses to Z-ajoene treatment in A549 and H1299 cells, together with increased expressions of the ERS pathway components, BiP, PERK, ATF4, and CHOP. This finding demonstrates that the anticancer potential of Z-ajoene is triggered via ERS.

Apoptosis is strictly regulated by many proteins and pathways, of which the Bcl-2 family has a crucial role [27], including pro-apoptotic (Bax, Bim, Bcl-xs, Bak, Bid, Bad, and Bik) and anti-apoptotic (Bcl-2, Bcl-xl, Bcl-w, and A1) subfamilies [28]. Bax-type apoptotic proteins allow small molecules such as ions and cytochrome C to penetrate the

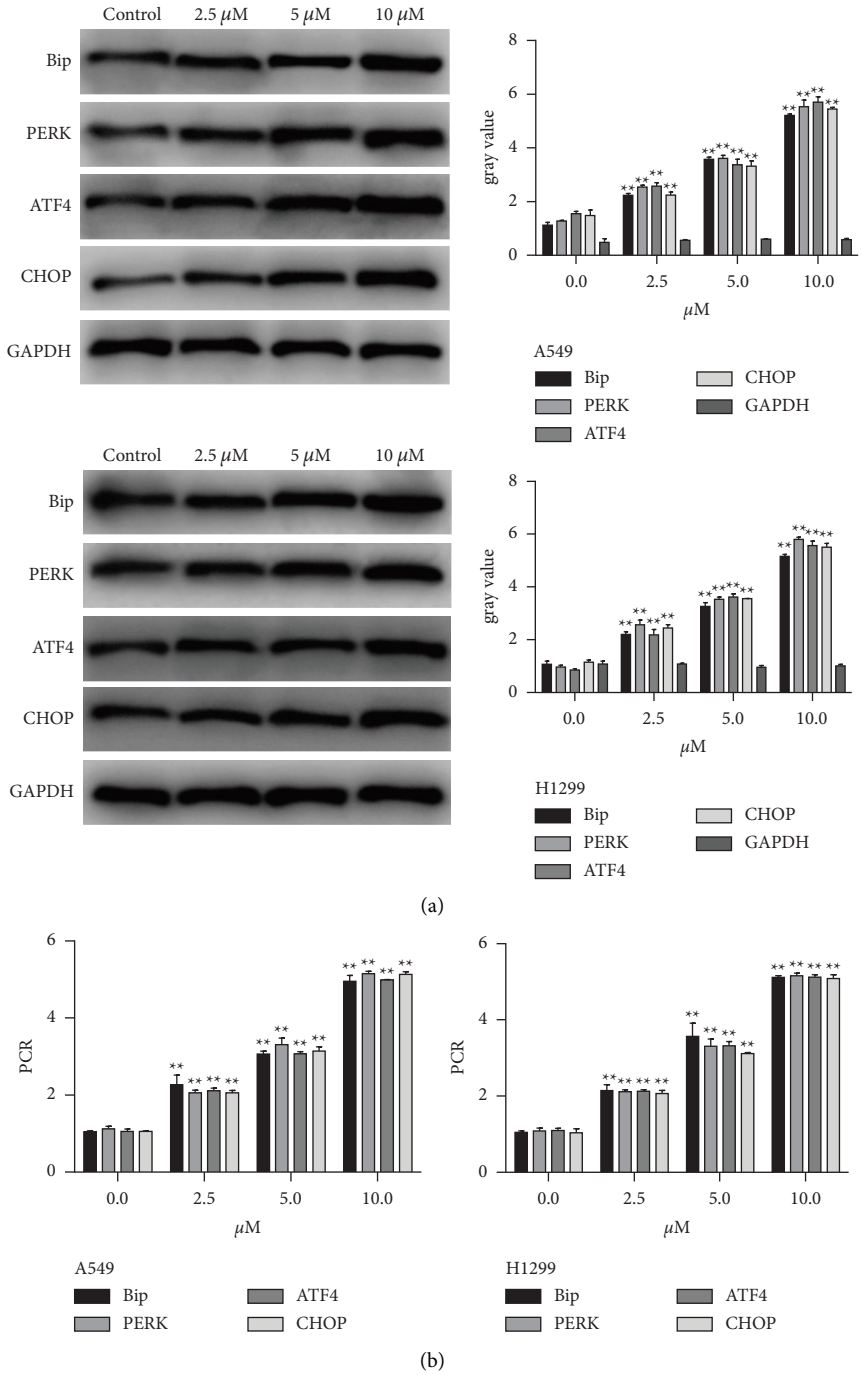

Figure 2: Z-Ajoene increases the expressions of ERR pathway components. (a) Significant increases in Bip, PERK, ATF4, and CHOP protein expressions were detectable in A549 or H1299 cells treated with Z-ajoene. (b) The same Bip, PERK, ATF4, and CHOP mRNA expression patterns were found in Z-ajoene treated cells.

mitochondrial membrane into the cytoplasm, leading to cell apoptosis. In our study, compared to untreated controls, Bax, caspase-3, and caspase-9 protein expressions were dose-dependently upregulated and anti-apoptoticBcl-2 down-regulated with the Z-ajoene treatment, which supports an apoptotic effect of Z-ajoene against NSCLC A549 and H1299 cells.

DLG1 is a crucial component gene of the cell polarity module SCRIB-LGL-DLG. A negative correlation of DLG1 expression with YAP activity, or the inhibitory of DLG1

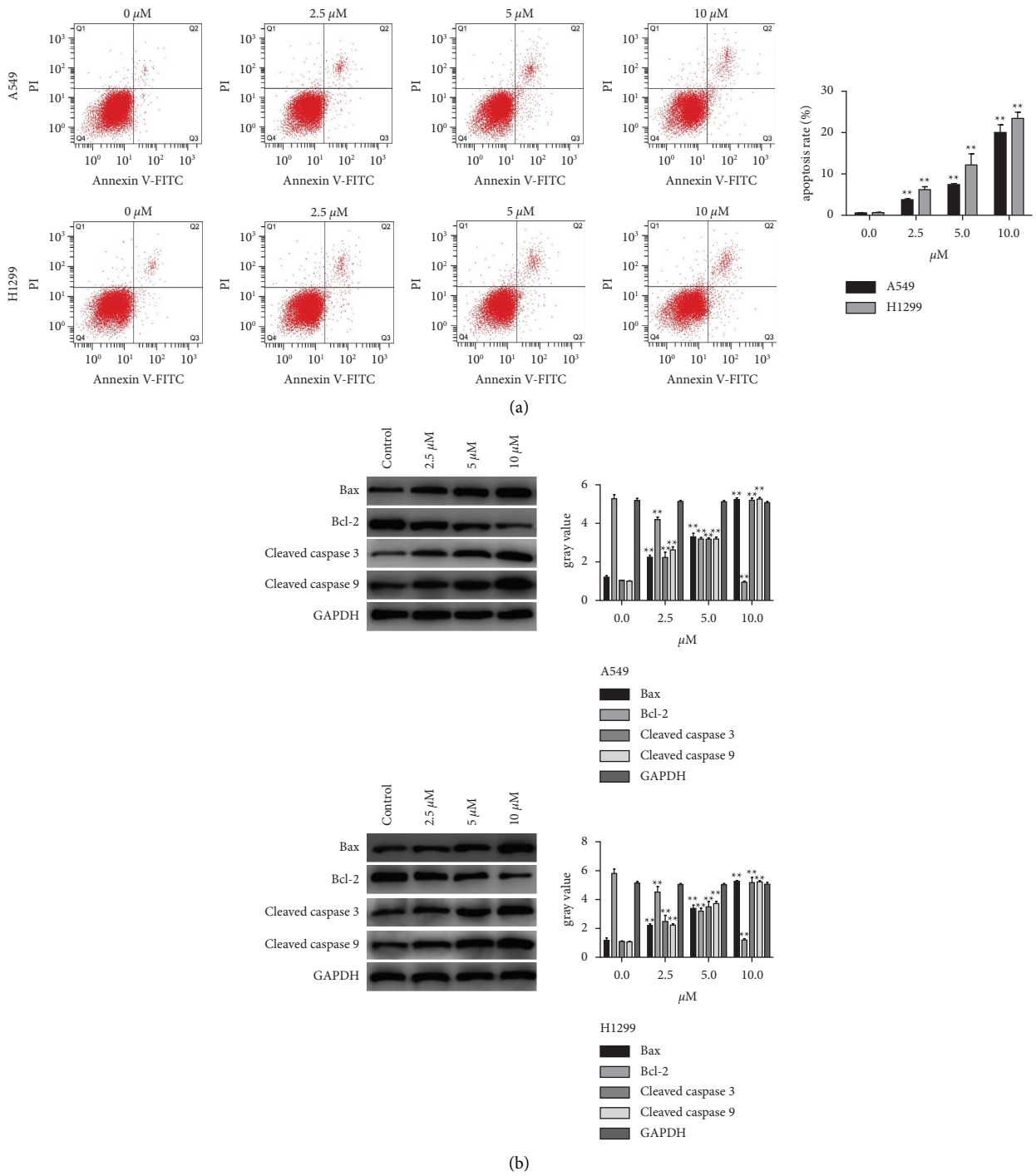

Figure 3: Z-Ajoene induces NSCLC cell apoptosis. (a) Enhanced cell apoptosis was detectable in Z-ajoene-treated cells, as indicated by flow cytometry. (b) Western blot showed increased expressions of pro-apoptotic Bax, cleaved caspase 3, and cleaved caspase 9 and a decreased expression of anti-apoptoticBcl-2 in Z-ajoene-treated cells.

molecule on YAP activity, has been reported [29–31]. The Hippo/YAP signaling pathway plays an important role in cell growth regulation and organ size control during biological growth and development [32]. In the Hippo signaling, the upstream activator of the core effector YAP, LATS1/2, is stimulated by MST1/2-induced phosphorylation to boost YAP phosphorylation. Phosphorylated YAP is maintained in the cytoplasm, ubiquitinated, and degraded to make the downstream pathway of YAP in a static state, thus inhibiting YAP-mediated gene transcription. YAP degradation can be inhibited by oxidative stress, ischemia or hypoxia, physical factors, G protein-coupled receptors, or other signalings to increase YAP activity, allowing activated YAP to bind to TAZ and enter the nucleus to initiate relevant

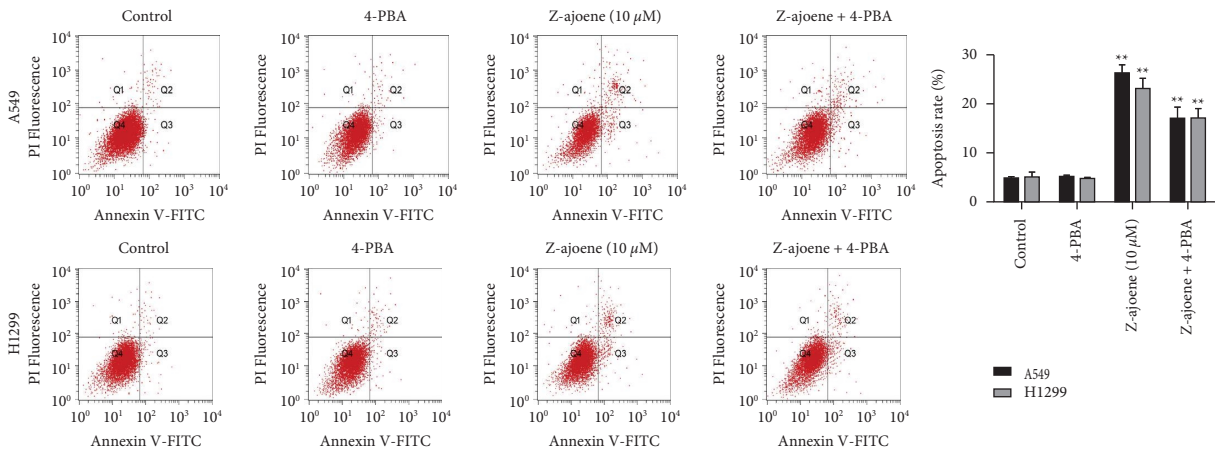

(a)

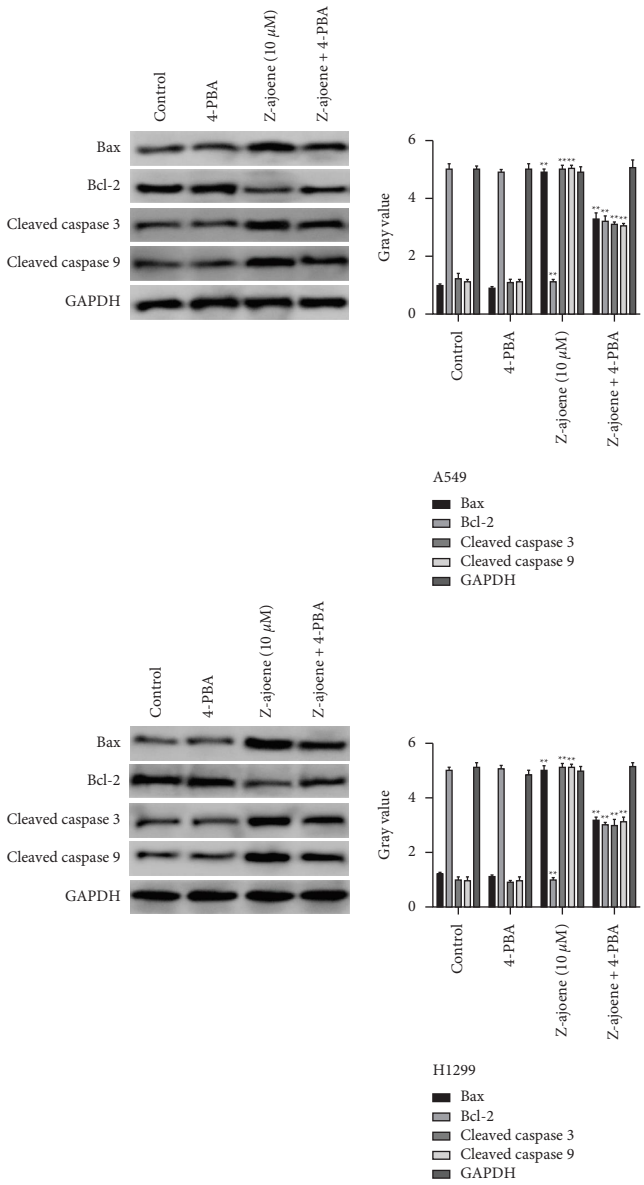

(b)

Figure 4: Z-Ajoene-induced NSCLC cell apoptosis is associated with enhanced ERS. (a) Flow cytometry revealed reduced apoptosis in cells co-treated with Z-ajoene and 4-PBA (an ERS inhibitor). (b) Western blot showed lower Bax, cleaved caspase 3, and cleaved caspase 9 expressions and higher Bcl-2 expression detected in cells cotreated with Z-ajoene and 4-PBA versus Z-ajoene-treated controls.

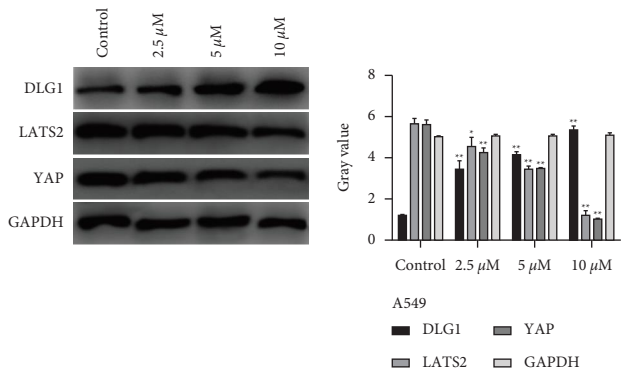
Control
2.5 μM
5 μM
10 μM
DLG1
LATS2
YAP
GAPDH
Gray value
Control 2.5 μM 5 μM 10 μM
A549
DLG1
YAP
LATS2
GAPDH

(a)

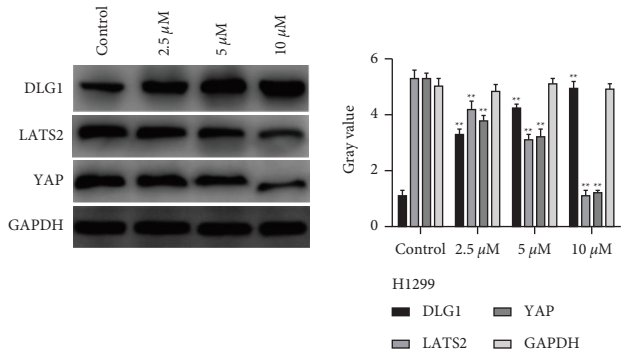
Control
2.5 μM
5 μM
10 μM
DLG1
LATS2
YAP
GAPDH
Gray value
Control 2.5 μM 5 μM 10 μM
H1299
DLG1
YAP
LATS2
GAPDH

(b)

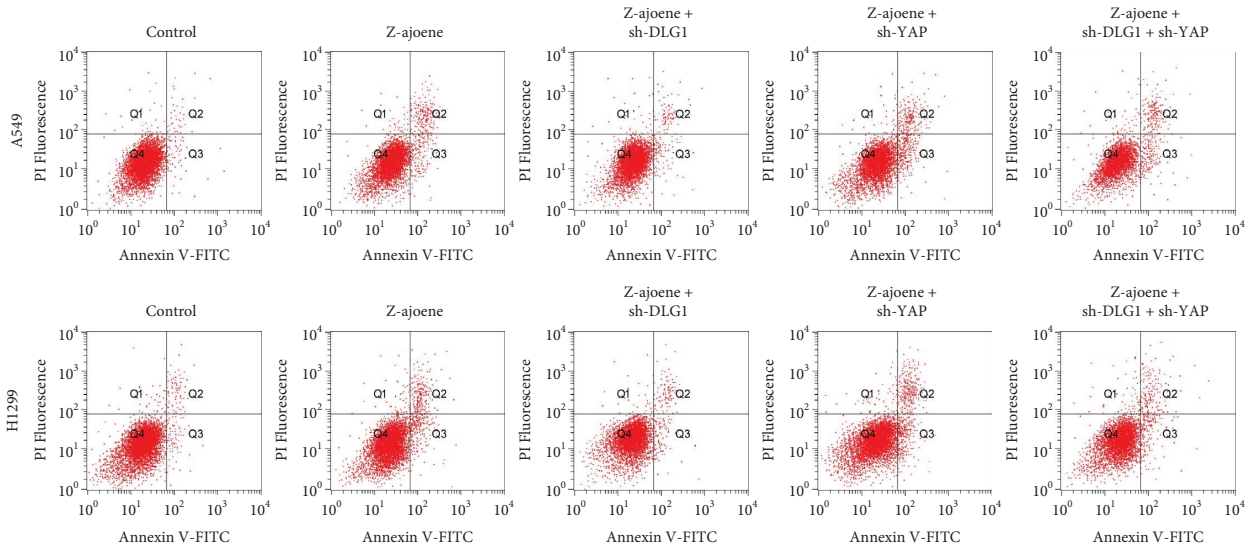
Control
Z-ajoene
Z-ajoene + sh-DLG1
Z-ajoene + sh-YAP
Z-ajoene + sh-DLG1 + sh-YAP
A549
H1299
PI Fluorescence
Annexin V-FITC
Q1
Q2
Q3
Q4

(c)

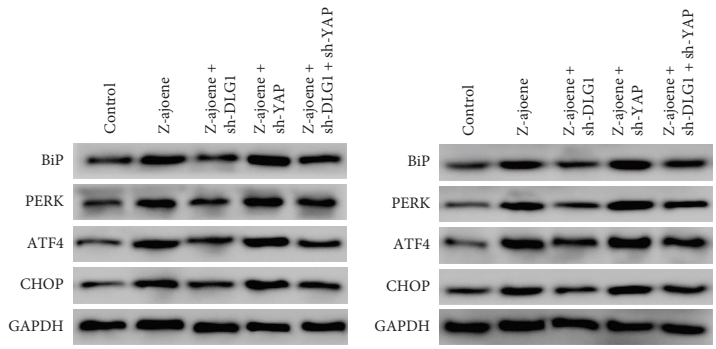

(d)

Figure 5: The pro-apoptotic effect of Z-Ajoene on NSCLC cell apoptosis is activated by ERS via DLG1/YAP signaling inhibition. (a) Western blot revealed DLG1, LATS2, and YAP protein expressions in A549 and H1299 cells treated with Z-ajoene. (b) The RT-qPCR assay revealed DLG1 and YAP mRNA expressions in A549 and H1299 cells. (c) The difference in cell apoptosis between groups was determined by flow cytometry. (d) Differences in Bip, PERK, ATF4, and CHOP protein expressions between groups were detected using the western blot analysis.

gene transcription [33]. Aberrant Hippo/Yap signaling may fuel cell proliferation and antagonize apoptosis for tumor occurrence and growth. In this study, Z-ajoene's regulation on YAP via DLG1 may be the mechanism responsible for its cytotoxic and apoptotic effects on NSCLC cells. Furthermore, our finding of LATS2 and YAP downregulation and DLG1 upregulation in a dose-dependent manner after the Z-ajoene treatment in A549 and H1299 cells is consistent with YAP regulation by DLG1, which was verified by YAP upregulation after DLG1 knockdown, together with a suppressed effect of Z-ajoene. Additional knockdown of the YAP gene reversed the effect of sh-DLG1 transfection into A549 and H1299 cells.

In summary, our study demonstrates that Z-ajoene induces ER stress through DLG1/YAP signal inhibition and promotes apoptosis in NSCLC cells. It is expected to offer more options for developing novel natural monotherapy or combination regimens for NSCLC.

Data Availability

The data used to support the findings of this study are available from the corresponding author upon request.

Conflicts of Interest

The authors declare that they have no conflicts of interest.

References

[1] R. L. Siegel, K. D. Miller, and A. Jemal, "Cancer statistics," *CA: A Cancer Journal for Clinicians*, vol. 68, no. 1, pp. 7–30, 2018.

[2] D. H. Johnson, J. H. Schiller, and P. A. Bunn, "Recent clinical advances in lung cancer management," *Journal of Clinical Oncology*, vol. 32, no. 10, pp. 973–982, 2014.

[3] Y. Kang, Y. L. Jia, Q. L. Wang et al., "<p>Long noncoding RNA KCNQ1OT1 promotes the progression of non-small cell lung cancer via regulating miR-204-5p/ATG3 Axis</p>," *OncoTargets and Therapy*, vol. 12, pp. 10787–10797, 2019.

[4] S. Chheang and K. Brown, "Lung cancer staging: clinical and radiologic perspectives," *Seminars in Interventional Radiology*, vol. 30, no. 02, pp. 99–113, 2013.

[5] Q. L. Tang, M. X. Li, L. Chen, F. Bi, and H. W. Xia, "miR-200b/c targets the expression of RhoE and inhibits the proliferation and invasion of non-small cell lung cancer cells," *International Journal of Oncology*, vol. 53, no. 4, pp. 1732–1742, 2018.

[6] Q. Li, Z. Yang, M. Chen, and Y. Liu, "Downregulation of microRNA-196a enhances the sensitivity of non-small cell lung cancer cells to cisplatin treatment," *International Journal of Molecular Medicine*, vol. 37, no. 4, pp. 1067–1074, 2016.

[7] E. Moravcikova, E. Krepela, V. S. Donnenberg et al., "BOK displays cell death-independent tumor suppressor activity in non-small cell lung carcinoma," *International Journal of Cancer*, vol. 141, no. 10, pp. 2050–2061, 2017.

[8] J. Rotow and T. G. Bivona, "Understanding and targeting resistance mechanisms in NSCLC," *Nature Reviews Cancer*, vol. 17, no. 11, pp. 637–658, 2017.

[9] M. Storm, X. Sheng, Y. J. Arnoldussen, and F. Saatcioglu, "Prostate cancer and the unfolded protein response," *Oncotarget*, vol. 7, no. 33, pp. 54051–54066, 2016.

[10] A. Gupta, D. E. Read, and S. Gupta, "Assays for induction of the unfolded protein response and selective activation of the three major pathways," *Methods in Molecular Biology*, vol. 1292, pp. 19–38, 2015.

[11] N. Hiramatsu, W. C. Chiang, T. D. Kurt, C. J. Sigurdson, and J. H. Lin, "Multiple mechanisms of unfolded protein response-induced cell death," *American Journal Of Pathology*, vol. 185, no. 7, pp. 1800–1808, 2015.

[12] Y. Li, Y. Guo, J. Tang, J. Jiang, and Z. Chen, "New insights into the roles of CHOP-induced apoptosis in ER stress," *Acta Biochimica et Biophysica Sinica*, vol. 47, no. 2, pp. 146-147, 2015.

[13] E. Block, "The chemistry of garlic and onions," *Scientific American*, vol. 252, no. 3, pp. 114–118, 1985.

[14] C. Silagy and A. Neil, "Garlic as a lipid lowering agent-ameta-analysis," *J R Coll Physicians Lond*, vol. 28, no. 1, pp. 39–45, 1994.

[15] C. Borek, "Antioxidant health effects of aged garlic extract," *Journal of Nutrition*, vol. 131, no. 3, pp. 1010–1015, 2001.

[16] H. I. El-Sayyad, A. M. Abou-El-Naga, A. A. Gadallah, and I. H. Bakr, "Protective effects of Allium sativum against defects of hypercholesterolemia on pregnant rats and their offspring," *International Journal of Clinical and Experimental Medicine*, vol. 3, no. 2, pp. 152–163, 2010.

[17] D. Y. Lee, H. Li, H. J. Lim, H. J. Lee, R. Jeon, and J. H. Ryu, "Anti-inflammatory activity of sulfur-containing compounds from garlic," *Journal of Medicinal Food*, vol. 15, no. 11, pp. 992–999, 2012.

[18] H. Y. Kay, J. Won Yang, T. H. Kim et al., "Ajoene, a stable garlic by-product, has an antioxidant effect through Nrf2-mediatedglutamate-cysteine ligase induction in HepG2 cells and primary hepatocytes," *Journal of Nutrition*, vol. 140, no. 7, pp. 1211–1219, 2010.

[19] C. Y. Han, S. H. Ki, Y. W. Kim et al., "Ajoene, a stable garlic by-product, inhibits high fat diet-induced hepatic steatosis and oxidative injury through LKB1-dependent AMPK activation," *Antioxidants and Redox Signaling*, vol. 14, no. 2, pp. 187–202, 2011.

[20] A. Pandrangi, "Cancer chemoprevention by garlic: a review," *Hereditary Genetics*, vol. 4, pp. 1–7, 2015.

[21] K. A. Hwang, Y. J. Hwang, I. G. Hwang, W. Heo, and Y. J. Kim, "Effects of low temperature-aged garlic on exercise performance and fatigue in mice," *Journal of Medicinal Food*, vol. 22, no. 9, pp. 944–951, 2019.

[22] X. Cao, L. Cao, W. C. Zhang, R. Z. Lu, J. S. Bian, and X. W. Nie, "Therapeutic potential of sulfur-containing natural products in inflammatory diseases," *Pharmacology and Therapeutics*, vol. 216, Article ID 107687, 2020.

[23] F. Q. Zhang, D. L. Chen, W. T. Yang, S. Z. Duan, and Y. B. Chen, "Combined effects of XAF1 and TRAIL on the apoptosis of lung adenocarcinoma cells," *Experimental and Therapeutic Medicine*, vol. 17, no. 6, pp. 4663–4669, 2019.

[24] X. H. Zhang and C. Xiao, "Ultrasonic diagnosis combined with targeted ultrasound contrast agent improves diagnostic sensitivity of ultrasonic for non-small cell lung cancer patients," *Experimental and Therapeutic Medicine*, vol. 16, no. 2, pp. 908–916, 2018.

[25] Y. P. Vandewynckel, D. Laukens, A. Geerts et al., "The paradox of the unfolded protein response in cancer," *Anticancer Research*, vol. 33, no. 11, pp. 4683–4694, 2013.

[26] N. L. Maas and J. A. Diehl, "Molecular pathways: the perks and pitfalls of targeting the unfolded protein response in cancer," *Clinical Cancer Research*, vol. 21, no. 4, pp. 675–679, 2015.

[27] S. García, M. Liz, J. J. Gómez-Reino, and C. Conde, "Akt activity protects rheumatoid synovial fibroblasts from Fas-induced apoptosis by inhibition of Bid cleavage," *Arthritis Research and Therapy*, vol. 12, no. 1, p. 33, 2010.

[28] A. Ashkenazi, W. J. Fairbrother, J. D. Leverson, and A. J. Souers, "From basic apoptosis discoveries to advanced selective BCL-2 family inhibitors," *Nature Reviews Drug Discovery*, vol. 16, no. 4, pp. 273–284, 2017.

[29] D. Wu, G. Liu, Y. Liu et al., "Zinc finger protein 191 inhibits hepatocellular carcinoma metastasis through discs large 1-mediatedyes-associated protein inactivation," *Hepatology*, vol. 64, no. 4, pp. 1148–1162, 2016.

[30] C. C. Yang, H. K. Graves, I. M. Moya et al., "Differential regulation of the Hippo pathway by adherens junctions and apical-basal cell polarity modules," *Proceedings of the National Academy of Sciences of the United States of America*, vol. 112, no. 6, pp. 1785–1790, 2015.

[31] M. Zhao, P. Szafranski, C. A. Hall, and S. Goode, "Basolateral junctions utilize warts signaling to control epithelial-mesenchymal transition and proliferation crucial for migration and invasion of Drosophila ovarian epithelial cells," *Genetics*, vol. 178, no. 4, pp. 1947–1971, 2008.

[32] K. F. Harvey, X. Zhang, and D. M. Thomas, "The Hippo pathway and human cancer," *Nature Reviews Cancer*, vol. 13, no. 4, pp. 246–257, 2013.

[33] G. T. K. Boopathy and W. Hong, "Role of hippo pathway-YAP/TAZ signaling in angiogenesis," *Frontiers in Cell and Developmental Biology*, vol. 7, p. 49, 2019.

Hindawi
Evidence-Based Complementary and Alternative Medicine
Volume 2023, Article ID 5885387, 9 pages
https://doi.org/10.1155/2023/5885387

Research Article

RAB11A Promotes Cell Malignant Progression and Tumor Formation of Prostate Cancer via Activating FAK/AKT Signaling Pathway

Weifang Chen[1] and Junjun Wang[2]

[1]*Department of Hematology Oncology, Zhejiang Putuo Hospital, Zhoushan 316100, China*
[2]*Department of Urology, Xiaoshan First Affiliated Hospital of Hangzhou Normal University, Hangzhou 311200, China*

Correspondence should be addressed to Junjun Wang; wjj_198763@126.com

Received 8 August 2022; Revised 25 August 2022; Accepted 24 November 2022; Published 31 January 2023

Academic Editor: Shoib Baba

Background. RAB11A, a member of the GTPase family, acts as a regulator in diverse cancers development. The dysregulation of the FAK/AKT signaling pathway is mainly related to tumorigenesis. This study aimed to investigate the possible effect of RAB11A in prostate cancer and further explore the potential mechanisms. *Results*. In this study, we illustrated the tumor-promoting effects of RAB11A based on *in vivo* and *in vitro* experiments. RAB11A expression was upregulated in prostate cancer cells. RAB11A knockdown decreased the prostate cancer cell proliferation, migration, and invasion. RAB11A also induced the epithelial-mesenchymal transition. PF562271 suppressed the malignant characteristics of prostate cancer cells caused by RAB11A knockdown. Furthermore, the interference of RAB11A reduced the tumor growth and the protein levels of p-FAK/FAK and p-AKT/AKT *in vivo*. *Conclusion*. RAB11A promotes cell malignant progression and tumor formation in prostate cancer via activating FAK/AKT signaling pathway.

1. Introduction

Prostate cancer is one of the most commonly diagnosed cancers in men worldwide, with approximately 191,930 cases and 33,330 deaths each year [1]. The incidence of prostate cancer is related to race and familial inheritance, especially in Africa and the USA [2]. Prostate cancer is usually diagnosed in the elderly (age >65 years) and ranks as the second cancer-related death in men [1]. Malignant transformation in the prostate is a multistage process that is initiated by localized prostate cancer, followed by adenocarcinoma with local invasion, and ends with metastatic prostate cancer [3]. Therapies for prostate cancer are mainly based on the pathologic evaluation of a prostate biopsy [4]. Surgery and radiotherapy are the main therapeutic approaches for early prostate cancer; however, they cannot effectively prevent tumor metastasis. Currently, the understanding of tumorigenesis mechanism of prostate cancer remains limited, which is an obstacle in the development of cancer therapies.

RAB11A is the first identified member of the small GTPase family, playing a crucial role in polarization during collective cell migration [5]. Previous studies found that RAB11A plays a critical role in cancer malignant progression through regulating the growth factor signaling [6, 7]. By activating of WNT signaling, RAB11A enhanced the proliferative capability and motility of esophageal cancer cells [8]. RAB11A is overexpressed in colorectal carcinoma and suppresses the expression of E-cadherin, which induces epithelial-mesenchymal transition (EMT) [9]. Besides, RAB11A is up-regulated in human gastric cancer cells and facilitates the proliferation and invasion of cancer cells through the FAK/AKT pathway [10]. These studies suggest RAB11A as an oncoprotein during cancer progression. However, the potential effects and mechanisms of RAB11A in prostate cancer remain unknown.

The focal adhesion kinase (FAK) signaling pathway is related to cell motility, which positively regulates tumorigenesis and metastasis [11]. FAK is upregulated in multiple cancers, such as gastric and prostate cancers, suggesting the deactivation of FAK signaling might be a possible approach for the treatment of cancer [10, 12]. FAK is an upstream target of ATP-dependent tyrosine kinase (AKT), and AKT acts as a migratory regulator in cancer cells [13]. Meanwhile, the activation of AKT could enhance the migration and invasion capabilities of cancer cells [14, 15]. Previous studies showed the FAK/AKT signaling pathway is activated in prostate cancer [12, 16]. Therefore, the FAK/AKT signaling pathway might be an effective target for cancer treatment, but its role in prostate cancer remains majorly elusive.

Therefore, the aim of the present study was to investigate the potential role of RAB11A in the development of prostate cancer. Meanwhile, the potential mechanism of RAB11A against prostate cancer was explored through *in vitro* and *in vivo* experiments to identify a novel potential target for the treatment of prostate cancer.

2. Materials and Methods

2.1. Cell Culture. A human prostatic epithelial cell line (RWPE1), purchased from the American Type Culture Collection (ATCC, Manassas, USA), was grown in defined keratinocyte serum-free medium (D-KSFM, Gibco, Carlsbad, CA, USA) at 37°C in 5% CO_2 with saturated humidity. Prostate cancer cell lines (PC-3, VCaP, and DU145; ATCC, Manassas, USA) were cultured in minimum essential medium (MEM, Gibco, Carlsbad, CA, USA) with 10% fetal bovine serum (FBS, Gibco) in an incubator (Heracell 150i, Thermo Scientific, Carlsbad, CA, USA) at 37°C in 5% CO_2 and saturated humidity. To prevent the contamination, the penicillin-streptomycin liquid (Solarbio, Beijing, China) was added to the medium.

2.2. Cell Transfection and Treatment. SiRNA targeting RAB11A (si-RAB11A) sequences were designed via the designer of small interfering RNA (DSIR, https://biodev.extra.cea.fr/dsir/dsir.php) (Table S1).

When the confluency of PC-3 cells was up to 70–90%, they were transfected with si-RAB11A, overexpressing (oe)-RAB11A, and empty vector (si-NC and oe-NC) plasmids (40 μL, 1×10^8 TU/mL). After transfection for 48 h, the medium was discarded, and complete medium with 2.5 μg/mL puromycin was added to filter out the stable transfected cell line. The stable transfected cells were conducted for subsequent experiment. To analyze the effect of RAB11A on FAK/AKT signaling pathways, PC-3 cells were pretreated with 0.5 μM PF562271 (a FAK inhibitor) for 24 h before the transfection.

2.3. Animal Model. Animal experimental procedures were approved by the Institutional Animal Care and Use Committee of Xiamen University (XMULAC20220034-1). A total of 10 male BALA/c nude mice, obtained from GemPharmatech Co. Ltd. (Nanjing, China), were cultured for 5-6 weeks, weighed 18–21 g, and were raised under specific nonpathogen conditions at 24–26°C and 40%–60% humidity. Mice were put into two groups at random ($n = 5$ each group): si-NC and si-RAB11A groups. After one week of adaptation, mice were subcutaneously injected with 3×10^6 PC-3 cells transfected with si-NC or si-RAB11A. Ten days after transplantation, tumor sizes were detected every five days, and the volume was calculated: tumor volume (v) = 1/2 × length × (width^2). After 30 days, mice were sacrificed via intraperitoneal injection with 160 mg/kg pentobarbital sodium, and death was considered as the asystole. Tumor tissues in each mouse were collected, weighed, and imaged.

2.4. Reverse Transcription-Quantitative PCR (RT-qPCR) Analysis. Total RNAs were extracted from cells and tumor tissues by Trizol (Invitrogen). cDNA was reversely transcribed using FastKing gDNA Dispelling RT Supermix (TIANGEN, KR118-02) and stored at −20°C. The SYBR Green PCR Master Mix (Lifeint, Guangzhou, China) was used to amplify cDNA in a cycler apparatus of the real-time system (MX3000P, Agilent Stratagene, California, USA). The thermocycling conditions were as follows: 95°C for 3 min, 40 cycles of annealing at 95°C for 12 s, and extension at 62°C for 40 s. The $2^{-\Delta\Delta Ct}$ method was employed to analyze the relative expression of genes. The composition of the RT-qPCR reaction mixture was listed at Table 1. Primer sequences used for RT-qPCR were presented in Table S2.

2.5. Western Blot Analysis. The transfected cell and tumor tissues lysing were accomplished with the radio immunoprecipitation assay buffer (RIPA, Beyotime, Shanghai, China) for total protein extraction. Protein concentration was determined using a bicinchoninic acid assay kit (BCA, Beyotime). Proteins were separated on 10% sodium dodecyl sulfate polyacrylamide gel electrophoresis (SDS-PAGE) by electrophoresis and transferred to polyvinylidene fluoride (PVDF) membrane. The membrane was blocked with 5% fat-free milk at room temperature for 1 h. Then, the membrane was incubated overnight at 4°C with primary antibodies, as listed at Table S3. Membranes were washed with TBST (a buffer combined with Tris buffered saline and Tween, Beyotime; 1 : 10) for 10 min thrice and incubated with secondary antibodies for 1 h. Finally, protein bands were visualized by the ECL reagents (Applygen, Beijing, China) and were quantified by Image J software.

2.6. Cell Counting Kit (CCK)-8 Assay. The cell viability assay was implemented with a CCK-8 assay kit (Beyotime). Briefly, transfected cells were digested by trypsin and then centrifuged at 1,000 g for 5 min to discard the supernatant. The fresh complete medium was used to suspend the cells. After suspension, cells (1×10^5/mL) were seeded into 96-well plates with 40 μL/well and incubated at 37°C with 5% CO_2. After 24 h, each well was added with 10 μL CCK-8 solution and incubated for 2 h. The absorbance value at 450 nm was measured by a microplate reader (DR-3518G, Wuxi Hiwell Diatek, Wuxi, China).

Table 1: The composition of the RT-qPCR reaction mixture.

Components	Volume (μL)
2 × mixture	10 μL
PCR forward primer (10 μM)	1 μL
PCR reverse primer (10 μM)	1 μL
cDNA template	1 μL
ddH_2O	7 μL
Total	Up to 20 μL

2.7. Colony Formation Assay. Cells (200 cells/well) were seeded into 6-well plates and cultured in 2 mL complete medium for 2 weeks. After 2 weeks of cell culture, the medium was discarded, and cells were rinsed with PBS twice. Following the fixation with 1 mL methanol for 15 min, cells were stained with crystal violet. Subsequently, the plate was reversely put on a white paper and then captured for further colony cell number counting by Image J software.

2.8. Wound Healing Assay. The cells in the logarithmic period were digested by trypsin for about 1 min, which was ended by the addition of complete medium. Then, the cells were centrifuged at 1,000 g for 5 min to discard the supernatant, and adjusted density with fresh complete medium. Cells (1×10^8 cells/well) were seeded in 6-well plates with complete medium. After 24 h incubation, cells were scratched with pipette tip, washed with PBS three times, and then put into a chamber at 37°C with 5% CO_2. Cell migration was observed between 0 and 24 h. The cell migration at 0 h was captured as a control for further comparison with the migration condition at 24 h.

2.9. Transwell Invasion Assay. The Transwell chamber was pretreated with 50 μL Matrigel (50 mg/L, dilution: 1 : 4) and incubated at 37°C for 2 h. After digestion by trypsin, cells were washed and resuspended by PBS to a cell density of 1×10^6/mL. The cells were suspended in serum-free medium. Upper and lower chambers of Transwell were added with 200 μL cell suspension and 600 μL medium with 10% FBS, respectively. Following incubation at 37°C with 5% CO_2 for 24 h, the medium was discarded, and cells were fixed with formaldehyde for 30 min. After fixation, cells were stained with 0.1% crystal violet for 20 min, and imaged three random regions under a microscope (SC180, Olympus, Japan).

2.10. Statistical Analysis. Data are presented as mean ± standard deviation. GraphPad Prism 7.0 software (GraphPad software, USA) was employed to analyze all experimental data. A one-way ANOVA was applied to compare data obtained from multiple groups. Statistical significance was regarded as $P < 0.05$.

3. Results

3.1. RAB11A Expression is Upregulated in Prostate Cancer Cells. RAB11A is a crucial regulator in multiple cancers. We first used RT-qPCR and western blot assays to measure the expression level of RAB11A in prostate cancer cells. Results showed both the mRNA and protein expression of RAB11A were remarkably overexpressed in human prostate cancer cell lines (DU145, VCaP, and PC-3) compared with those in normal RWPE1 cells ($P < 0.05$). Notably, the expression level of in PC-3 cells was relatively highest ($P < 0.01$) (Figure 1).

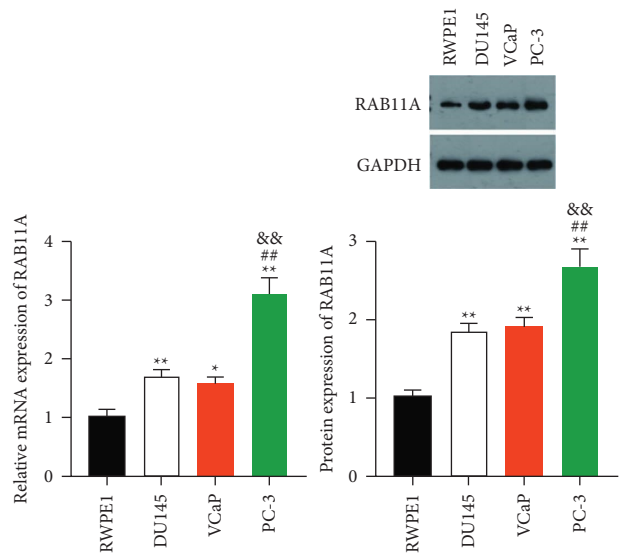

Figure 1: RAB11A expression is up-regulated in prostate cancer cells. The mRNA and protein expression of RAB11A in human prostate cancer cell lines (DU145, VCaP, and PC-3) and normal RWPE1 cell lines were detected by RT-qPCR and western blotting, respectively. $^*P < 0.05$, $^{**}P < 0.01$ vs. RWPE1; ## $P < 0.01$ vs. DU145; && $P < 0.01$ vs. VCaP.

3.2. RAB11A Promotes Prostate Cancer Cell Proliferation. Since RAB11A expression was obviously higher in PC-3 cells relative to normal cells, we examined the effects of RAB11A on PC-3 by transfecting PC-3 cell lines with siRNA-RAB11A (si-RAB11A), overexpress RAB11A (oe-RAB11A), and a negative control (NC). The mRNA and protein levels of RAB11A were reduced by si-RAB11A and enhanced by oe-RAB11A ($P < 0.01$) (Figure 2(a)). CCK-8 and colony formation assays showed that, compared to the NC groups, the interference of RAB11A remarkably reduced the proliferation of PC-3 cells, and RAB11A overexpression enhanced cell proliferation ($P < 0.01$) (Figures 2(b) and 2(c)).

3.3. RAB11A Facilitates the Migration, Invasion, and Epithelial-Mesenchymal Transition (EMT) of Prostate Cancer Cells. Next, we determined the influence of RAB11A on the invasion and migration of cancer cells. Wound healing assay demonstrated the decreased migratory potential of PC-3 cells with RAB11A knockdown and the increased migration with RAB11A overexpression ($P < 0.01$) (Figure 3(a)). Transwell assay suggested that RAB11A overexpression markedly enhanced cell invasion, while RAB11A knockdown presented the opposite effect ($P < 0.01$) (Figure 3(b)). Subsequently, we used western blot assay to detect the levels of E-cadherin, N-cadherin, and vimentin. Results revealed

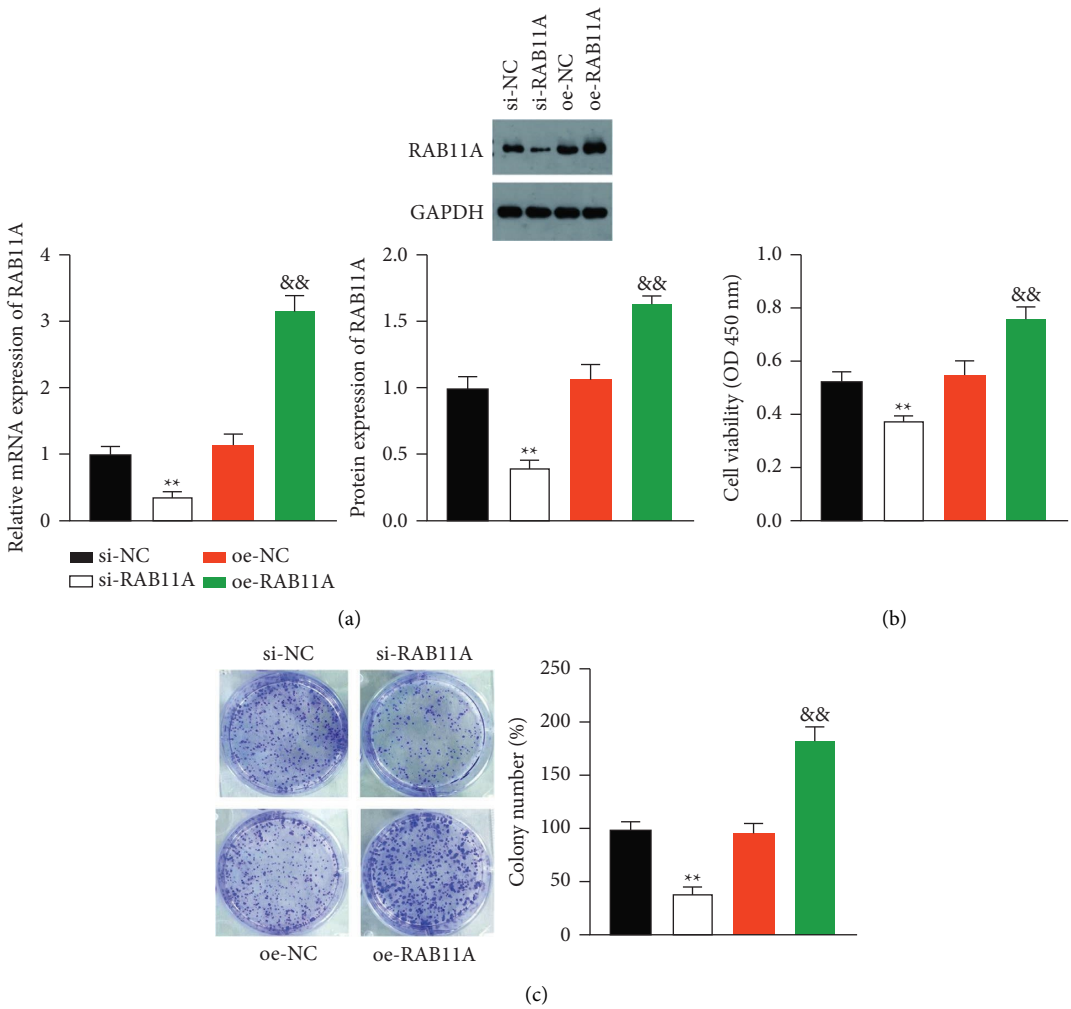

Figure 2: RAB11A promotes prostate cancer cell proliferation. (a) The mRNA and protein levels of RAB11A in PC-3 cells were detected by RT-qPCR and western blotting, respectively. (b) The viability of PC-3 cells was analyzed by the CCK-8 assay. (c) The proliferation of PC-3 cells was examined by a clone formation assay. PC-3 cells were transfected with si-NC, si-RAB11A, oe-NC, or oe-RAB11A. $^{**}P < 0.01$ vs. si-NC; && $P < 0.01$ vs. oe-NC.

that the knockdown of RAB11A, compared with the NC group, enhanced the level of the epithelial marker E-cadherin but suppressed the expression of mesenchymal markers N-cadherin and vimentin; meanwhile, RAB11A overexpression presented opposite effects ($P < 0.01$) (Figure 3(c)).

3.4. RAB11A Promotes Proliferation, Migration, Invasion, and EMT of Prostate Cancer Cells via Activating FAK/AKT Signaling Pathway. Activation of FAK/AKT promotes prostate cancer cell aggression. Thus, we hypothesized that the potential mechanism of RAB11A in prostate cancer might be associated with the FAK/AKT signaling pathway. To verify this, we pretreated PC-3 cells with the FAK inhibitor PF562271 before transfection with si-RAB11A. Results showed that PF562271 did not affect the RAB11A expression level in transfected PC-3 cells (Figures 4(a) and 4(b)). Besides, CCK-8 and clone formation assays demonstrated that PF562271 remarkably reduced the proliferative capability of the PC-3 cells with si-RAB11A ($P < 0.01$) (Figures 4(c) and 4(d)). Meanwhile, wound healing and Transwell experiments revealed that the migration and invasion of PC-3 cells with si-RAB11A were remarkably inhibited by PF562271 addition ($P < 0.01$) (Figures 5(a) and 5(b)). In addition, western blot experiment demonstrated that PF562271 suppressed the expression of N-cadherin and vimentin and increased E-cadherin expression in PC-3 cells transfected with si-RAB11A ($P < 0.01$) (Figure 5(c)). Furthermore, RAB11A knockdown decreased the protein expression of p-FAK/FAK and p-AKT/AKT, and PF562271 addition enhanced the inhibitory effect of si-RAB11A on the FAK/AKT pathway in PC-3 cells ($P < 0.01$) (Figure 5(d)).

3.5. RAB11A Promotes the Tumor Formation of Prostate Cancer via Activating FAK/AKT Signaling In Vivo. To evaluate the effects and mechanism of RAB11A in prostate cancer *in vivo*, a xenograft mouse tumor model was created by transfecting with si-RAB11A. The images of euthanized

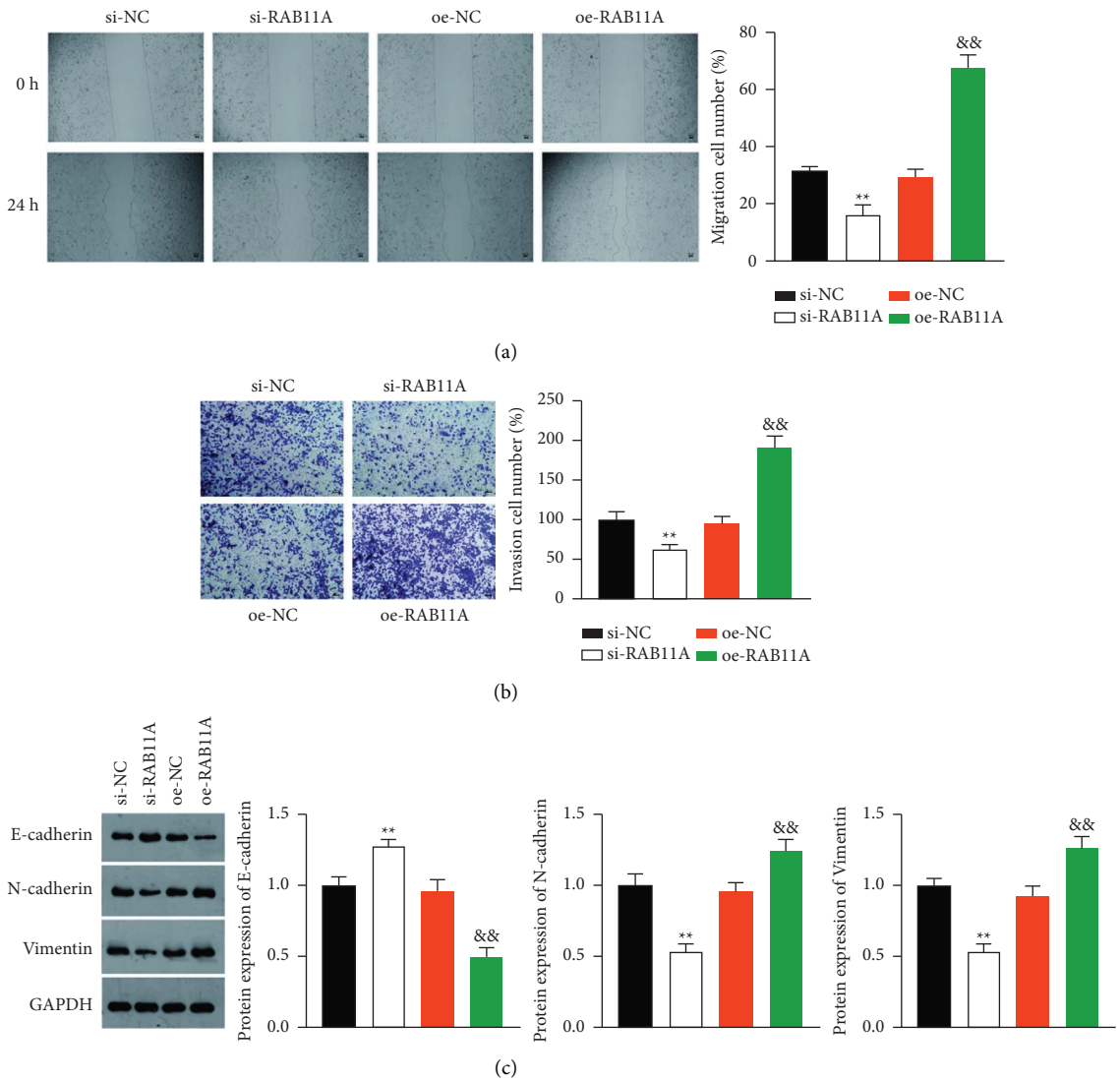

Figure 3: RAB11A promotes the migration and invasion of prostate cancer cells. (a) Cell migration ability was detected by wound healing assay (scale bar = 50 μm); (b) Cell invasion ability was detected by Transwell assay (scale bar = 50 μm); (c) The expressions of E-cadherin, N-cadherin, and vimentin in PC-3 cells were detected by western blot analysis. PC-3 cells were transfected with si-NC, si-RAB11A, oe-NC, or oe-RAB11A. $^{**}P < 0.01$ vs. si-NC; && $P < 0.01$ vs. oe-NC.

mice and the sizes of collected tumors are presented in Figure 6(a), showing the absence of RAB11A reduced tumor sizes. The weight and volume of tumor tissues in the si-RAB11A group were significantly lower than si-NC group ($P < 0.01$) (Figure 6(b)). RT-qPCR showed that RAB11A expression, compared with the si-NC group, was remarkably decreased by si-RAB11A ($P < 0.01$) (Figure 6(c)). On the other hand, the protein levels of FAK, AKT, p-FAK, and p-AKT were detected by western blot assay. Results showed the p-FAK/FAK and p-AKT/AKT protein levels are obviously decreased in si-RAB11A group ($P < 0.01$) (Figure 6(d)).

4. Discussion

Prostate cancer is the secondary diagnosed malignancy in men worldwide, with high mortality. The etiology of prostate cancer remains elusive because of the lacked evidence of genetic and pathology [17]. Previous studies showed there are several signaling pathways were mainly involved in prostate cancer, including MEK/ERK, FAK/AKT, and p75NTR signaling pathway [12, 18, 19]. Risk factors regulating these signaling pathways could be regarded as a potential target in the treatment of prostate cancer. RAB11A is overexpressed in diverse types of human cancers, such as lung and gastric cancer [6, 10]. In this work, we found that the RAB11A is upregulated in prostate cancer cells and promotes the progression of prostate cancer *in vitro* and *in vivo* through activating FAK/AKT signaling.

RAB11A is a major GTPase of vesicular trafficking and membrane dynamics, the alterations of which promote tumorigenesis [20]. It has been reported that RAB11A facilitates gastric cancer progression and metastasis [10]. Our data showed a similar effect of RAB11A overexpression in prostate cancer, promoting the proliferation, invasion, and

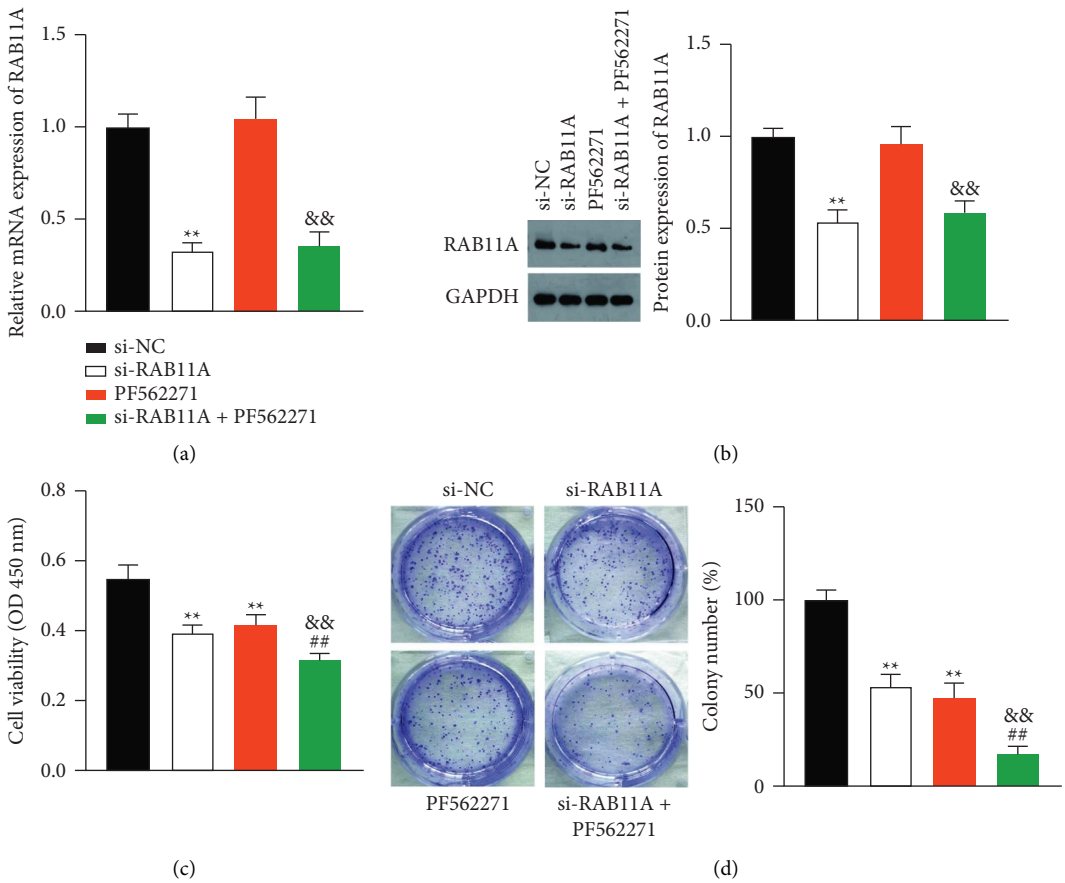

Figure 4: RAB11A promotes proliferation of prostate cancer cells via the activating FAK/AKT signaling pathway. (a) The mRNA expression of RAB11A in PC-3 cells was detected by RT-qPCR. (b) The protein expression levels of RAB11A in PC-3 cells were detected by western blotting. (c) PC-3 cell viability was analyzed by CCK-8 assay. (d) The proliferation of PC-3 cells was examined by clone formation assay. The PC-3 cells were pretreated with the FAK inhibitor PF562271 before the transfection with si-RAB11A. $^{**}P < 0.01$ vs. si-NC; $^{\#\#}P < 0.01$ vs. si-RAB11A; && $P < 0.01$ vs. PF562271.

migration of cancer cells. Meanwhile, the RAB11A expression was positively related with mesenchymal markers (N-cadherin and vimentin) but negatively with epithelial marker E-cadherin. These results demonstrate that RAB11A plays an oncological role in prostate cancer.

FAK is an important regulator of cell migration and invasion [21, 22]. FAK signaling pathway was activated in multiple human cancers including prostate cancer [16]. AKT is activated by FAK stimulation, regulating cell migration and invasion [23]. Accumulating evidence suggests that the activation of FAK/AKT signaling promotes tumorigenesis. CCK3 contributes to the EMT process in prostate cancer by activating FAK/AKT signaling [12]. Knockdown of RABL3, which belongs to the Rab subfamily, inhibits the proliferation and invasion of oral squamous cell carcinoma through deactivating the FAK/AKT pathway [24]. As another member of the Rab subfamily, RAB11A in the present study showed similar functions, facilitating the proliferation, migration, and invasion of prostate cancer. Therefore, we speculated that RAB11A promotes prostate cancer progression via the FAK/AKT pathway. Our data showed that si-RAB11A reduced the expression of p-FAK/FAK and p-AKT/AKT. PF562271 (a FAK inhibitor) enhanced the inhibitory effect of RAB11A on the FAK/AKT signaling pathway and on the malignant progression of prostate cancer. These results demonstrate that RAB11A could potentially promote the malignant progression of prostate cancer by activating the FAK/AKT signaling pathway. Meanwhile, *in vivo* experiment showed that the interference of RAB11A reduced the tumor growth and downregulated the protein levels of p-FAK/FAK and p-AKT/AKT in tumor tissues of prostate cancer. Taken together, our data suggest that RAB11A, as an oncogenous protein, promotes prostate cancer malignant progression and tumorigenesis through activating FAK/AKT signaling.

In conclusion, the current study identified the role of RAB11A as a tumor promoter overexpressed in human prostate cancer. The possible mechanism of RAB11A promoting prostate cancer is associated with the activation of the FAK/AKT pathway. Meanwhile, this study suggests the FAK/AKT signaling pathway as a therapeutic target to regulate the progression and development of prostate cancer. However, the understanding of the underlying intermediate mechanism by which RAB11A regulates the FAK/AKT signaling pathway remains unrevealed.

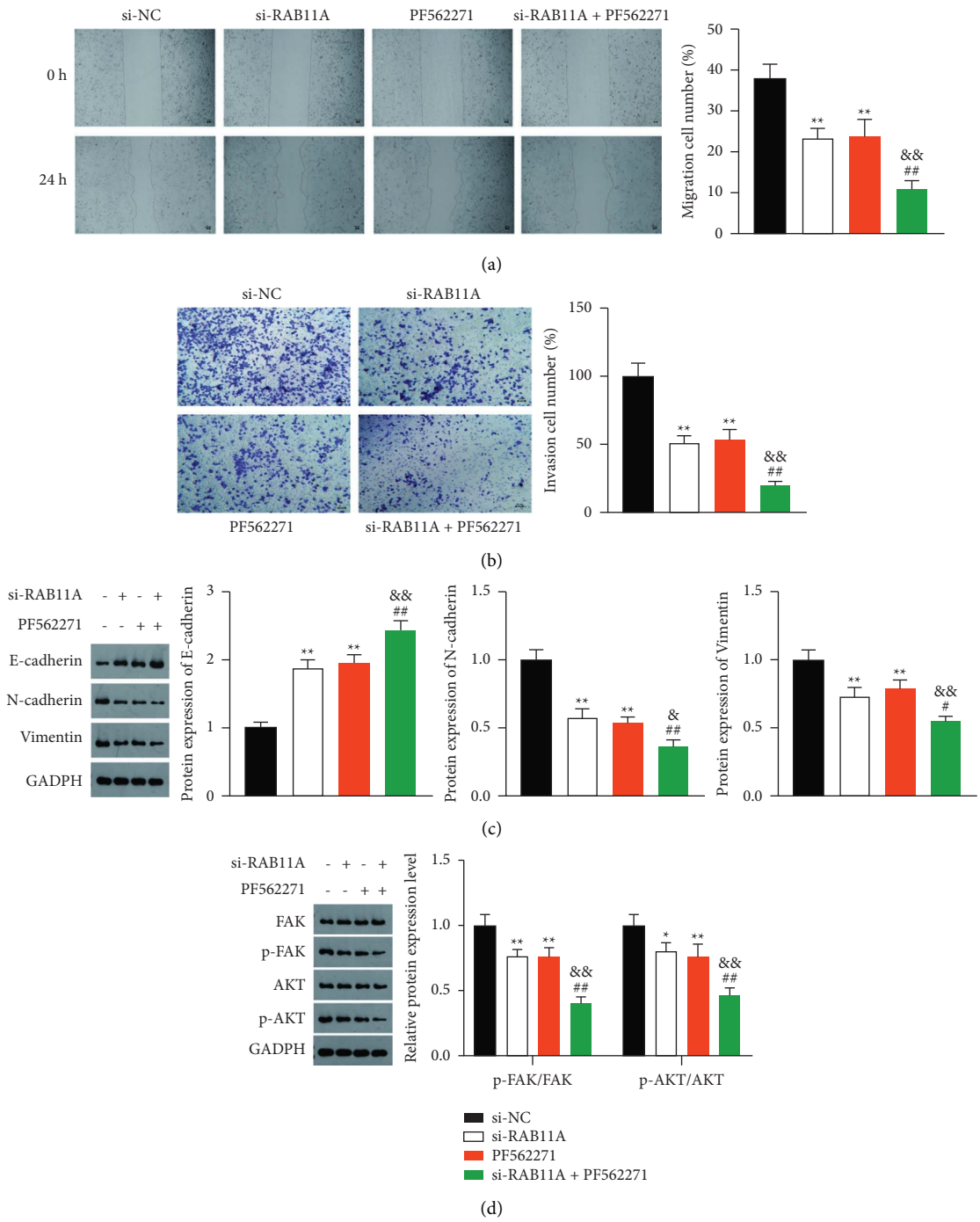

Figure 5: RAB11A promotes migration, invasion, and EMT of prostate cancer cells via activating the FAK/AKT signaling pathway. (a) The migration of PC-3 cells was analyzed by wound healing assay. (b) The invasion of PC-3 cells was analyzed by Transwell assay (scale bar = 50 μm). (c) The protein levels of E-cadherin, N-cadherin, and vimentin were analyzed by western blot analysis. (d) The protein levels of p-FAK/FAK and p-AKT/AKT were analyzed by western blot analysis. The PC-3 cells were pretreated with the FAK inhibitor PF562271 before the transfection with si-RAB11A. $^{*}P < 0.05$, $^{**}P < 0.01$ vs. si-NC; $^{\#}P < 0.05$, $^{\#\#}P < 0.01$ vs. si-RAB11A; $\&P < 0.05$, $\&\&P < 0.01$ vs. PF562271.

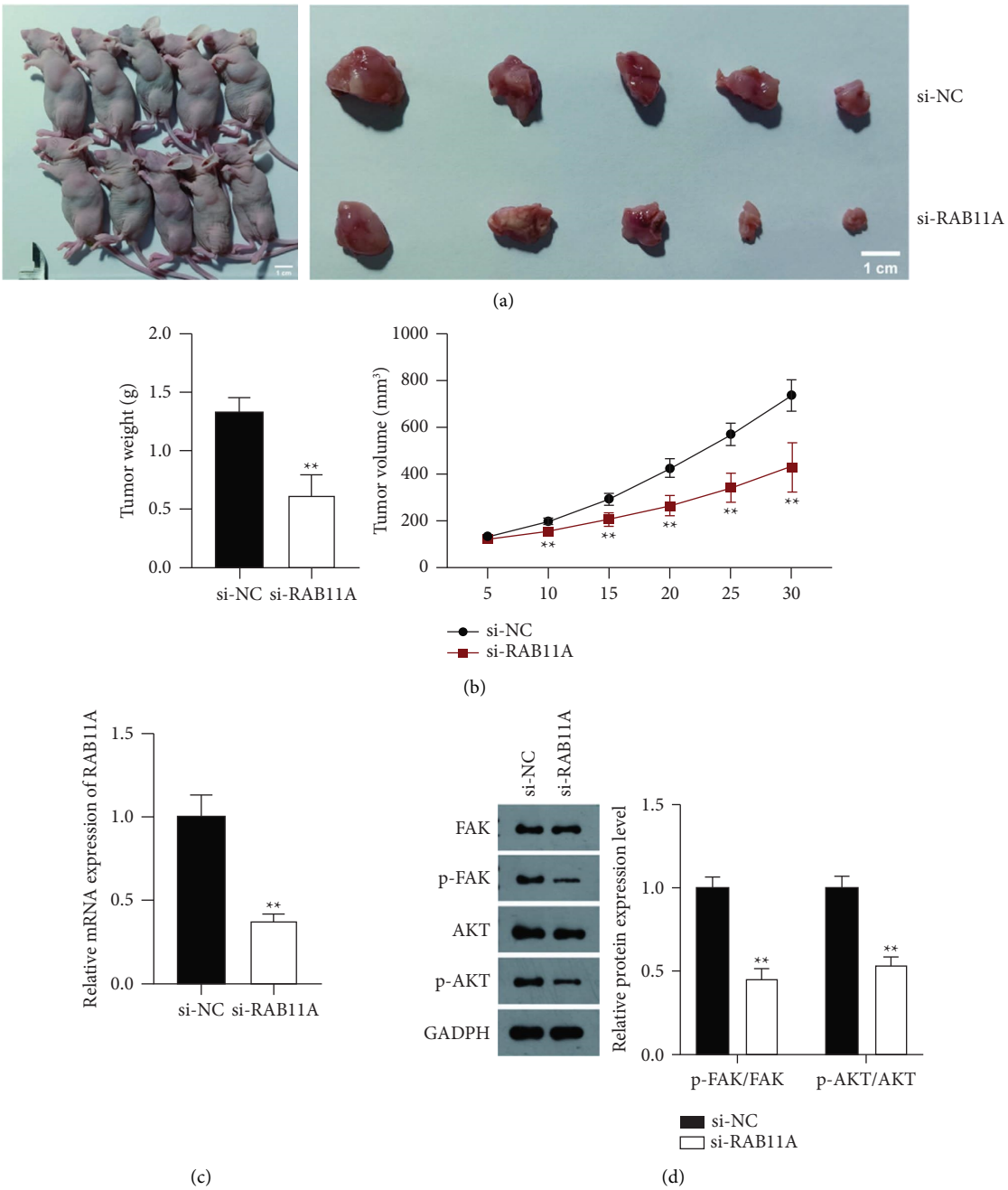

Figure 6: RAB11A promotes the tumor formation of prostate cancer via activating the FAK/AKT signaling pathway *in vivo*. (a) Tumor size (scale bar = 1 cm); (b) tumor weight and volume. (c) The mRNA expression of RAB11A in tumor tissues of mice was detected by RT-qPCR. (d) The protein levels of p-FAK/FAK and p-AKT/AKT in tumor tissues were measured by western blotting. Mice were subcutaneously injected with PC-3 cells that were transfected with si-NC or si-RAB11A. After 30 days transfection, mice were euthanized, and tumor tissues were collected. $^{**}P < 0.01$ vs. si-NC.

Data Availability

The data used to support the findings of this study are available from the corresponding author upon request.

Ethical Approval

This study was approved by the Ethic Committee of Affiliated Hospital of Xiamen University (XMULAC20220034-1).

Conflicts of Interest

The authors declare that there are no conflicts of interest regarding the publication of this paper.

Supplementary Materials

Table S1: the sequence of si-RAB11A. Table S2: primer sequences used for RT-qPCR. Table S3: the information of antibodies. (*Supplementary Materials*)

References

[1] R. L. Siegel, K. D. Miller, and A. Jemal, "Cancer statistics 2020," *CA: A Cancer Journal for Clinicians*, vol. 70, no. 1, pp. 7–30, 2020.

[2] F. Ugwumba and I. Nnabugwu, "Prostate cancer characteristics: a descriptive analysis of clinical features at presentation in the last decade in a black African community," *Annals of African Medicine*, vol. 21, no. 2, pp. 153–157, 2022.

[3] S. Bhattacharjee, K. Ikromjanov, K. S. Carole et al., "Cluster analysis of cell nuclei in H&E-Stained histological sections of prostate cancer and classification based on traditional and modern artificial intelligence techniques," *Diagnostics*, vol. 12, no. 1, p. 15, 2021.

[4] X. Liu, W. Li, I. Puzanov, D. Goodrich, G. Chatta, and D. Tang, "Prostate cancer as a dedifferentiated organ: androgen receptor, cancer stem cells, and cancer stemness," *Essays in Biochemistry*, vol. 66, no. 4, pp. 291–303, 2022.

[5] D. Ramel, X. Wang, C. Laflamme, D. J. Montell, and G. Emery, "Rab11 regulates cell-cell communication during collective cell movements," *Nature Cell Biology*, vol. 15, no. 3, pp. 317–324, 2013.

[6] Q. Dong, L. Fu, Y. Zhao et al., "Rab11a promotes proliferation and invasion through regulation of YAP in non-small cell lung cancer," *Oncotarget*, vol. 8, no. 17, pp. 27800–27811, 2017.

[7] N. Porther and M. Barbieri, "The role of endocytic Rab GTPases in regulation of growth factor signaling and the migration and invasion of tumor cells," *Small GTPases*, vol. 6, no. 3, pp. 135–144, 2015.

[8] D. Zhao, B. Wang, and H. Chen, "RAB11A mediates the proliferation and motility of esophageal cancer cells via WNT signaling pathway," *Acta Biochimica Polonica*, vol. 67, no. 4, pp. 531–538, 2020.

[9] Y. C. Chung, W. C. Wei, S. H. Huang et al., "Rab11 regulates E-cadherin expression and induces cell transformation in colorectal carcinoma," *BMC Cancer*, vol. 14, no. 1, pp. 587–589, 2014.

[10] J. Du, L. Fu, J. Hao, X. Lin, and Q. Dong, "Rab11a is overexpressed in gastric cancer and regulates FAK/AKT signaling," *Journal of oncology*, vol. 2020, pp. 1–13, 2020.

[11] H. Yoon, J. P. Dehart, J. M. Murphy, and S. T. S. Lim, "Understanding the roles of FAK in cancer: inhibitors, genetic models, and new insights," *Journal of Histochemistry and Cytochemistry*, vol. 63, no. 2, pp. 114–128, 2015.

[12] P. C. Chen, H. C. Tai, T. H. Lin et al., "CCN3 promotes epithelial-mesenchymal transition in prostate cancer via FAK/Akt/HIF-1α-induced twist expression," *Oncotarget*, vol. 8, no. 43, pp. 74506–74518, 2017.

[13] K. Nguyen, Y. Yan, B. Yuan et al., "ST8SIA1 regulates tumor growth and metastasis in TNBC by activating the FAK-AKT-mTOR signaling pathway," *Molecular Cancer Therapeutics*, vol. 17, no. 12, pp. 2689–2701, 2018.

[14] K. Dohoon, K. Sunhong, K. Hyongjong et al., "Akt/PKB promotes cancer cell invasion via increased motility and metalloproteinase production," *The FASEB Journal*, vol. 15, no. 11, pp. 1953–1962, 2001.

[15] M. Scaltriti, "The Epidermal Growth Factor Receptor Pathway," *A Model for Targeted Therapy Aacr Education Book*, vol. 12, no. 18, pp. 5268–5272, 2008.

[16] P. Xing, Y. Wang, L. Zhang, C. Ma, and J. Lu, "Knockdown of lncRNA MIR4435-2HG and ST8SIA1 expression inhibits the proliferation, invasion and migration of prostate cancer cells *in vitro* and *in vivo* by blocking the activation of the FAK/AKT/β-catenin signaling pathway," *International Journal of Molecular Medicine*, vol. 47, no. 6, p. 93, 2021.

[17] H. E. Taitt, "Global trends and prostate cancer: a review of incidence, detection, and mortality as influenced by race, ethnicity, and geographic location," *American Journal of Men's Health*, vol. 12, no. 6, pp. 1807–1823, 2018.

[18] P. Dasgupta, P. Kulkarni, N. S. Bhat et al., "Activation of the Erk/MAPK signaling pathway is a driver for cadmium induced prostate cancer," *Toxicology and Applied Pharmacology*, vol. 401, Article ID 115102, 2020.

[19] C. Liu, W. Wang, P. Lin et al., "GDI2 is a target of paclitaxel that affects tumorigenesis of prostate cancer via the p75NTR signaling pathway," *Biochemical and Biophysical Research Communications*, vol. 562, pp. 119–126, 2021.

[20] E. Ferro, C. Bosia, and C. C. Campa, "RAB11-Mediated trafficking and human cancers: an updated review," *Biology*, vol. 10, no. 1, p. 26, 2021.

[21] J. S. Chen, X. H. Huang, Q. Wang et al., "FAK is involved in invasion and metastasis of hepatocellular carcinoma," *Clinical & Experimental Metastasis*, vol. 27, no. 2, pp. 71–82, 2010.

[22] N. Sima, X. Cheng, F. Ye, D. Ma, X. Xie, and W. Lu, "The overexpression of scaffolding protein NEDD9 promotes migration and invasion in cervical cancer via tyrosine phosphorylated FAK and SRC," *PLoS One*, vol. 8, no. 9, Article ID e74594, 2013.

[23] Y. Huang, G. Feng, J. Cai et al., "Sin1 promotes proliferation and invasion of prostate cancer cells by modulating mTORC2-AKT and AR signaling cascades," *Life Sciences*, vol. 248, Article ID 117449, 2020.

[24] Z. Xu, H. Li, C. Lin, B. Zeng, Y. Chen, and Y. Luo, "Knockdown of RABL3 suppresses the proliferation and invasion of oral squamous cell carcinoma through inactivating the FAK/AKT pathway," *Journal of Bioenergetics and Biomembranes*, vol. 53, no. 2, pp. 203–211, 2021.

Hindawi
Evidence-Based Complementary and Alternative Medicine
Volume 2023, Article ID 9764181, 1 page
https://doi.org/10.1155/2023/9764181

Retraction

Retracted: Application Value of Metagenomics Next-Generation Sequencing (mNGS) in Detection of Mucormycosis after Chemotherapy in Childhood Acute Leukemia

Evidence-Based Complementary and Alternative Medicine

Received 1 August 2023; Accepted 1 August 2023; Published 2 August 2023

This article has been retracted by Hindawi following an investigation undertaken by the publisher [1]. This investigation has uncovered evidence of one or more of the following indicators of systematic manipulation of the publication process:

(1) Discrepancies in scope
(2) Discrepancies in the description of the research reported
(3) Discrepancies between the availability of data and the research described
(4) Inappropriate citations
(5) Incoherent, meaningless and/or irrelevant content included in the article
(6) Peer-review manipulation

The presence of these indicators undermines our confidence in the integrity of the article's content and we cannot, therefore, vouch for its reliability. Please note that this notice is intended solely to alert readers that the content of this article is unreliable. We have not investigated whether authors were aware of or involved in the systematic manipulation of the publication process.

In addition, our investigation has also shown that one or more of the following human-subject reporting requirements has not been met in this article: ethical approval by an Institutional Review Board (IRB) committee or equivalent, patient/participant consent to participate, and/or agreement to publish patient/participant details (where relevant).

Wiley and Hindawi regrets that the usual quality checks did not identify these issues before publication and have since put additional measures in place to safeguard research integrity.

We wish to credit our own Research Integrity and Research Publishing teams and anonymous and named external researchers and research integrity experts for contributing to this investigation.

The corresponding author, as the representative of all authors, has been given the opportunity to register their agreement or disagreement to this retraction. We have kept a record of any response received.

References

[1] W. Li, H. Zhu, L. Wen, M. Quan, and L. Wang, "Application Value of Metagenomics Next-Generation Sequencing (mNGS) in Detection of Mucormycosis after Chemotherapy in Childhood Acute Leukemia," *Evidence-Based Complementary and Alternative Medicine*, vol. 2022, Article ID 7366432, 5 pages, 2022.

Hindawi
Evidence-Based Complementary and Alternative Medicine
Volume 2022, Article ID 7366432, 5 pages
https://doi.org/10.1155/2022/7366432

Research Article

Application Value of Metagenomics Next-Generation Sequencing (mNGS) in Detection of Mucormycosis after Chemotherapy in Childhood Acute Leukemia

Wenzi Li,[1] Hua Zhu,[2] Li Wen,[1] Meijie Quan,[1] and Li Wang[1]

[1]*Department of Hematology and Oncology, Hebei Province Children's Hospital, Shijiazhuang City 050031, Hebei Province, China*
[2]*Hebei Province Children's Hospital Orthopedics Department, Shijiazhuang City 050031, Hebei Province, China*

Correspondence should be addressed to Li Wang; liwang1232022@163.com

Received 10 June 2022; Accepted 15 July 2022; Published 19 August 2022

Academic Editor: Shuli Yang

Objective. To analyze the application of macrogenomics next-generation sequencing (mNGS) in the detection of post-chemotherapy trichomoniasis cases in children with acute leukemia. *Methods*. To retrospectively analyze the clinical data of 7 patients with acute leukemia combined with trichomoniasis after chemotherapy in the department of hematology and oncology of Hebei Children's Hospital, and to summarize the characteristics of their postchemotherapy clinical data, diagnostic and therapeutic processes, and outcomes. *Results*. Among the 7 children, 6 cases had acute lymphoblastic leukemia and 1 case had acute myeloid leukemia. mNGS detected trichoderma infection, including 1 case of pulmonary cerebral type and 6 cases of pulmonary type. After treatment, 1 case died, 2 cases were cured, and 4 cases improved. *Conclusion* **.** The clinical manifestations of trichomoniasis after combined chemotherapy in pediatric acute leukemia lack specificity. Early application of the mNGS assay is of great value.

1. Introduction

Pulmonary trichomycosis is an invasive pulmonary fungal disease caused by pathogenic infections of the order Trichophyton [1]. It occurs in immunocompromised populations, especially in immunodeficient hosts undergoing chemotherapy and hematopoietic stem cell transplantation [2]. Childhood acute leukemia is the most common hematologic malignancy in children[3]. The cure rate has gradually increased with the continuous improvement of chemotherapy regimens [4]. The combination of pulmonary trichomoniasis after chemotherapy can seriously affect the prognosis of children [5]. Because of the difficulty in treating this devastating infection, rapid initiation of antifungal therapy is the cornerstone [6]. However, the early diagnosis of pulmonary trichomycosis lacks specificity and relies mainly on histopathology and fungal culture, with long lead times and low positive rates [7]. In recent years, with the advent of mNGS assays, the detection rate of pathogenic organisms in children with postchemotherapy coinfection in leukemia has improved [8]. In this study, we retrospectively analyzed seven children with acute leukemia who had early infection detected by the mNGS method after chemotherapy for leukemia from January 2020 to December 2021, and analyzed the clinical characteristics, treatment, and outcome of these children [9]. The value of this method in the early diagnosis of pulmonary trichinosis after chemotherapy in children with acute leukemia was further discussed [10].

2. Cases and Methods

The clinical data of 7 children with acute leukemia complicated with mucormycosis treated in the Hematology and Oncology Department of Hebei Children's Hospital from 2020 to 1 to 2021–12 were collected. Mucormycosis was diagnosed in all 7 patients by the mNGS assay. There were 6 males and 1 female. The underlying diseases, clinical manifestations, laboratory and imaging examinations, use of

antifungal drugs, surgical and other outcomes of 7 children were retrospectively analyzed. Reference (6) criteria for the evaluation of clinical efficacy: ① Cure: the symptoms and signs disappeared completely, and the lesions were obviously absorbed or completely absorbed by imaging examination; ② Improved: the symptoms and signs improved, and there was no significant change in the absorption of the lesions; ③ Worsening: new symptoms appeared. Symptoms and signs of infection, imaging examination progressed or did not improve; ④ death.

3. Results

3.1. Clinical Features. The clinical features of the 7 patients are shown in Table 1. Basic disease: 1 case of acute myeloid leukemia. The primary disease was not relieved when the infection occurred. During the second course of induction chemotherapy, the patient was in a state of agranulocytosis when the infection occurred, and the agranulocytosis lasted for 45 days. 6 cases of acute lymphoblastic leukemia, all patients achieved complete remission. During consolidation chemotherapy, they were in agranulocytosis state when infection occurred, and the duration of agranulocytosis was 8–18 days. All the children had been applied with more than two kinds of broad-spectrum antibiotics during hospitalization.

The time from symptom onset to diagnosis of pathogenic bacteria in 7 cases was 2–15 days, with an average of 7.85 days. Among the 7 cases of mucormycosis, 6 cases were of the pulmonary type, and they all showed varying degrees of fever and cough at the beginning of the disease, and the Case 4 showed rapid breathing. In 1 case of the pulmonary brain type, fever and cough were the first symptoms, followed by headache and convulsions.

3.2. Auxiliary Examination. 7 children were in an agranulocytosis state during the course of the disease. The blood culture, sputum culture, sputum fungal smear, galactomannan (GM test) and 1,3 β D glucan (G test) were all negative. In Case 1, pathogenic bacteria were found through peripheral blood (PB) mNGS. The pathogenic bacteria were found in the PB and cerebrospinal fluid (CSF) mNGS of the lung-cerebral type (Case 2). In cases 4 and 5, pathogenic bacteria were found by mNGS of bronchoalveolar lavage fluid (BAL). In cases 3 and 6, pathogenic bacteria were found by mNGS in PB and BAL. In Case 7, pathogenic bacteria were found in the mNGS of PB but not found in the mNGS of BAL. Chest computed tomography (CT) manifestations of 6 children with pulmonary type were patchy shadow, nodular shadow, mass shadow, and consolidation. The cranial magnetic resonance (MRI) findings of a child with pulmonary cerebral type showed diffuse abnormal enhancement on the brain surface, sulci, and brain stem margins, as in Table 1.

3.3. Treatment and Outcome. All children were given liposomal amphotericin B formulation (LAmB) for injection and posaconazole oral liquid combined with antifungal therapy on the basis of controlling the primary disease. At the same time, amphotericin B was given by aerosol inhalation. The dose of amphotericin B liposome is 1–3 mg/kg·d. During the course of treatment, hypokalemia occurred in all 7 children. Renal function abnormalities occurred in 3 children, which improved after dose reduction or drug withdrawal. Cases 3, 5, 6, and 7 underwent bronchoalveolar lavage through fiberoptic bronchoscopy many times, but there was no significant improvement in repeated chest computed tomography scans. Case 6 underwent surgical resection of the diseased lung lobe due to lung consolidation and cavity formation. The postoperative pathological report was a fungal infection (Figures 1 and 2). Cases 1 and 7 were complicated with pulmonary hemorrhage due to severe cough during the follow-up consolidation chemotherapy. Case 1 improved after emergency surgery to remove the lesion, and Case 7 improved after timely invasive ventilator support. In Case 2, the condition of the child continued to progress, and during hospitalization, there were multiple convulsions, all of which were generalized seizures, and later the child died of multiple organ failure.

4. Discussion

Mucormycosis is a rare but extremely fatal invasive fungal disease. Several studies have shown that the underlying disease in patients is also related to the site of infection; pulmonary mucormycosis is more common in patients with hematologic malignancies and neutropenia, nasal orbital cerebral mucormycosis is more common in patients with diabetes, and trauma usually leads to cutaneous mucormycosis [11]. Pulmonary mucormycosis infection is one of the most common types of infections in patients with mucormycosis, and its nonspecific symptoms include fever, cough, dyspnea, and chest pain [12]. The lesions usually involve the lung parenchyma but may also extend to the chest wall, pulmonary artery, aorta, mediastinum, or pericardium, and hemoptysis may be caused by infiltration into the pulmonary artery [13]. In the present study, all children with mucormycosis were in a granulocytopenic state, including six cases of pulmonary mucormycosis and one case of pulmonary cerebral mucormycosis [14]. All patients had varying degrees of cough and fever at the beginning of the disease, and 2 patients developed hemoptysis during the progression of the disease.

Several studies have shown that the mortality rate of localized infections with mucormycosis is 20%–50%, while the mortality rate of disseminated mucormycosis can be as high as 70%–90% [15]. As treatment of this devastating infection is very difficult, rapid initiation of antifungal therapy is the cornerstone. Early diagnosis and treatment will help to reduce patient mortality. However, the diagnosis of mucormycosis depends on histopathology and culture. Mucormycosis readily invades blood vessels and destroys the tissue of affected organs, leading to vascular thrombosis and tissue necrosis with the formation of black crusts [16]. Hematoxylin-eosin (HE) staining, hyperoside (PAS) staining, and hexosamine silver staining can be selected for definite infection, with hexosamine silver staining being preferred, and may show broad, irregular hyphae in tissue

Table 1: Overview of our 7 pediatric mucormycosis cases.

Number	Age/ sex	Underlying diseases	Main clinical manifestations	Specimen source/ pathogenic bacteria/reads	Imaging performance	The involved organs	Antifungal drugs	Operative	Survival outcome
1	15/M	AML	Fever and cough	PB/Rhizopus mi Crosporus/(reads 125)	High-density shadow under the left lung	Lungs	LAmB posaconazole	Yes	Cure
2	11/F	ALL	Fever, cough, headache, and convulsions	PB/Rhizopus delemar/Reads 42 CSF/Rhizopus delemar/Reads 316	Cranial MRI: diffuse and abnormal enhancement on the brain surface, sulcus and brainstem margin chest CT: shadow of left lung	Lungs brain	LAmB posaconazole	No	Die
3	3/M	ALL	Fever and cough	PB/Rhizopus microsporus/reads 10 BAL/Rhizopus Microsporus/reads 10	High-density shadow in the lower lobe of both lungs	Lungs	LAmB posaconazole	No	Improved
4	1/M	ALL	Fever, cough breathe fast	BAL/Rhizomucor pusillus/reads 6	Real changes in the upper lobe of the left lung	Lungs	LAmB posaconazole	No	Improved
5	1/M	ALL	Fever, cough	BAL/Rhizomucor pusillus/Reads 3742	Double lung field multiple size unequal nodular sheet high-density shadow	Lungs	LAmB posaconazole	No	Improved
6	3/M	ALL	Fever cough	BAL/Rhizomucor pusillus/reads2 PB/ Rhizomucor pusillus/reads 40	Large upper lobe of the right lung	Lungs	LAmB posaconazole	Yes	Cure
7	7/F	ALL	Fever cough	PB/ Cunninghamella bertholletiae/reads 3	High-density shadow of emerging nodules in the lower lobe of the right lung	Lungs	LAmB posaconazole	No	Improved

ALL, acute lymphoblastic leukemia; AML, acute myeloid leukemia; CT, computerized tomography; MRI, magnetic resonance; PB, peripheral blood; BAL, bronchoalveolar lavage fluid; CSF, cerebral spinal fluid; LAmB, liposomal amphotericin B formulation.

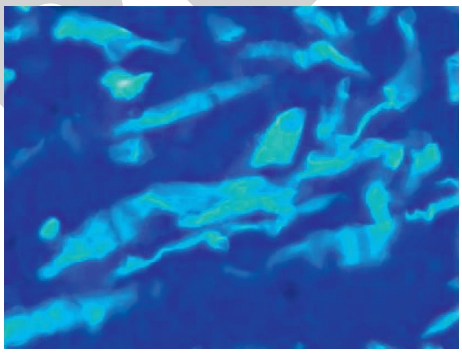

Figure 1: Immunofluorescence of fungal hyphae.

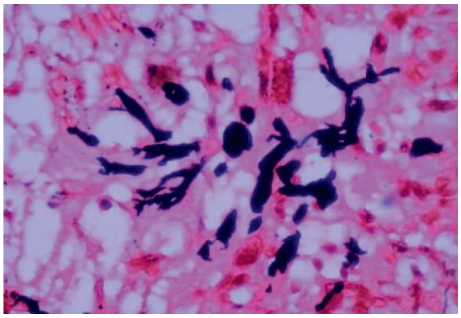

Figure 2: Hexamine silver staining showed that the fungal hyphae were short black rod-like structures.

specimen sections without separation or with little separation or righting branching [17]. In general, tissue cultures may be negative and blood cultures are rarely positive, even when there are characteristic histopathological changes of mucormycetes. Serological tests for galactomannan (GM test) and 1,3-beta-D glucan (G test) of mucor were negative [5]. In our study, blood cultures, sputum cultures, fungal smears in sputum, G and GM tests were negative in all

children sent for examination. Only one case of resected diseased lung lobe was positive for hexosamine-silver staining, a characteristic change of mucormycosis infection, and no pathogenic evidence was found in other children by conventional laboratory tests [18].

In recent years, a new detection technology, metagenomic next-generation sequencing (mNGS), has emerged. mNGS does not require traditional microbial culture, does not require specific amplification, and can simultaneously detect known or unknown bacteria, fungi, viruses, parasites, and other pathogens in the same sample without bias [19]. The DNA or RNA in the sample is detected and then analyzed in comparison with the information database to know the species of pathogenic microorganisms contained in the sample [20]. Currently, mNGS has been gradually applied to the diagnosis of difficult clinical infections, and the types of specimens mainly include venous blood, cerebrospinal fluid, bronchoalveolar lavage fluid, sputum, pleural effusion, ascites, pharyngeal secretions, lesion punctures, and pathological tissues [21].

In our study, we used the mNGS assay to obtain evidence of pathogenic bacteria by infecting children with PB, BAL, and CSF. Four different mucus genera were identified [22]. In Case 2, the pathogenic bacteria were consistent in CSF and peripheral blood. Pathogenic bacteria in peripheral blood and alveolar lavage fluid were concordant in patients 3, 4, 5, and 6, respectively [23]. In all cases, it took only 1–2 days from specimen submission to report the test results. The time was greatly reduced. In combination with the test results, the treatment plan was rapidly adjusted and effective interventions were given, resulting in the survival of most of the children with a good prognosis [24].

5. Conclusion

The lack of specificity in the clinical manifestations of children with acute leukemia after chemotherapy makes it difficult to rely on clinical diagnosis at an early stage and to give effective interventions early, resulting in an extremely poor prognosis and high mortality. Therefore, early diagnosis and treatment are particularly important. mNGS is a novel detection technology that can shorten the time to detect pathogenic bacteria and can enable clinicians to give effective treatment plans in a timely manner, thus improving the prognosis of children, increasing their cure rate and reducing mortality. Therefore, mNGS detection technology is of great value in the early diagnosis of combined mucormycosis after chemotherapy for pediatric acute leukemia.

Data Availability

The experimental data used to support the findings of this study are available from the corresponding author upon request. The original contributions presented in the study are included in the article/supplementary materials. Further inquiries can be directed to the corresponding author.

Ethical Approval

The studies involving human participants were reviewed and approved by Hebei Province Children's Hospital.

Consent

The patients/participants provided their written informed consent to participate in this study. Written informed consent was obtained from the individual (s) for the publication of any potentially identifiable images or data included in this article.

Conflicts of Interest

The authors declare that there are no conflicts of interest regarding this work.

Authors' Contributions

Wenzi li, Hua zhu, Meijie Quan, Li Wen, Li wang, Huali Li, Jiamin Wang, Yanrong Zhao, Mingli Yang, Xianbin Meng, and Ling Liu analyzed and interpreted patient data. Wenzi li and Hua zhu wrote the manuscript. All authors read and approved the final manuscript.

Acknowledgments

This study was supported by the Hebei Province Medical Science Research Project Planning Fund (20211015).

References

[1] H. Inaba and C. G. Mullighan, "Pediatric acute lymphoblastic leukemia," *Haematologica*, vol. 105, no. 11, p. 2524, 2020.

[2] N. V. Sipsas, M. N. Gamaletsou, and A. Anastasopoulou, "Therapy of mucormycosis," *Journal of Fungi*, vol. 4, no. 3, p. 90, 2018.

[3] W. Jeong, C. Keighley, R. Wolfe et al., "The epidemiology and clinical manifestations of mucormycosis: a systematic review and meta-analysis of case reports," *Clinical Microbiology and Infections*, vol. 25, no. 1, pp. 26–34, 2019.

[4] A. M. Al-Azab, A. A. Zaituon, K. M. Al-Ghamdi, and F. M. A. Al-Galil, "Surveillance of dengue fever vector Aedes aegypti in different areas in Jeddah city Saudi Arabia," *Advances in Animal and Veterinary Sciences*, vol. 10, no. 2, pp. 348–353, 2022.

[5] O. A. Cornely, A. Alastruey-Izquierdo, D. Arenz et al., "Global guideline for the diagnosis and management of mucormycosis: an initiative of the European confederation of medical mycology in cooperation with the mycoses study group education and Research consortium," *The Lancet Infectious Diseases*, vol. 19, no. 12, pp. e405–e421, 2019.

[6] C. C. Tsang, J. L. L. Teng, S. K. P. Lau, and P. C. Y. Woo, "Rapid genomic diagnosis of fungal infections in the age of next-generation sequencing," *Journal of Fungi*, vol. 7, no. 8, p. 636, 2021.

[7] A. M. Casto, D. N. Fredricks, and J. A. Hill, "Diagnosis of infectious diseases in immunocompromised hosts using metagenomic next generation sequencing-based diagnostics," *Blood Reviews*, vol. 53, Article ID 100906, 2022.

[8] X. Ma, S. Zhang, H. Xing et al., "Invasive pulmonary aspergillosis diagnosis via peripheral blood metagenomic next-generation sequencing," *Frontiers of Medicine*, vol. 9, Article ID 751617, 2022.

[9] J. D. Jenks, J. P. Gangneux, I. S. Schwartz et al., "Diagnosis of breakthrough fungal infections in the clinical mycology

Hindawi
Evidence-Based Complementary and Alternative Medicine
Volume 2022, Article ID 1150390, 16 pages
https://doi.org/10.1155/2022/1150390

Research Article

The Prognostic Value of AT-Rich Interaction Domain (ARID) Family Members in Patients with Hepatocellular Carcinoma

Siyi Li,[1,2] Zhulin Wu,[3] Qiuyue Li,[4] Qiting Liang,[4,5] Hengli Zhou,[4,5] Yafei Shi,[6] Rong Zhang,[1,2] and Huafeng Pan[4,5]

[1]*Joint Laboratory for Translational Cancer Research of Chinese Medicine of the Ministry of Education of the People's Republic of China, Guangzhou 510405, China*
[2]*International Institute for Translational Chinese Medicine, Guangzhou University of Chinese Medicine, Guangzhou 510405, China*
[3]*The Fourth Clinical Medical College of Guangzhou University of Chinese Medicine, Shenzhen 518033, Guangdong, China*
[4]*Science and Technology Innovation Center, Guangzhou University of Chinese Medicine, Guangzhou 510405, China*
[5]*Institute of Clinical Pharmacology, Guangzhou University of Chinese Medicine, Guangzhou 510405, China*
[6]*Basic Medical College of Guangzhou University of Chinese Medicine, Guangzhou 510405, China*

Correspondence should be addressed to Huafeng Pan; gzphf@gzucm.edu.cn

Received 15 June 2022; Accepted 19 July 2022; Published 18 August 2022

Academic Editor: Shoib Baba

Objective. Hepatocellular carcinoma (HCC) is one of the most lethal malignancies with a poor prognosis. The AT-rich interaction domain (ARID) family plays an essential regulatory role in the pathogenesis and progression of cancers. This study aims to evaluate the prognostic value and clinical significance of human ARID family genes in HCC. *Methods*. ONCOMINE and The Cancer Genome Atlas (TCGA) databases were employed to retrieve ARIDs expression profile and clinicopathological information of HCC. Kaplan–Meier plotter and MethSurv were applied to the survival analysis of patients with HCC. CBioPortal was used to analyze genetic mutations of ARIDs. Gene Expression Profiling Interactive Analysis (GEPIA) and Metascape were used to perform hub gene identification and functional enrichment. *Results*. Expression levels of 11 ARIDs were upregulated in HCC, and 2 ARIDs were downregulated. Also, 4 ARIDs and 5 ARIDs were correlated with pathologic stages and histologic grades, respectively. Furthermore, higher expression of ARID1A, ARID1B, ARID2, ARID3A, ARID3B, ARID5B, KDM5A, KDM5B, KDM5C, and JARID2 was remarkably correlated with worse overall survival of patients with HCC, and the high ARID3C/KDM5D expression was related to longer overall survival. Multivariate Cox analysis indicated that ARID3A, KDM5C, and KDM5D were independent risk factors for HCC prognosis. Moreover, ARIDs mutations and 127 CpGs methylation in all ARIDs were observed to be significantly associated with the prognosis of HCC patients. Besides, our data showed that ARIDs could regulate tumor-related pathways and distinct immune cells in the HCC microenvironment. *Conclusions*. ARIDs present the potential prognostic value for HCC. Our findings suggest that ARID3A, KDM5C, and KDM5D may be the prognostic biomarkers for patients with HCC.

1. Introduction

Liver cancer is the leading cause of mortality among malignancies according to the statistics from the GLOBOCAN database [1]. Hepatocellular carcinoma (HCC), the most prevalent subtype of liver cancer, accounts for 75%–85% of all liver cancer cases worldwide in 2020 [2]. In addition, the five-year survival rate of HCC is approximately 18.1% due to lack of information for early diagnosis and limited therapeutic strategy [3]. Most of the patients with HCC are at stages of an interim or advanced period when they are diagnosed, who are not applicable for surgical treatment [4]. Some drugs, such as regorafenib, nivolumab, and lenvatinib, have been developed for HCC treatment [5]. However, drug

resistance and adverse effects restrain the overall therapeutic efficacy of these drugs [6]. Therefore, it is urgently needed to find effective markers for detection, diagnosis, and prognosis of patients with HCC in the early stage.

Human AT-rich interaction domain (ARID) family composes of 15 members, including ARID1A, ARID1B, ARID2, AIRD3A, ARID3B, ARID3C, ARID4A, ARID4B, ARID5A, ARID5B, KDM5A (JARID1A), KDM5B (JARID1B), KDM5C (JARID1C), KDM5D (JARID1D), and JARID2. According to sequence identity among individual members, the ARID family was classified into 7 subfamilies, containing ARID1, ARID2, ARID3, ARID4, ARID5, KDM5, and JARID2. The ARID family genes have the ability of DNA binding, which may participate in the modification of chromatin structure and play a positive or negative role in regulating the transcription of target genes [7]. As transcriptional regulators, ARIDs have been found to be associated with cell growth, differentiation, and development, which is also closely associated with cancers [8]. For instance, a previous study has found many meaningful ARID family biomarkers in breast cancer [9]. ARID family is associated with the immune infiltrate and tumor microenvironment of digestive cancer [10]. In addition, ARID1A silencing promotes epithelial-mesenchymal transition and enhances the sensitivity of pancreatic tumor cells to NVP-AUY922, which is a promising biomarker for the identification of pancreatic ductal adenocarcinomas [11]. ARID family members are also identified as novel biomarkers for immune checkpoint inhibitor therapy in malignancies by pan-cancer analysis [12]. Nevertheless, the prognostic value of ARIDs in HCC has not been thoroughly studied.

In the current study, the expression, mutation, and methylation of different ARIDs were analyzed, and their correlation with clinicopathological parameters and survival of HCC patients was unveiled. Besides, the predicted functions and immune regulating roles of ARIDs were also analyzed.

2. Methods

2.1. Gene Expression Analysis of ARIDs. First of all, the differential expression of ARIDs between HCC and normal tissues was analyzed using the ONCOMINE (https://www.oncomine.org) database [13]. We followed the methods of Wu et al. with some modifications [14]. Screening criteria were as follows: cancer type = liver cancer; gene = ARID family members; data type = mRNA; analysis type = cancer versus normal analysis; threshold values: p value < 0.05, fold change > 1.5, and gene rank = top 10%. By default, the difference between normal and HCC tissue groups was analyzed using the t-test. Subsequently, differences in ARID family gene expression between HCC and normal samples were compared. Moreover, The Cancer Genome Atlas (TCGA, https://tcga-data.nci.nih.gov/tcga/) [15] dataset was also used to analyze the mRNA expression of 15 ARID family members in HCC tissues, and result visualization was performed with "ggplot2" package in R software (version 3.6.3). In addition, the association between ARID family members and clinicopathologic parameters (pathologic stage and histologic grade) was evaluated using the TCGA HCC dataset. Clinical information for pathological stages I and II (early stage) and stages III and IV (advanced stage), and histologic grades of patients with HCC were obtained from the TCGA database. HCC patients who lacked information on pathologic stage or histologic grade were excluded, and results were visualized with violin plots using the "ggplot2" package in R software.

2.2. Prognostic Value of ARID Family Genes. Association between the ARIDs expression and HCC prognosis was evaluated by the online software Kaplan–Meier (KM) plotter (https://www.kmplot.com) [16, 17]. Patients with HCC in TCGA dataset were divided into two groups based on the optimal cutoff value of ARIDs expression, and overall survival (OS) was selected as the outcome. To evaluate the independent prognostic factors of ARIDs, univariate and multivariate Cox analyses were conducted for both ARIDs and clinicopathological data (age, gender, stage, and T stage) using the TCGA HCC dataset, and factors with p value < 0.1 were selected for multivariate analysis. Additionally, MethSurv, an online tool for methylation visualization (https://biit.cs.ut.ee/methsurv/) [18] was applied to perform DNA methylation-based survival analysis of ARIDs using the TCGA dataset.

2.3. Genetic Mutations in ARID Family Genes. Mutations of ARID family members in HCC were analyzed via the cBioPortal tool (https://cbioportal.org) [19] by referring to a previous study [20]. Furthermore, KM plots were utilized to evaluate the correlation between genetic mutations in ARIDs and the survival time of HCC patients with cBioPortal. In cBioPortal analysis, HCC patients were classified into the altered and unaltered groups. OS, progression-free survival (PFS), and disease-free survival (DFS) were all considered as endpoints.

2.4. Functional Enrichment Analyses. Hub genes screening and functional enrichment analyses were carried out according to the previously reported methods [21]. Before functional enrichment analysis, the top 10 similar genes of each ARID family member were acquired using the Gene Expression Profiling Interactive Analysis (GEPIA, https://gepia.cancer-pku.cn/) [22]. Functions of ARID family genes were identified using the Metascape database (https://metascape.org) [23]. Additionally, Gene Ontology (GO) analysis was used to determine the biological functions of these genes based on three categories, including cellular components, molecular functions, and biological processes. Kyoto Encyclopedia of Genes and Genomes (KEGG) analysis was applied to identify signaling pathways related to ARIDs and their similar genes. Moreover, protein-protein interaction (PPI) network establishment and independent functional enrichment analyses of Molecular Complex Detection (MCODE) components were carried out in Metascape.

2.5. Immune Infiltrates Correlation Analysis. Tumor Immune Estimation Resource (TIMER, https://cistrome.shinyapps.io/timer/), an online tool for comprehensive analysis of tumor-infiltrating immune cells [24], was used to assess the correlation between ARID family genes and immune infiltrates. We followed the methods of Qin et al. to perform the immune infiltrates correlation analysis [25]. The relationships of ARIDs expression with tumor-infiltrating immune cells (B cell, $CD4^+$ T cell, $CD8^+$ cell, macrophage, neutrophil, and dendritic cell) were identified by purity-corrected partial Spearman's correlation (partial-cor) and statistical significance, and the results were shown in scatterplots provided by TIMER.

2.6. Real-Time Quantitative Reverse Transcription Polymerase Chain Reaction (RT-qPCR). Total RNA was extracted from LO2 and HepG2 cells using TRIzol reagent. We synthesized cDNA from total RNA using the One Step PrimeScript RT-PCR Kit. Next, RT-qPCR was conducted and analyzed using the ChamQTM Universal SYBR qPCR Master Mix (Vazyme, Nanjing, China) and the ABI 7500 sequence detection system. The cycling condition for RT-qPCR was 95°C for 3 min, 45 cycles of 95°C for 5 s, 60°C for 30 s, and 72°C for 10 s. Each experiment was conducted in triplicate. Primer sequences are listed in Table 1.

2.7. Statistical Methods. In the TCGA HCC dataset, differences between normal and HCC tissue groups were analyzed by *t*-test or Mann–Whitney *U* test. ANOVA test or Kruskal–Wallis test was used for multiple comparisons. Correlations among ARIDs were estimated using the Spearman test. Survival curves were plotted by the KM method, with hazard ratios (HRs) with 95% confidence intervals (CIs) and log-rank *p* values. In this paper, statistical analyses were conducted using the *R* software (version 3.6.3) or online databases. p value < 0.05 are statistically significant.

3. Results

3.1. Gene Expression Analysis of ARIDs. As displayed in Figure 1, 15 ARIDs were identified in distinct cancers, containing breast cancer, liver cancer, brain cancer, and central nervous system (CNS) cancer. The expression levels of ARID1A, ARID2, ARID3A, ARID3B, ARID4B, ARID5B, KDM5A, KDM5B, KDM5D, and JARID2 were upregulated, and expression levels of ARID1B, ARID4A, ARID4B, and KDM5D were downregulated in all types of liver cancers (including hepatocellular adenoma, liver cell dysplasia, HCC, and cirrhosis). Furthermore, data from four datasets [26–28] in ONCOMINE demonstrated that ARID1A, ARID2, ARID3A, ARID4B, KDM5A, KDM5B, and JARID2 were markedly upregulated in HCC than that in normal groups (Table 2). Furthermore, based on the TCGA dataset, mRNA expression of ARID1A, ARID1B, ARID2, ARID3A, ARID3B, ARID4B, KDM5A, KDM5B, KDM5C, KDM5D, and JARID2 was remarkably overexpressed, and ARID3C and ARID4A were underexpressed in HCC (Figure 2). In addition, no significant difference was found regarding ARID5A or ARID5B mRNA expression in the TCGA HCC dataset. Subsequently, obvious correlations among ARIDs were discovered using the Spearman test (Supplementary Figure 1).

3.2. Correlations between Clinical Features and ARIDs Expression in HCC. To identify correlations of ARIDs expression with clinicopathological factors, the clinical data of pathologic stage and histologic grade were analyzed based on the TCGA database. Results showed that higher expression levels of ARID1A, ARID2, and KDM5C were closely associated with advanced pathologic stages of patients with HCC (Figures 3(a), 3(c), and 3(m)). Increased ARID3C expression was related to the late pathologic stage (Figure 3(f)). Moreover, violin plots displayed that the expression levels of ARID2, ARID3A, ARID3C, ARID5B, KDM5C, and JARID2 were remarkably related to grades (Figures 4(a)–4(o). Higher expression levels of ARID2, ARID3A, ARID5B, KDM5C, and JARID2 tended to be correlated to higher histologic grade (Figures 4(c), 4(d), 4(j), 4(m), and 4(o)). ARID3C expression was negatively associated with the histologic grade of patients with HCC (Figure 4(f)).

3.3. Prognostic Value of ARIDs Members in HCC. The prognostic value of ARID family members in HCC was identified using a KM plotter. KM plot presented that high expression levels of 10 ARIDs, including ARID1A, ARID1B, ARID2, ARID3A, ARID3B, ARID5B, KDM5A, KDM5B, KDM5C, and JARID2, were associated with the shorter OS of all patients with HCC (Figures 5(a)–5(d), 5(e), and 5(j)–5(o)). Conversely, high mRNA expression levels of ARID3C and KDM5D were obviously associated with better OS time (Figures 5(f) and 5(n)). In addition, the association between ARID4A/ARID5B/ARID5A expression and OS in patients with HCC did not show statistical significance (Figures 5(g)–5(i)). Also, the prognostic value of CpGs was analyzed using MethSurv, and a total of 127 –CpGs in ARIDs were found to be associated with the prognosis of patients with HCC (Supplementary Table 1). In univariate Cox analysis, pathologic stage, *T* stage, and some ARIDs (including ARID2, ARID3A, ARID3B, KDM5B, KDM5C, and KDM5D) were correlated to OS of HCC patients (Supplementary Tables 2–16). Furthermore, multivariate Cox analysis indicated that high expression levels of ARID3A, KDM5C, and KDM5D were independently correlated with worse OS in patients with HCC.

3.4. Genetic Mutations of ARIDs in Patients with HCC. The genetic alterations of ARID family members in the TCGA dataset are displayed in Figure 6(a). Among 366 patients with HCC, 288 patients have genetic mutations of ARID family genes, with 78.69% mutation rate of ARIDs. The percentages of genetic mutations of ARIDs in HCC ranged from 7% to 33%, and the top 3 alteration rates in ARID family genes were KDM5D (33%), ARID3C (15%),

Table 1: Primer sequences for RT-qPCR.

Gene	Forward (5′-3′)	Reverse (5′-3′)
ARID1A	GCAGCCAAGGAGAGCAGAGTAATC	CTGAGCGAGACTGAGCAACACTG
ARID1B	ATGAACCGCACAGACGATATGATGG	TGGAGGCTGAGGACGACATATAAGG
ARID2	TACTGCCATGTCGTCGTCCTCTAC	GCTGGTGAATGTTGCTGCTGTTG
ARID3B	GACGGAGGTTTGGAAGATGAGGATG	GGTGCTGGAAGTAGATTGGACATGG
ARID3C	GCTCGACCTGTACGCTCTGTTTC	TGATGGTGGTGGGTAGGCTGAG
ARID5A	AGATGATGCCAGGAAAGACCAAAGC	CACAAAGGACACAGAAGACCCAGAG
ARID5B	AGCAAGAAATTCAGGAGGGCAAGG	TCGGTGTGTCTGTAGAGGCTATGG
KDM5A	AATGTGATGGTGGCTGTGATGAGTG	AAGGAAGGAGGTGGTGCTGGAC
KDM5B	CCGCCTCCTAGATTCCAGCAATTC	GTTCTGGCTTCCGTTGTCTCCTC
KDM5C	CCGCCTCCTAGATTCCAGCAATTC	GTTCTGGCTTCCGTTGTCTCCTC
KDM5D	AGAAGCATCCACCAGCCACATTG	TCTCATCCACATCAGCAATCCAAGC
JARID2	CGTCGTGTTCTGTCTGGAGTGTG	ATCGTAGCGGTACATCAACTTCAGC

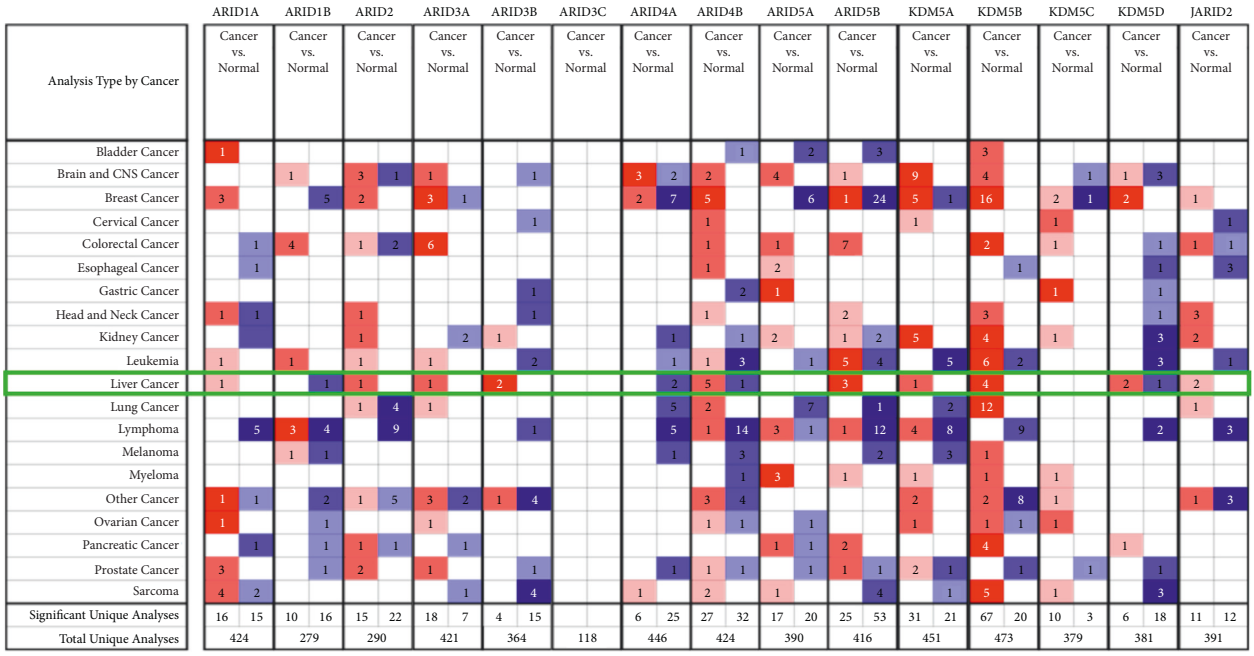

Figure 1: The mRNA expression of AT-rich interaction domain (ARID) family members in multiple cancers and hepatocellular carcinoma (HCC) based on ONCOMINE. Blue and red colors, respectively, indicate low and high expression. The number in each box represents the number of datasets that fulfill the criteria for this study.

Table 2: Transcriptional levels of AT-rich interaction domains (ARIDs) between HCC and normal liver tissues (ONCOMINE).

No	Gene name	Fold change	p value	T-test	Datasets
1	ARID1A	1.903	4.62E-6	5.073	Roessler Liver (22)
2	ARID2	1.645	1.29E-6	6.204	Wurmbach Liver (21)
3	ARID3A	2.320	3.60E-12	7.407	Chen Liver (20)
4	ARID4B	1.541	7.11E-11	6.815	Chen Liver (20)
5	ARID4B	2.115	6.32E-9	7.949	Roessler Liver (22)
6	ARID4B	2.135	1.26E-7	6.917	Wurmbach Liver (21)
7	ARID4B	1.871	2.44E-42	15.272	Roessler Liver 2 (22)
8	KDM5A	1.739	7.49E-6	5.075	Wurmbach Liver (21)
9	KDM5B	2.242	1.84E-8	6.837	Wurmbach Liver (21)
10	KDM5B	2.226	4.12E-41	15.473	Roessler Liver 2 (22)
11	KDM5B	1.579	7.87E-8	5.510	Chen Liver (20)
12	KDM5B	1.625	2.20E-5	4.981	Roessler Liver (22)
13	JARID2	1.583	1.57E-35	13.970	Roessler Liver 2 (22)
14	JARID2	1.909	9.63E-5	4.717	Wurmbach Liver (21)

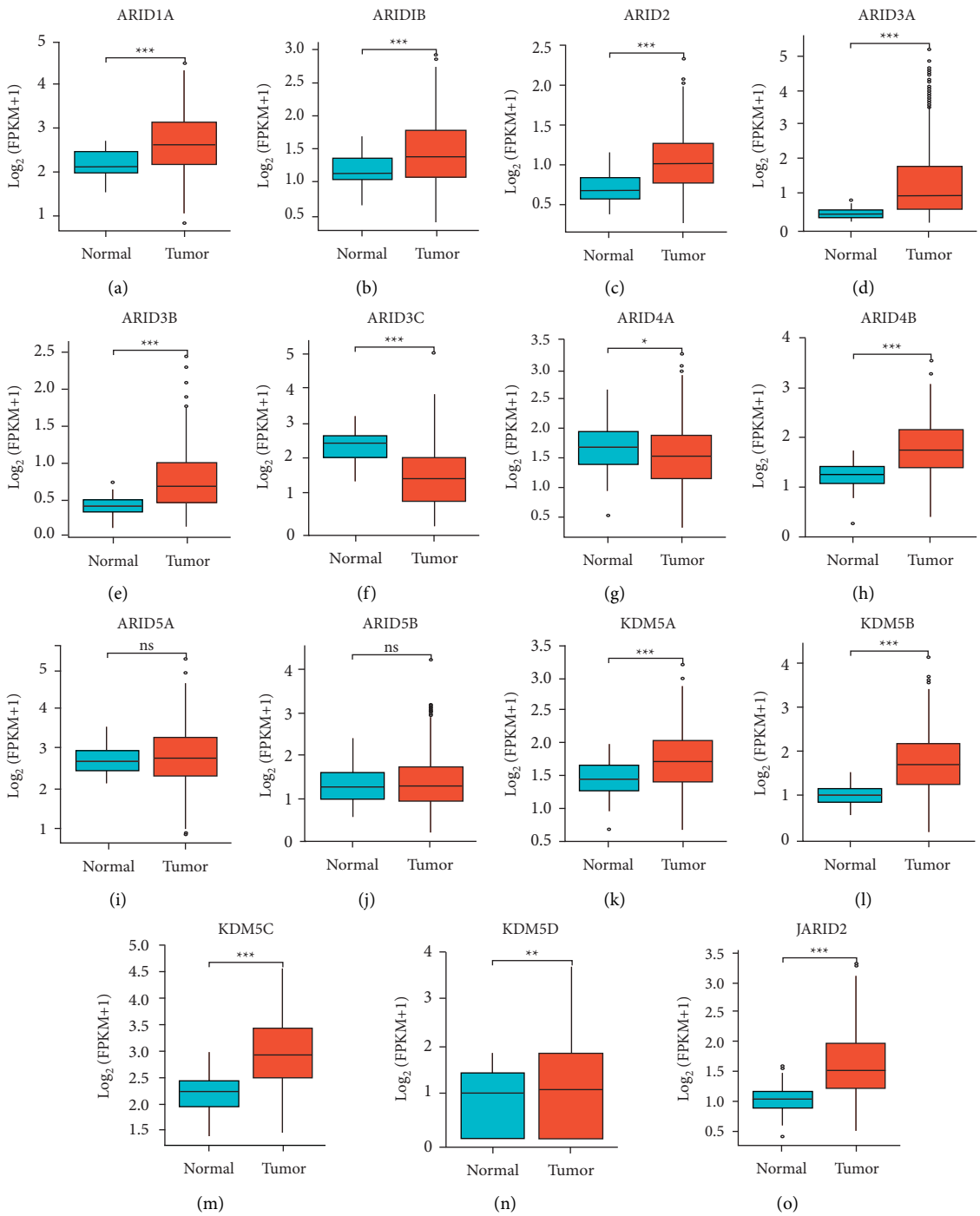

Figure 2: Expression of 15 ARID family members in HCC and normal tissues. (a-o) The mRNA expression levels of ARIDs were increased in HCC compared with normal tissues based on The Cancer Genome Atlas (TCGA) dataset. ns represents $p \geq 0.05$, * represents $p < 0.05$, ** represents $p < 0.01$, and *** represents $p < 0.001$.

and ARID1A (15%). The KM survival plot of OS indicated that the mutations of ARIDs were related to the poor prognosis of patients with HCC (Figure 6(b)). As displayed in Figures 6(c) and 6(d), genetic alterations in ARID family genes were related to worse PFS ($p = 0.0139$) and DFS ($p = 0.0317$) of patients with HCC. Collectively, genetic mutations of ARID family members may remarkably influence the survival of patients with HCC.

3.5. Functional Analyses of ARIDs in HCC. The top 10 similar genes of each ARID family gene were collected from the GEPIA database (Supplementary Table 17). The functions of ARIDs were predicted using Metascape with the thresholds of p -value < 0.05, min overlap = 3, and min enrichment = 3. Following the removal of the duplicate genes, 140 genes were collected, including 15 ARID family genes and 125 similar genes. As shown in Figure 7(a),

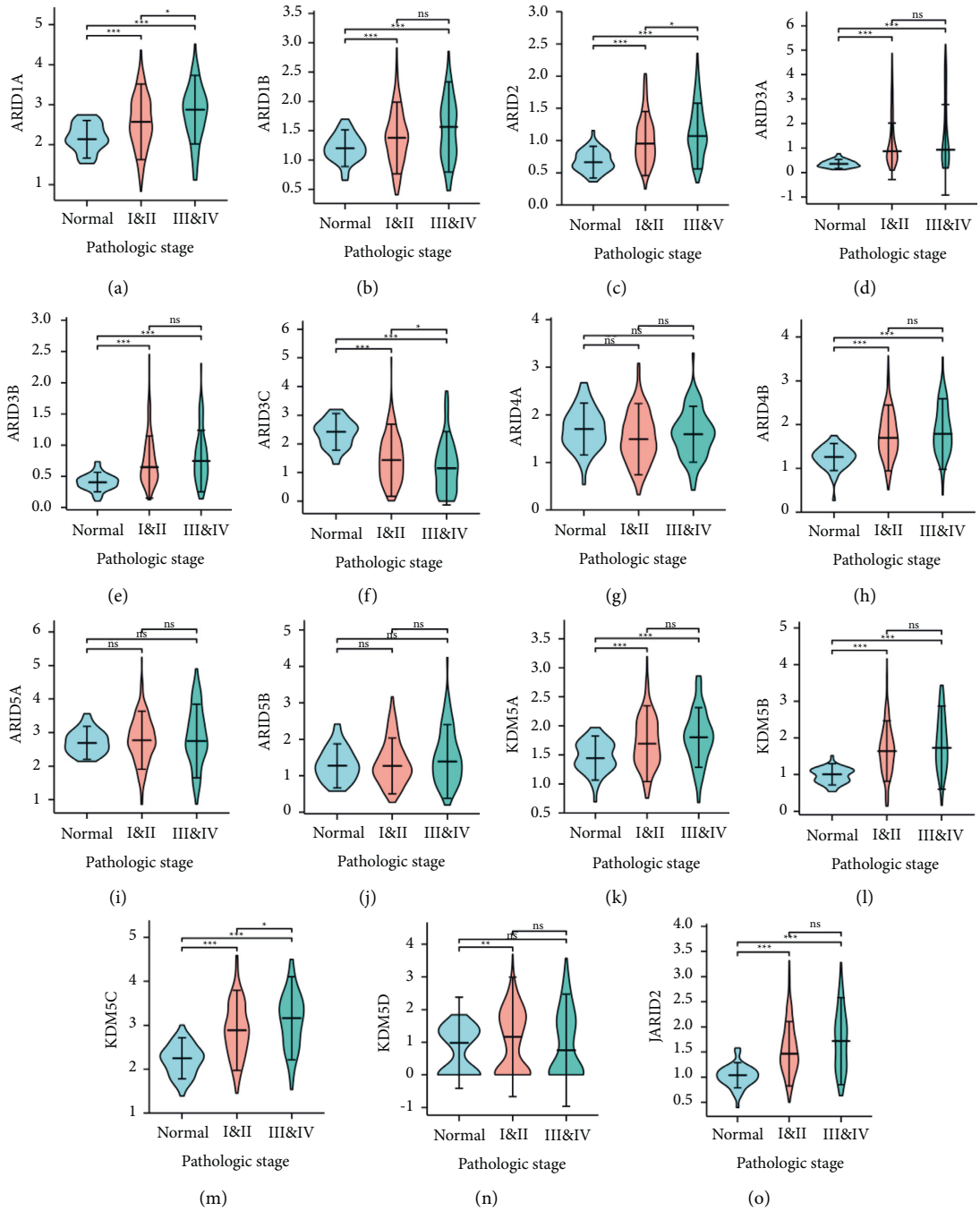

Figure 3: The relationship between the expression of different ARIDs and pathologic stages (TCGA dataset). (a–o) Violin plots showing the expression of the 15 ARID family genes with the pathologic stages (normal, stage I/II, and stageIII/IV). ARID1A, ARID2, and KDM5C were highly expressed in advanced stage (a, c, m) and lower mRNA expression of ARID3C was detected in the early stage (f). * indicates $p < 0.05$, ** indicates $p < 0.01$, *** indicates $p < 0.001$, and ns represents $p \geq 0.05$.

KEGG pathways, including transcriptional misregulation in cancer, mircoRNAs in cancer, ubiquitin-mediated proteolysis, transforming growth factor (TGF)-beta signaling pathway, bacterial invasion of epithelial cells, endocytosis, choline metabolism in cancer, and Wnt signaling, were correlated with the biological functions of ARIDs in HCC. Moreover, the enriched GO terms of these genes were classified into three groups: 9 biological processes, 4 molecular functions, and 7 cellular component terms. As displayed in Figures 7(b) and 7(c), these genes were mainly related to chromatin binding, protein polyubiquitination, mRNA transport, and covalent chromatin modification. Additionally, the two most crucial MCODE components were identified from PPI analysis. Results showed that biological functions were mostly related to ubiquitin-mediated proteolysis (MCODE 1), and RNA transport (MCODE (2) (Figure 7(e)).

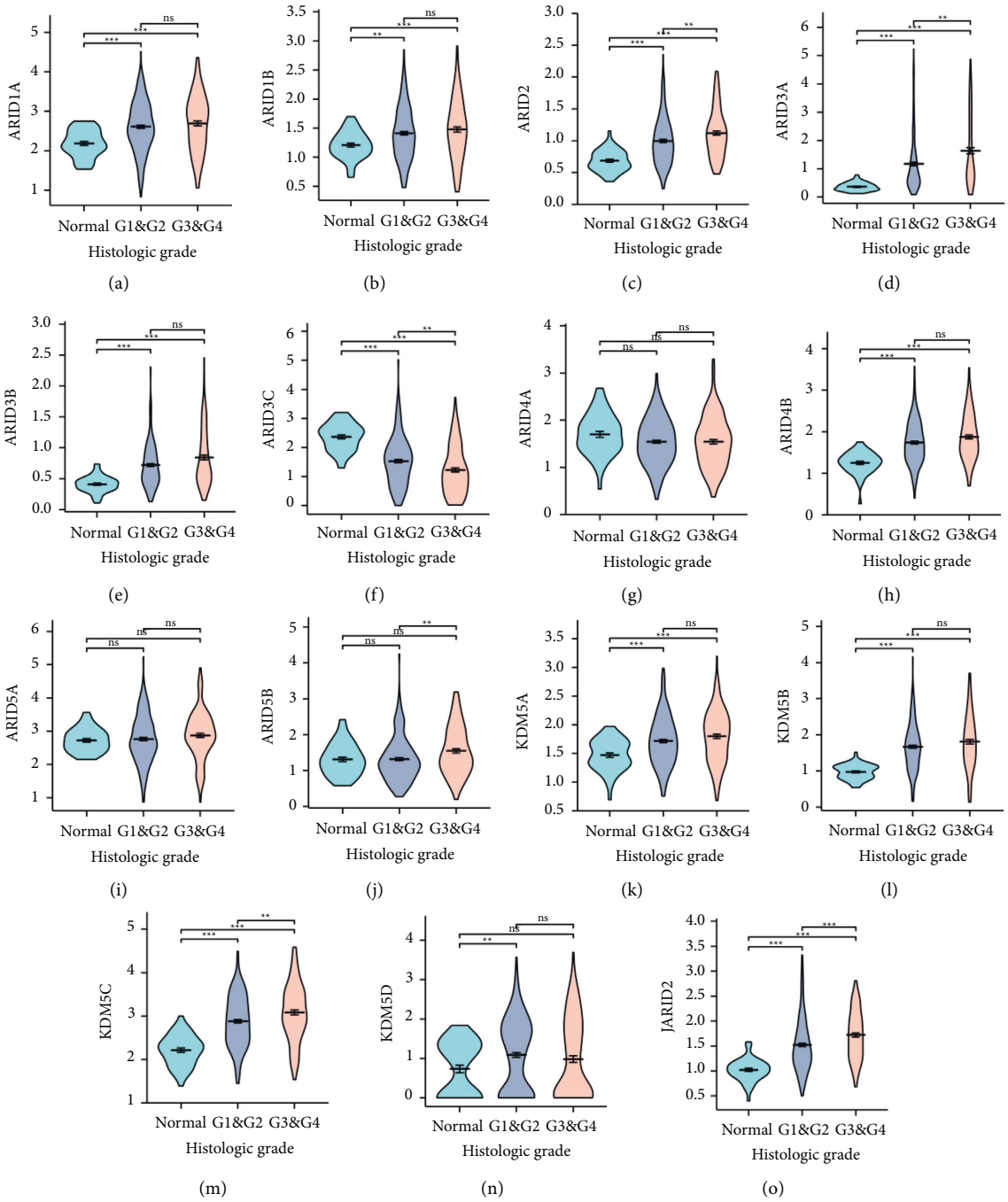

Figure 4: Association between the expression of distinct ARIDs and histologic grades. (a–o) Violin plots showing the expression of the 15 ARID family genes with grades (normal, G1/2, and G3/4). ARID2, ARID3A, ARID3B, ARID5B, KDM5C, and JARID2 were highly expressed in G3/4 (c, d, e, j, m, o), and lower mRNA expression of ARID3C was found in G1/2 (f). ** indicates $p < 0.01$, *** indicates $p < 0.01$, and ns represents $p > 0.05$.

3.6. Immune Regulating Roles of ARIDs. As shown in Figures 8 and Figure 9, results from the TIMER database showed that the expression of ARID1A, ARID2, and ARID4A was positively related to tumor purity ($p < 0.05$), indicating that these three genes were lowly expressed in the HCC immune microenvironment. Conversely, a negative correlation between ARID5A/ARID5B and tumor purity was found. Moreover, except for ARID3C and KDM5D, other ARID family members were significantly associated with all six types of immune cells (B cell, $CD4^+$ T cell, $CD8^+$ T cell, macrophage, neutrophil, and dendritic cell) in HCC microenvironment.

4. Discussion

Hepatocellular carcinoma (HCC) is a common malignancy belonging to liver cancer with high mortality. Patients with HCC are often diagnosed at the middle or advanced stage

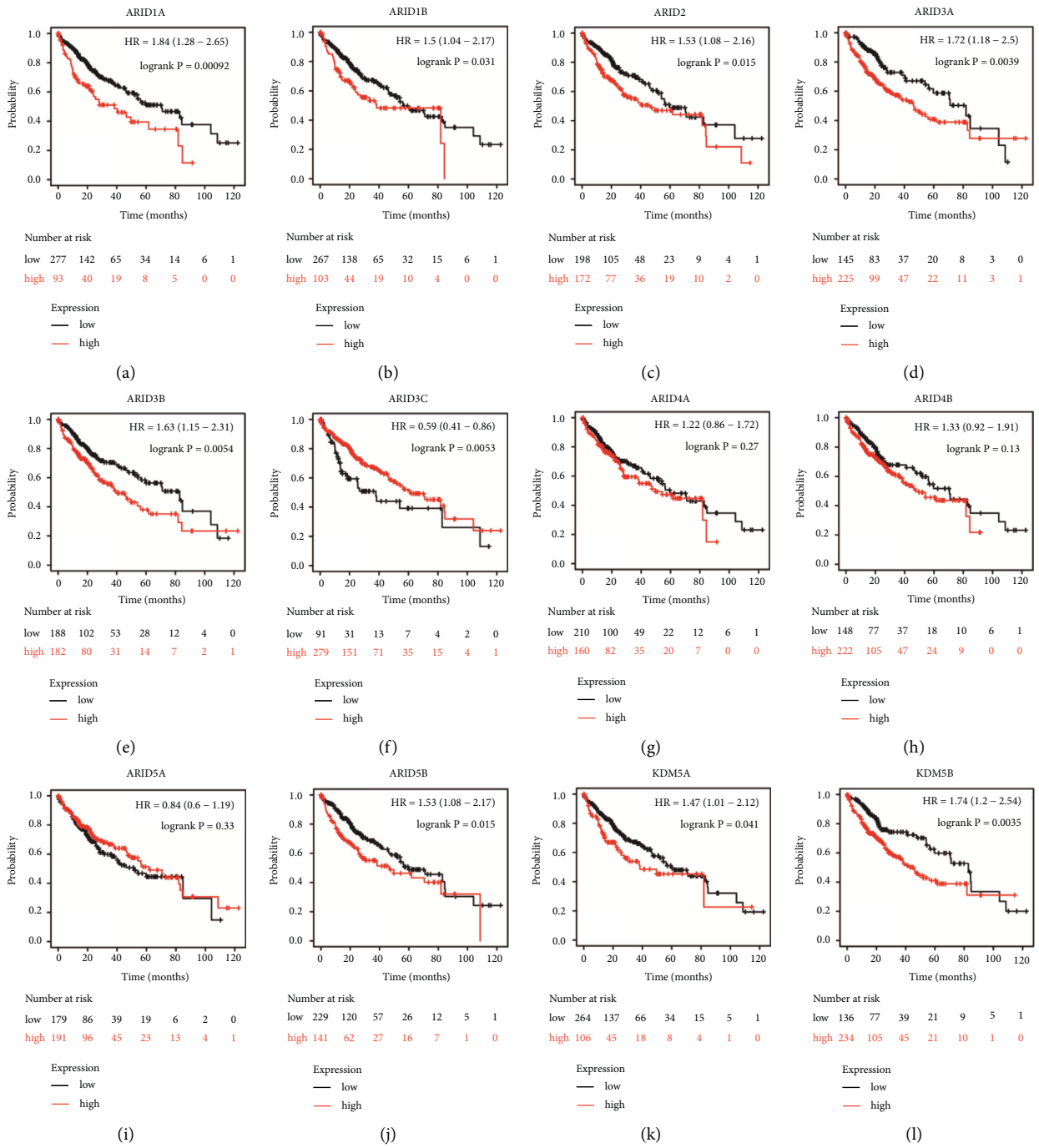

Figure 5: Continued.

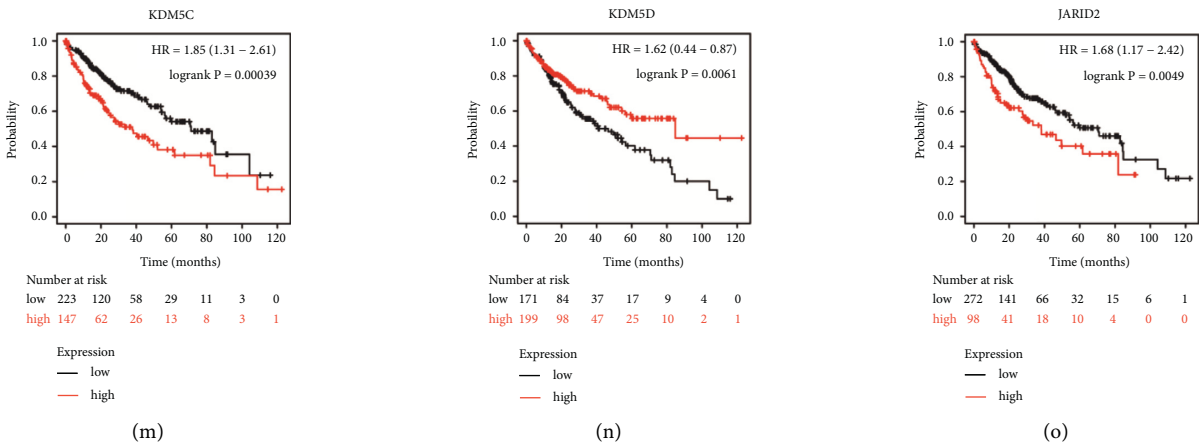

(m) (n) (o)

Figure 5: The prognostic value of ARID family genes in HCC patients (Kaplan–Meier plotter). (a–o) The Kaplan–Meier survival curves comparing HCC patients with high (red) and low (black) expressions of ARIDs were plotted. High expression levels of ARID1A (a), ARID1B (b), ARID2 (c), ARID3A (d), ARID3B (e), ARID5B (j), KDM5A (k), KDM5B (l), KDM5C (m), and JARID2 (o) were significantly correlated with shorter overall survival (OS) in HCC patients. High expression levels of ARID3C (f) and KDM5D (n) were remarkably associated with better OS. Others showed no correlation with OS time.

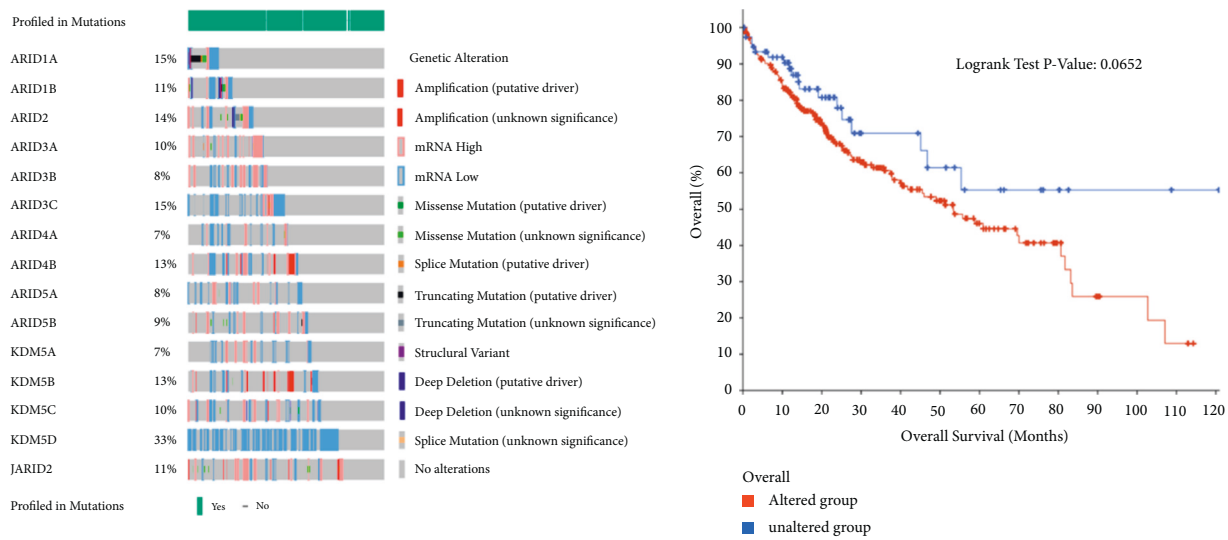

(a) (b)

Figure 6: Continued.

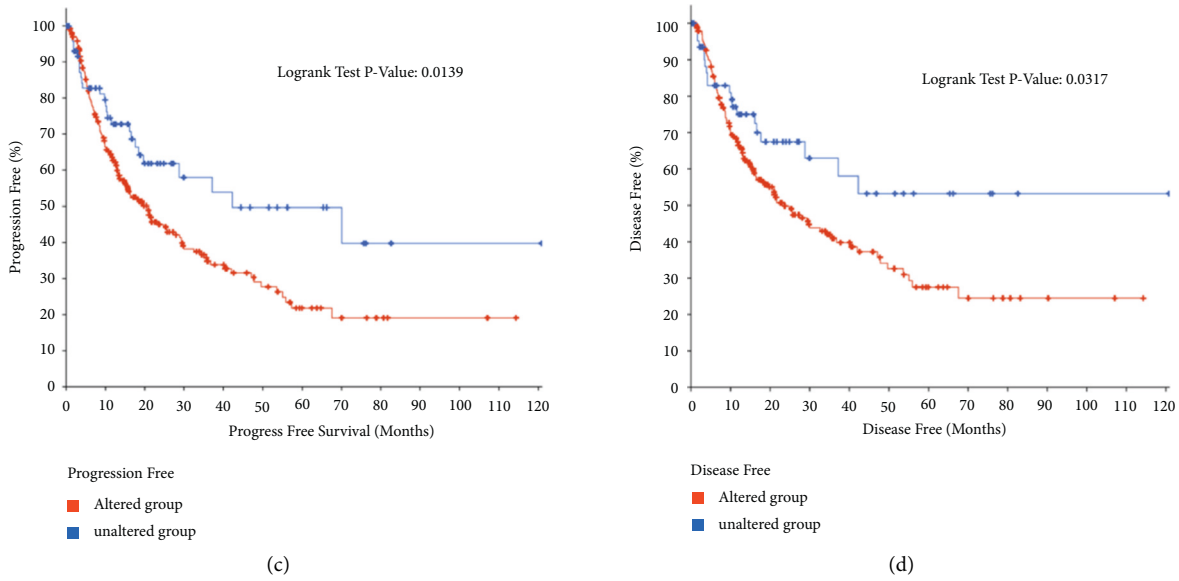

(c) (d)

Figure 6: Alteration frequency of ARID family genes and their correlation with prognosis of HCC patients (cBioPortal database). (a) The ARIDs mutation rate was 78.69% (288/366) in patients with clear cell renal cell carcinoma (ccRCC). The top three highest alteration rates in ARID family genes were KDM5D (33%), ARID3C (15%), and ARID1A (15%), respectively. (b) Genetic alterations in ARIDs showed no correlation with OS time. (c) Genetic alterations in ARID family genes were remarkably related to progression-free survival (PFS) of ccRCC patients ($p < 0.05$). (d) Genetic alterations in ARID family genes were significantly related to disease-free survival (DFS) of HCC patients ($p < 0.05$).

with a poor prognosis. Therefore, the identification of novel prognostic and diagnostic markers is urgently needed. As transcriptional regulators, ARIDs regulate cellular growth, differentiation, and development in a variety of cancers [29]. Zhang et al. identified the prognostic value of ARIDs and provided insight to explore the ARID-targeting regents for breast cancer treatment [9]. Sun et al. revealed the association between ARIDs, prognosis, and the tumor microenvironment in HCC, indicating that ARIDs are prospective therapeutic targets for HCC [30]. Growing evidence demonstrates that ARID family genes act as tumor promoters or suppressors to regulate the occurrence and development of cancers [8]. A pan-cancer analysis for ARID family members exhibits that ARIDs are novel biomarkers for immune checkpoint inhibitor therapy [12].

ARID1A is highly expressed in primary HCC, and the overexpression of ARID1A could accelerate tumor initiation [31]. Consistently, our study found that ARID1A was highly expressed in HCC and associated with pathologic stage and OS time. However, loss of homozygous or heterozygous ARID1A in HCC may accelerate progression [31]. Therefore, ARID1A plays a context-dependent function in tumor inhibition and carcinogenesis in HCC. Hu et al. reported that ARID1A deficiency could increase tumor mutation burden, upregulate the programmed cell death ligand 1 (PD-L1) expression, and modulate the immune microenvironment [32], which supports our findings. Interestingly, growth-promoting effect was observed for the knockdown of ARID1B in HCC [33], which is contrary to our results. The abnormality of ARID1B may destroy the function of Switch/sucrose-nonfermentable (SWI/SNF) complex in the regulation of gene expression and antioncogenic and oncogenic pathways, which are related to the carcinogenesis of HCC [34]. Additional studies are still needed to explore the modulatory pathways of ARID1A and ARID1B.

Our data showed that ARID2 was highly expressed in HCC and associated with clinicopathological factors and poor prognosis. ARID2 is an important tumor suppressor in HCC, but recent genomic studies have found frequent mutations of ARID2 in HCC [35]. The nucleotide change of ARID2 is also considered to be the driver of HCC [36]. Furthermore, inactivating mutations of ARID2 in three main types of HCC, including hepatitis C virus (HCV)-related, hepatitis B virus (HBV)-related, and alcohol-related HCC were found [37]. Combined with previous studies, our discoveries further confirmed that ARID2 may be a promising prognostic and therapeutic target for HCC.

ARID3 subfamily, containing ARID3A, ARID3B, and ARID3C, regulates gene expression by binding to specific DNA common sites, playing a key role in transcriptional regulation [38]. Our study found that ARID3A and ARID3B were overexpressed in HCC and associated with poor OS. In particular, ARID3A was an independent prognostic factor for predicting OS of patients with HCC, and HCC patients with advanced grades tended to have higher mRNA expression of ARID3A. ARID3A is reportedly involved in a variety of biological processes and maybe correlated with tumorigenesis. Also, overexpression of ARID3A could potentiate cancer cell proliferation, migration, and invasion [39]. In addition, previous research has shown that ARID3A and ARID3B jointly regulate gene expression in B-cells and cancers, regulate stem cell-related genes, and promote the

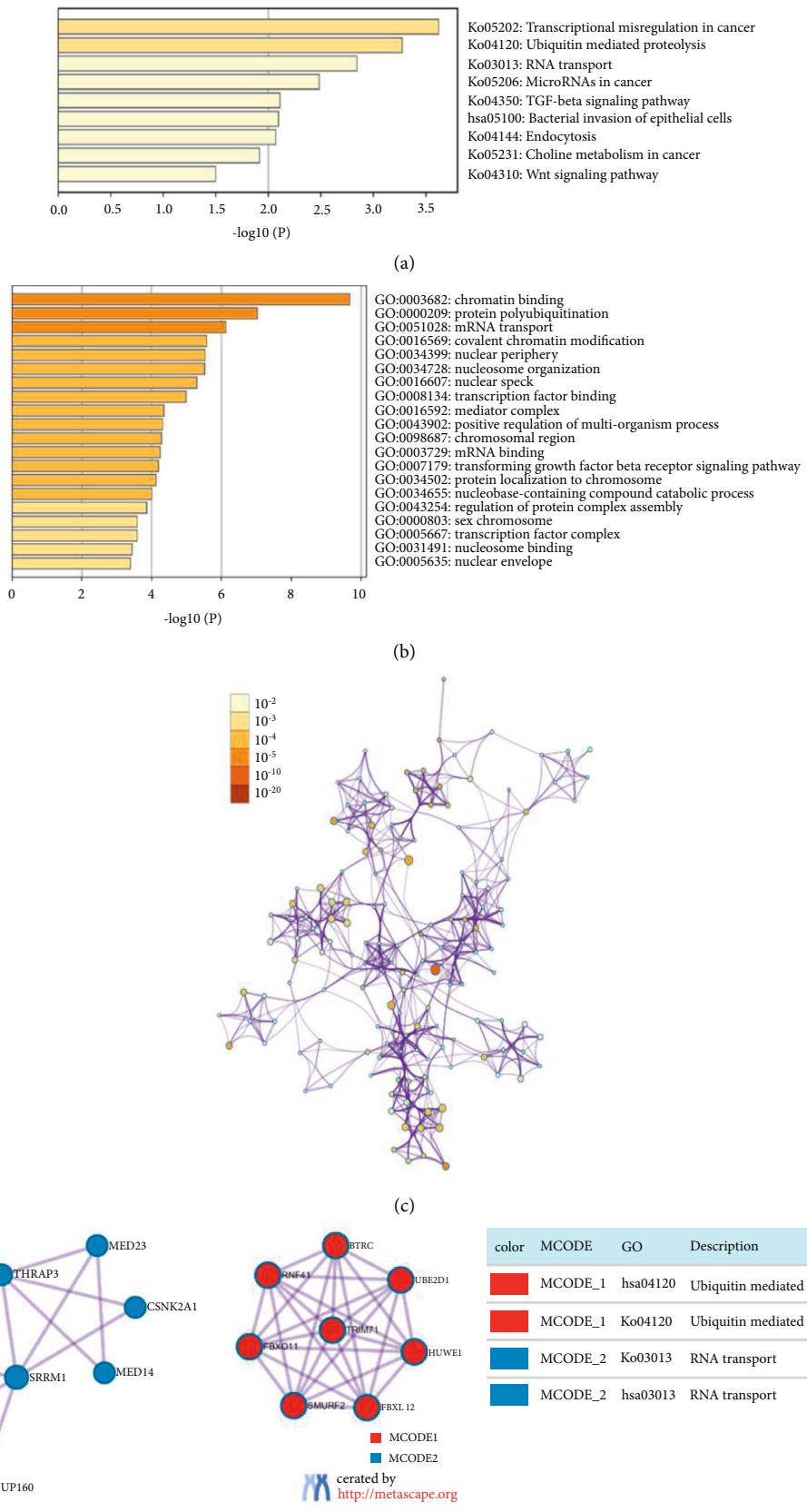

Figure 7: Functional enrichment analysis of ARID family members and their similar genes in HCC patients (GEPIA and Metascape). (a) Barplot of KEGG pathways colored by the value of -log10 (p value). (b) Barplot of GO enriched terms colored by -log10 (p value). (c) The network of GO enriched terms. (d) Two key MCODE components form the PPI network. (e) Independent functional enrichment analysis of MCODE components.

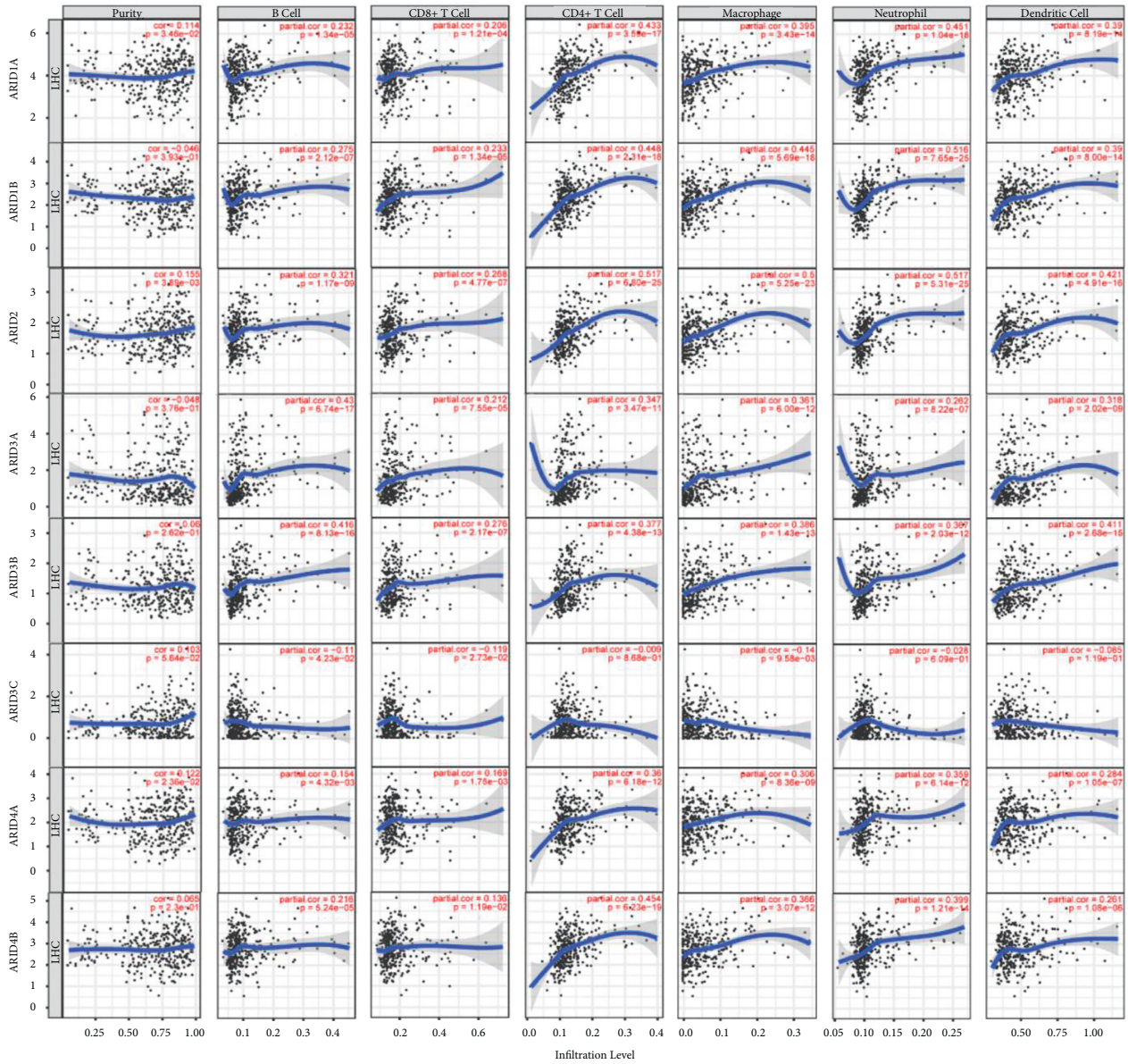

Figure 8: Relationship between the expression of ARID1A, ARID1B, ARID2, ARID3A, ARID3B, ARID3C, ARID4A, and ARID4B and immune infiltration level by TIMER in HCC. The left-most panels show tumor purity, and the associations of tumor-infiltrating immune cells and these genes in HCC were displayed.

phenotype of tumor stem cells [38]. Additionally, ARID3C was observed to be a protective prognostic factor for HCC. ARID3C has been identified as one of the main downstream targets of β-catenin, and ARID3C knockdown could inhibit cell proliferation of ovarian cancer [40]. Studies on ARID3C in HCC are still limited, but our data provided some light into this field.

ARID4A plays a dual role in cancer progression. In patients with prostate cancer, the down-regulation of ARID4A promotes tumor progression [41]. ARID4A is a tumor suppressor in breast cancer, the expression of which indicates better OS in patients with breast cancer [9]. However, our data demonstrated that ARID4A was not significantly correlated with OS or clinicopathological in HCC. Moreover, it has been reported that the expression of ARID4B in HCC tissues was upregulated compared to that in adjacent normal liver tissues, which is an independent prognostic factor for predicting OS and DFS of patients with HCC [42]. Although we also found that ARID4B was upregulated in HCC, OS is not significantly different between the low and high ARID4B expression groups. Thus, research with a larger sample size is warranted.

ARID5 subfamily includes ARID5A and ARID5B. The research found that ARID5A regulates the inflammatory process, low expression of which is correlated with poor prognosis of lung cancer patients [43]. ARID5A is also a prognostic biomarker for glioma, which is correlated with immune infiltration [44]. ARID5B is associated with histone deacetylase-1, thereby affecting cell proliferation and differentiation [45]. In our study, KM survival curves displayed

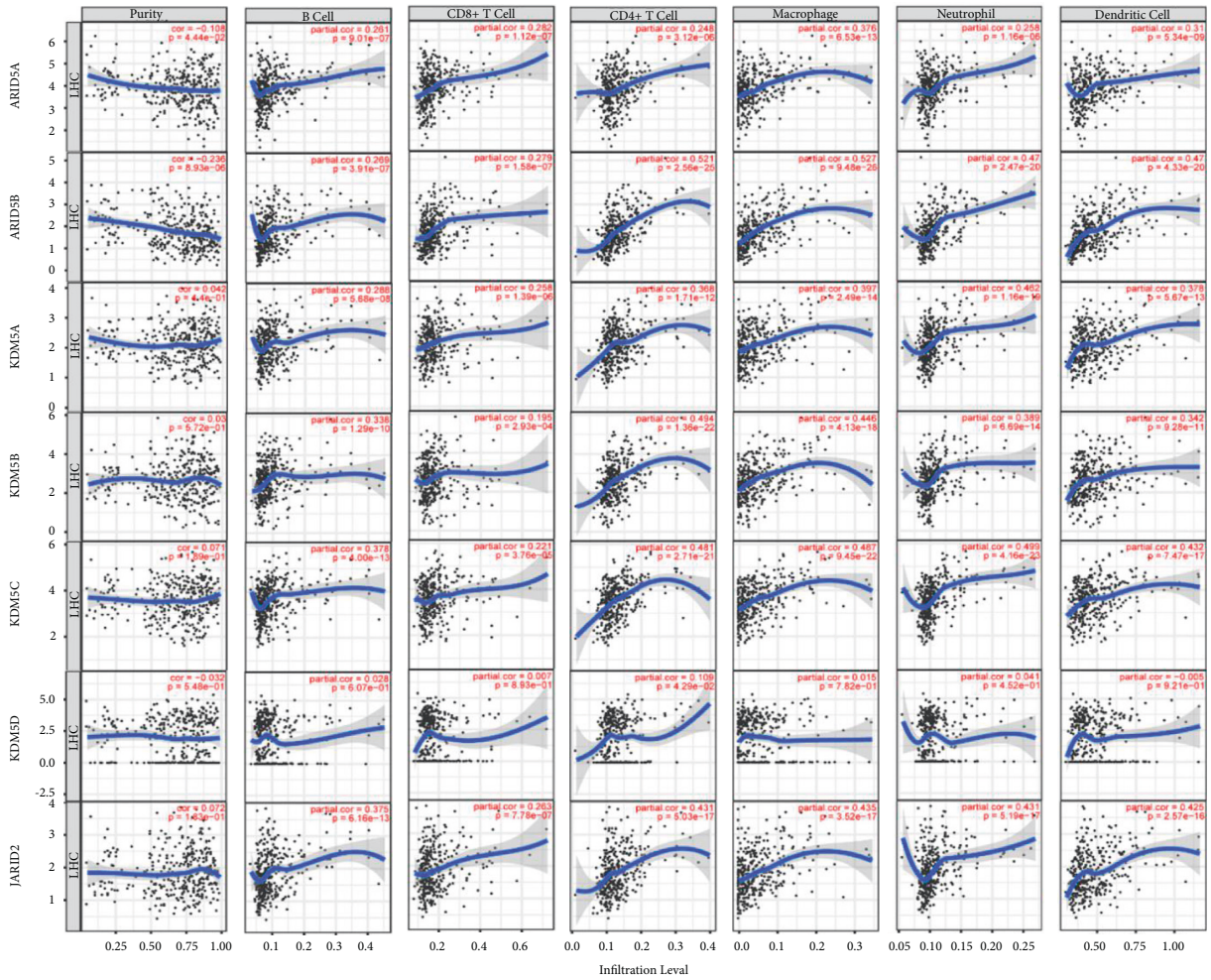

Figure 9: Relationship between the expression of ARID5A, ARID5B, KDM5A, KDM5B, KDM5C, KDM5D, and JARID2 and immune infiltration level by TIMER in HCC. The left-most panels show tumor purity, and the associations of tumor-infiltrating immune cells and these 7 genes in HCC were shown.

that high ARID5B expression was associated with worse OS time, but the association between ARID5A and OS of patients with HCC did not reach statistical significance.

Our results revealed that KDM5A, KDM5B, KDM5C, and KDM5D were upregulated in HCC tissues. A previous study indicates that KDM5A depletion leads to reduced cell migration, invasion, and proliferation of HCC, which may promote angiogenesis by activating the PI3K/AKT pathway [46]. Also, KDM5B is highly expressed in HCC, promoting the occurrence of HCC by regulating the YTHDF3/ITGA6 axis [47]. Meanwhile, we found that high expression levels of KDM5A, KDM5B, and KDM5C were associated with shorter OS, and high expression of KDM5D was correlated with longer OS time. In particular, patients with HCC at an advanced stage or grade have higher KDM5C mRNA expression. Evidence has demonstrated that the overexpression of KDM5C could predict a poor prognosis of HCC patients undergoing radical resection and promotes the HCC cell invasion, metastasis, and epithelial-mesenchymal transition, suggesting that KDM5C may be a potential therapeutic target for HCC [48]. Multivariate Cox analysis showed that KDM5C or KDM5D was an independent prognostic factor for the prediction of OS. KDM5D regulates the epithelial-mesenchymal transformation and metastasis of gastric cancer, which is a novel target for cancer treatment [49]. Besides, JARID2 was elevated in HCC, high expression of which was remarkably related to late grade and worse prognosis. Preceding research has shown that the expression of JARID2 in HCC is significantly upregulated, which is closely associated with the metastasis of HCC. JARID2 could also promote invasion, metastasis, and epithelial-mesenchymal transition of HCC cells via the PTEN/AKT pathway [50].

The frequent mutations of ARIDs have been well-established using the cBioPortal database, which is supported by previous studies [8, 33]. ARIDs mutations are correlated with poor prognosis in patients with HCC. CpGs methylation in all ARIDs may serve as prognostic markers for HCC patients. To further study the potential mechanism of ARIDs in HCC, functional analysis was performed, and the results showed that ARIDs and their similar genes were involved in the signaling pathways related to inflammatory

responses and cancer. Evidence showed that inefficient proteolysis can lead to the dysregulated cell cycle transition, which eventually results in tumorigenesis. Therefore, ubiquitin ligases related to cell cycle regulation are expected to become a therapeutic strategy for cancer [51]. Additionally, abnormal activation of the Wnt/β-catenin signal plays an important role in precancerous dysplasia, malignant transformation of hepatocytes, and malignant expansion of tumor cells [52]. According to PPI analysis, ARIDs mostly interact with UBE2D1, HUWE1, FBXO11, and MED23, and these hub genes play essential roles in the tumorigenesis and progression of HCC [53–56]. Several studies focus on the association between hub genes and HCC, however, the exact mechanisms remain to be further studied. Most of the ARID family genes were closely related to immune cells in the HCC microenvironment, suggesting that ARIDs could regulate the immune condition of HCC and may be potential predictors for immune checkpoints during treatment. However, survival analyses in this study were based on public databases. Therefore, more validations are needed to verify our discoveries. Besides, the functional analysis also needs to be verified by *in vitro* and *in vivo* experiments.

5. Conclusions

ARIDs mutations, 127 CpGs methylation in all ARIDs, and the expression levels of ARID1A/B, ARID2, ARID3A/B/C, ARID5B, KDM5A/B/C/*D*, and JARID2 were related to the prognosis of patients with HCC. Moreover, ARID3A, KDM5C, and KDM5D were also independent risk factors for the prognostic prediction of HCC. ARIDs may be associated with the regulation of cancer-associated pathways and immune function. Our findings revealed that ARIDs are potential prognostic biomarkers for HCC. ARID family members can be as promising therapeutic targets for HCC. Further research is still needed to validate these results and promote the clinical application of ARID family members in HCC.

Data Availability

The datasets analyzed for this study can be found in the TCGA, ONCOMINE, Kaplan–Meier Plotter, MethSurv, cBioPortal, GEPIA, Metascape, and TIMER web resources, and requests to further access to datasets can be directed to 1257003447@qq.com.

Conflicts of Interest

The authors declare that there are no conflicts of interest regarding the publication of this paper.

Authors' Contributions

SYL, ZLW, and HFP designed the study. SYL, ZLW, QTL, HLZ, and YFS analyzed the data. SYL and ZLW wrote the draft of the manuscript. RZ and HFP edited the manuscript. All authors read and approved the final manuscript.

Acknowledgments

The authors would like to thank TCGA, ONCOMINE, Kaplan–Meier Plotter, MethSurv, cBioPortal, GEPIA, Metascape, and TIMER databases for providing open access. This work was supported by National Natural Science Foundation of China (Grant number 82174319), Natural Science Foundation of Guangdong Province (Grant number 2021A1515110932), China Postdoctoral Science Foundation (Grant number 2022M710030), and Key Laboratory (Pi Wei diseases and Pi-deficiency syndrome) of State Administration of Traditional Chinese Medicine (Grant number 202110071448237400).

Supplementary Materials

Supplementary Figure 1: Spearman correlation of ARID family genes. Supplementary Table 1: the prognostic values of CpGs in the ARID family (MethSurv database, $p < 0.05$). Supplementary Table 2: univariate and multivariate Cox analyses of ARID1A. Supplementary Table 3: univariate and multivariate Cox analyses of ARID1B. Supplementary Table 4: univariate and multivariate Cox analyses of ARID2. Supplementary Table 5: univariate and multivariate Cox analyses of ARID3A. Supplementary Table 6: univariate and multivariate Cox analyses of ARID3B. Supplementary Table 7: univariate and multivariate Cox analyses of ARID3C. Supplementary Table 8: univariate and multivariate Cox analyses of ARID4A. Supplementary Table 9: univariate and multivariate Cox analyses of ARID4B. Supplementary Table 10: univariate and multivariate Cox analyses of ARID5A. Supplementary Table 11: univariate and multivariate Cox analyses of ARID5B. Supplementary Table 12: univariate and multivariate Cox analyses of KDM5A. Supplementary Table 13: univariate and multivariate Cox analyses of KDM5B. Supplementary Table 14: univariate and multivariate Cox analyses of KDM5C. Supplementary Table 15: univariate and multivariate Cox analyses of KDM5D. Supplementary Table 16: nivariate and multivariate Cox analyses of JARID2. Supplementary Table 17: top 10 similar genes of each ARID family member (GEPIA). (*Supplementary Materials*)

References

[1] F. Bray, J. Ferlay, I. Soerjomataram, R. L. Siegel, L. A. Torre, and A. Jemal, "Global cancer statistics 2018: globocan estimates of incidence and mortality worldwide for 36 cancers in 185 countries," *Ca-a Cancer Journal for Clinicians*, vol. 68, no. 6, pp. 394–424, 2018.

[2] H. Sung, J. Ferlay, R. L. Siegel et al., "Global cancer statistics 2020: Globocan estimates of incidence and mortality worldwide for 36 cancers in 185 countries," *CA: A Cancer Journal for Clinicians*, vol. 71, no. 3, pp. 209–249, 2021.

[3] S. Hassanipour, M. Vali, S. Gaffari-Fam et al., "The survival rate of hepatocellular carcinoma in asian countries: a systematic review and meta-analysis," *Excli Journal*, vol. 19, pp. 108–130, 2020.

[4] Z. Wu, L. Yang, L. He, L. Wang, and L. Peng, "Systematic elucidation of the potential mechanisms of core Chinese materia medicas in treating liver cancer based on network

pharmacology," *Evidence-based Complementary and Alternative Medicine*, vol. 2020, Article ID 4763675, 13 pages, 2020.

[5] A. Jindal, A. Thadi, and K. Shailubhai, "Hepatocellular carcinoma: etiology and current and future drugs," *Journal of Clinical and Experimental Hepatology*, vol. 9, no. 2, pp. 221–232, 2019.

[6] J. Jia, L. Che, A. Cigliano et al., "Pivotal role of fatty acid synthase in c-myc driven hepatocarcinogenesis," *International Journal of Molecular Sciences*, vol. 21, no. 22, p. 8467, 2020.

[7] R. D. Kortschak, P. W. Tucker, and R. Saint, "Arid proteins come in from the desert," *Trends in Biochemical Sciences*, vol. 25, no. 6, pp. 294–299, 2000.

[8] C. Lin, W. Song, X. Bi et al., "Recent advances in the arid family: focusing on roles in human cancer," *OncoTargets and Therapy*, vol. 7, pp. 315–324, 2014.

[9] J. Zhang, S. Hou, Z. You et al., "Expression and prognostic values of arid family members in breast cancer," *Aging (Albany NY)*, vol. 13, no. 4, pp. 5621–5637, 2021.

[10] Y. Lu, Z. Liu, W. Wang, X. Chen, X. Zhou, and W. Fu, "Expression signature of the at-rich interactive domain gene family identified in digestive cancer," *Frontiers of Medicine*, vol. 8, Article ID 775357, 2021.

[11] H. Tomihara, F. Carbone, L. Perelli et al., "Loss of arid1a promotes epithelial-mesenchymal transition and sensitizes pancreatic tumors to proteotoxic stress," *Cancer Research*, vol. 81, no. 2, pp. 332–343, 2021.

[12] Y. Zhu, C. Yan, X. Wang et al., "Pan-cancer analysis of arid family members as novel biomarkers for immune checkpoint inhibitor therapy," *Cancer Biology & Therapy*, vol. 23, no. 1, pp. 104–111, 2022.

[13] D. R. Rhodes, S. Kalyana-Sundaram, V. Mahavisno et al., "Oncomine 3.0: genes, pathways, and networks in a collection of 18, 000 cancer gene expression profiles," *Neoplasia*, vol. 9, no. 2, pp. 166–180, 2007.

[14] Z. Wu, L. He, L. Yang, X. Fang, and L. Peng, "Potential role of neu1 in hepatocellular carcinoma: a study based on comprehensive bioinformatical analysis," *Frontiers in Molecular Biosciences*, vol. 8, Article ID 651525, 2021.

[15] The Cancer Genome Atlas Research Network, J. N. Weinstein, E. A. Collisson et al., "The cancer genome atlas pan-cancer analysis project," *Nature Genetics*, vol. 45, no. 10, pp. 1113–1120, 2013.

[16] O. Menyhart, A. Nagy, and B. Gyorffy, "Determining consistent prognostic biomarkers of overall survival and vascular invasion in hepatocellular carcinoma," *Royal Society Open Science*, vol. 5, no. 12, Article ID 181006, 2018.

[17] A. Nagy, A. Lanczky, O. Menyhart, and B. Gyorffy, "Validation of mirna prognostic power in hepatocellular carcinoma using expression data of independent datasets," *Scientific Reports*, vol. 8, no. 1, p. 9227, 2018.

[18] V. Modhukur, T. Iljasenko, T. Metsalu, K. Lokk, T. Laisk-Podar, and J. Vilo, "Methsurv: a web tool to perform multivariable survival analysis using DNA methylation data," *Epigenomics*, vol. 10, no. 3, pp. 277–288, 2018.

[19] J. Gao, B. A. Aksoy, U. Dogrusoz et al., "Integrative analysis of complex cancer genomics and clinical profiles using the cbioportal," *Science Signaling*, vol. 6, no. 269, 2013.

[20] Z. Wu, Y. Zhang, X. Chen, W. Tan, L. He, and L. Peng, "Characterization of the prognostic values of the cxcr1-7 in clear cell renal cell carcinoma (ccrcc) microenvironment," *Frontiers in Molecular Biosciences*, vol. 7, Article ID 601206, 2020.

[21] W. Tan, S. Peng, Z. Li et al., "Identification of therapeutic targets and prognostic biomarkers among genes from the mediator complex family in the hepatocellular carcinoma tumour-immune microenvironment," *Computational and Mathematical Methods in Medicine*, vol. 2022, Article ID 2021613, 22 pages, 2022.

[22] Z. Tang, C. Li, B. Kang, G. Gao, C. Li, and Z. Zhang, "Gepia: a web server for cancer and normal gene expression profiling and interactive analyses," *Nucleic Acids Research*, vol. 45, pp. W98–W102, 2017.

[23] Y. Zhou, B. Zhou, L. Pache et al., "Metascape provides a biologist-oriented resource for the analysis of systems-level datasets," *Nature Communications*, vol. 10, no. 1, p. 1523, 2019.

[24] T. Li, J. Fan, B. Wang et al., "Timer: a web server for comprehensive analysis of tumor-infiltrating immune cells," *Cancer Research*, vol. 77, no. 21, pp. e108–e110, 2017.

[25] S. Qin, G. Liu, H. Jin et al., "The dysregulation of sox family correlates with DNA methylation and immune microenvironment characteristics to predict prognosis in hepatocellular carcinoma," *Disease Markers*, vol. 2022, Article ID 2676114, 21 pages, 2022.

[26] X. Chen, S. T. Cheung, S. So et al., "Gene expression patterns in human liver cancers," *Molecular Biology of the Cell*, vol. 13, no. 6, pp. 1929–1939, 2002.

[27] E. Wurmbach, Y. B. Chen, G. Khitrov et al., "Genome-wide molecular profiles of hcv-induced dysplasia and hepatocellular carcinoma," *Hepatology*, vol. 45, no. 4, pp. 938–947, 2007.

[28] S. Roessler, H. L. Jia, A. Budhu et al., "A unique metastasis gene signature enables prediction of tumor relapse in early-stage hepatocellular carcinoma patients," *Cancer Research*, vol. 70, no. 24, pp. 10202–10212, 2010.

[29] D. Wilsker, A. Patsialou, P. B. Dallas, and E. Moran, "Arid proteins: a diverse family of DNA binding proteins implicated in the control of cell growth, differentiation, and development," *Cell Growth & Differentiation*, vol. 13, no. 3, pp. 95–106, 2002.

[30] J. Sun and N. S. Cheng, "Comprehensive landscape of arid family members and their association with prognosis and tumor microenvironment in hepatocellular carcinoma," *Journal of Immunology Research*, vol. 2022, Article ID 1688460, 10 pages, 2022.

[31] X. Sun, S. C. Wang, Y. Wei et al., "Arid1a has context-dependent oncogenic and tumor suppressor functions in liver cancer," *Cancer Cell*, vol. 32, no. 5, pp. 574–589.e6, 2017.

[32] G. Hu, W. Tu, L. Yang, G. Peng, and L. Yang, "Arid1a deficiency and immune checkpoint blockade therapy: from mechanisms to clinical application," *Cancer Letters*, vol. 473, pp. 148–155, 2020.

[33] A. Fujimoto, Y. Totoki, T. Abe et al., "Whole-genome sequencing of liver cancers identifies etiological influences on mutation patterns and recurrent mutations in chromatin regulators," *Nature Genetics*, vol. 44, no. 7, pp. 760–764, 2012.

[34] L. Liu, N. Tian, C. Zhou et al., "A potentially functional variant of arid1b interacts with physical activity in association with risk of hepatocellular carcinoma," *Oncotarget*, vol. 8, no. 19, pp. 31057–31064, 2017.

[35] A. Oba, S. Shimada, Y. Akiyama et al., "Arid2 modulates DNA damage response in human hepatocellular carcinoma cells," *Journal of Hepatology*, vol. 66, no. 5, pp. 942–951, 2017.

[36] F. Pezzuto, L. Buonaguro, F. M. Buonaguro, and M. L. Tornesello, "Frequency and geographic distribution of

tert promoter mutations in primary hepatocellular carcinoma," *Infectious Agents and Cancer*, vol. 12, no. 1, p. 27, 2017.

[37] M. Li, H. Zhao, X. Zhang et al., "Inactivating mutations of the chromatin remodeling gene arid2 in hepatocellular carcinoma," *Nature Genetics*, vol. 43, no. 9, pp. 828-829, 2011.

[38] P. Dausinas, K. Pulakanti, S. Rao, J. M. Cole, R. Dahl, and K. D. Cowden Dahl, "Arid3a and arid3b induce stem promoting pathways in ovarian cancer cells," *Gene*, vol. 738, Article ID 144458, 2020.

[39] J. Tang, L. Yang, Y. Li et al., "Arid3a promotes the development of colorectal cancer by upregulating aurka," *Carcinogenesis*, vol. 42, no. 4, pp. 578–586, 2021.

[40] Y. Wang, J. Cao, W. Liu et al., "Protein tyrosine phosphatase receptor type r (ptprr) antagonizes the wnt signaling pathway in ovarian cancer by dephosphorylating and inactivating beta-catenin," *Journal of Biological Chemistry*, vol. 294, no. 48, pp. 18306–18323, 2019.

[41] Y. K. Liang, Z. D. Han, J. M. Lu et al., "Downregulation of arid4a and arid4b promote tumor progression and directly regulated by microrna-30d in patient with prostate cancer," *Journal of Cellular Biochemistry*, vol. 119, no. 9, pp. 7245–7255, 2018.

[42] R. Wang, Z. Yu, F. Chen, C. Liao, Q. Wang, and X. Huang, "Overexpression of arid4b predicts poor survival in patients with hepatocellular carcinoma," *Human Pathology*, vol. 73, pp. 114–121, 2018.

[43] P. Sarode, X. Zheng, G. A. Giotopoulou et al., "Reprogramming of tumor-associated macrophages by targeting beta-catenin/fosl2/arid5a signaling: a potential treatment of lung cancer," *Science Advances*, vol. 6, 2020 eaaz6105.

[44] Q. Zhou, J. Zhou, and J. Fan, "Expression and prognostic value of arid5a and its correlation with tumor-infiltrating immune cells in glioma," *Frontiers Oncology*, vol. 11, Article ID 638803, 2021.

[45] P. Joshi, T. M. Greco, A. J. Guise et al., "The functional interactome landscape of the human histone deacetylase family," *Molecular Systems Biology*, vol. 9, no. 1, p. 672, 2013.

[46] Y. S. Ma, T. M. Wu, B. Qian et al., "Kdm5a silencing transcriptionally suppresses the fxyd3-pi3k/akt axis to inhibit angiogenesis in hepatocellular cancer via mir-433 up-regulation," *Journal of Cellular and Molecular Medicine*, vol. 25, no. 8, pp. 4040–4052, 2021.

[47] J. C. Guo, Z. Liu, Y. J. Yang, M. Guo, J. Q. Zhang, and J. F. Zheng, "Kdm5b promotes self-renewal of hepatocellular carcinoma cells through the microrna-448-mediated ythdf3/itga6 axis," *Journal of Cellular and Molecular Medicine*, vol. 25, no. 13, pp. 5949–5962, 2021.

[48] X. Ji, S. Jin, X. Qu et al., "Lysine-specific demethylase 5c promotes hepatocellular carcinoma cell invasion through inhibition bmp7 expression," *BMC Cancer*, vol. 15, no. 1, p. 801, 2015.

[49] X. Shen, K. Hu, G. Cheng et al., "Kdm5d inhibit epithelial-mesenchymal transition of gastric cancer through demethylation in the promoter of cul4a in male," *Journal of Cellular Biochemistry*, vol. 120, no. 8, pp. 12247–12258, 2019.

[50] X. Lei, J. F. Xu, R. M. Chang, F. Fang, C. H. Zuo, and L. Y. Yang, "Jarid2 promotes invasion and metastasis of hepatocellular carcinoma by facilitating epithelial-mesenchymal transition through pten/akt signaling," *Oncotarget*, vol. 7, no. 26, pp. 40266–40284, 2016.

[51] F. Dang, L. Nie, and W. Wei, "Ubiquitin signaling in cell cycle control and tumorigenesis," *Cell Death & Differentiation*, vol. 28, no. 2, pp. 427–438, 2021.

[52] W. Wang, R. Smits, H. Hao, and C. He, "Wnt/β-Catenin signaling in liver cancers," *Cancers*, vol. 11, no. 7, p. 926, 2019.

[53] Y. Guo, J. Wang, H. Li et al., "Mediator subunit 23 overexpression as a novel target for suppressing proliferation and tumorigenesis in hepatocellular carcinoma," *Journal of Gastroenterology and Hepatology*, vol. 30, no. 6, pp. 1094–1103, 2015.

[54] Y. Ma, F. Deng, P. Li, G. Chen, Y. Tao, and H. Wang, "The tumor suppressive mir-26a regulation of fbxo11 inhibits proliferation, migration and invasion of hepatocellular carcinoma cells," *Biomedicine & Pharmacotherapy*, vol. 101, pp. 648–655, 2018.

[55] C. Zhou, F. Bi, J. Yuan, F. Yang, and S. Sun, "Gain of ube2d1 facilitates hepatocellular carcinoma progression and is associated with DNA damage caused by continuous il-6," *Journal of Experimental & Clinical Cancer Research*, vol. 37, no. 1, 2018.

[56] T. Kodama, J. Y. Newberg, M. Kodama et al., "Transposon mutagenesis identifies genes and cellular processes driving epithelial-mesenchymal transition in hepatocellular carcinoma," *Proceedings of the National Academy of Sciences of the United States of America*, vol. 113, no. 24, pp. E3384–E3393, 2016.

Hindawi
Evidence-Based Complementary and Alternative Medicine
Volume 2022, Article ID 7983530, 6 pages
https://doi.org/10.1155/2022/7983530

Research Article

Study on the Diagnostic Value of Contrast-Enhanced Ultrasound and Magnetic Resonance Imaging in Prostate Cancer

Xinnian Pang,[1] Jianhua Zhang,[2] Lvcou Chen,[1] Yang Yuan,[1] and Dong Xu[3]

[1]*Department of Ultrasound, Tiantai People's Hospital of Zhejiang Province, Taizhou 317500, Zhejiang, China*
[2]*Department of Urology, Tiantai People's Hospital of Zhejiang Province, Taizhou 317500, Zhejiang, China*
[3]*Department of Ultrasound, Zhejiang Cancer Hospital, Hangzhou 310022, Zhejiang, China*

Correspondence should be addressed to Xinnian Pang; pangxinnian@ecut.edu.cn

Received 28 June 2022; Accepted 25 July 2022; Published 8 August 2022

Academic Editor: Shuli Yang

Objective. The aim is to study the different roles of single and joint application of magnetic resonance imaging (MRI) and contrast-enhanced ultrasound (CEUS) in prostate malignant tumors. *Methods*. 72 patients with prostate masses who underwent CEUS and MRI examination in our hospital from October 2021 and March 2022 were enrolled in this research. The differentially diagnostic roles of CEUS, MRI, and CEUS combined MRI for prostate cancer was assessed on basis of pathological findings as the reference standard. The specificity and sensitivity of the joint application for prostate malignant tumors with various prostate-specific antigen (PSA) levels were also evaluated. *Results*. The sensitivity of CEUS, MRI, and the joint application for prostate cancer were 72.1%, 74.4%, and 90.7%, respectively. Compared with single application, the sensitivity of CEUS combined with MRI was significantly higher. The specificity of MRI, CEUS, and the combination of the two for prostate cancer were 82.8%, 79.3%, and 89.7%, respectively, and the statistical differences for specificity were not found. The area under ROC curve (AUC) of CEUS combined with MRI in prostate malignant tumor diagnosis was obviously more than that of CEUS and MRI ($P < 0.05$). CEUS combined with MRI has relative high sensitivity in these patients with different levels of PSA. *Conclusions*. Contrast-enhanced ultrasound combined with MRI can significantly improve the sensitivity and specificity of prostate cancer diagnosis so that patients can be better diagnosed in advance.

1. Introduction

In western countries, prostate malignant tumor is considered as the common cancer, especially in elderly men [1]. It was reported that the occurrence rate of prostate malignant tumor raised every year, which severely affected the physical and psychological status of these patients [2, 3]. Many studies reported that patients with prostatic cancer in the early phase who underwent timely treatment could gain a more than 5-year survival rate, while those in the end stage showed an obviously less than 5-year survival rate [4]. Early detection of prostate malignant tumor is extremely important for enhancing the quality of life and reducing the death rate. At present, biopsy under the guidance of ultrasound has become the standard method in the diagnosis of prostate malignant tumor. But the shortcomings of technologies are proverbial [5]. Therefore, novel imaging procedures should be recommended as an alternative to characterize and identify the prostate tumors.

Magnetic resonance imaging (MRI) is currently the optimal detection for the findings of prostate malignant tumors. However, using MRI alone has some limitations. It was reported that could MRI only find morphological information and was not able to obtain the internal microstructure of tumor tissues, resulting in difficult evaluation for the risk of prostate tumors [6]. Another study showed that diffusion-weighted MRI could well manifest the tissue of tumor with abundant vascularity; however, the diagnostic role for prostate malignant tumor was debated [7]. In conclusion, MRI has the advantages of thorough research

and clear morphological information and can better display tumor tissues with abundant blood vessels. In recent years, contrast-enhanced ultrasonography (CEUS) appeared with the development of advanced techniques in the ultrasound imaging. The value of CEUS in oncologic diagnosis attracts increasing emphasis due to the measurement of moving blood [8]. It was reported that improved cancer identification at CEUS was associated with the better examination of small blood flow in tumors [9]. So far, few data are found regarding the value of MRI plus CEUS for the prostate malignant tumor diagnosis. In this context, this research was performed to study the roles of MRI plus CEUS for prostate tumors and it will provide important evidences for assessing prostate malignant tumor.

2. Material and Methods

2.1. Basic Data. From October 2021 and March 2022, 72 patients with prostate masses were included in this research; hospital ethics committee approved this trial.

The signed informed consent was provided. The inclusion criteria were as follows: (1) those who were diagnosed as suspicious prostate cancer with over 30 years of age and elevated levels of prostate-specific antigen (PSA) (≥4.0 ng/mL). (2) Those who had no history of radiotherapy, chemotherapy, and endocrine treatment. (3) The examinations of contrast-enhanced ultrasonography, MRI, and prostate biopsy were performed. (4) Complete medical records were obtained and patients were able to cooperate in the research. The exclusion criteria were as follows: (1) History of malignant tumor. (2) History of prostate operation. (3) Hypersensitivity reaction of the contrast agent. (4) Accompaniment with disorders of the blood and immune system, prostatitis, and acute urinary tract infections. (5) Severe renal and hepatic insufficiency, cardio- and cerebrovascular disease, and mental disorders. All the patients were informed about the necessity for pathological detection and about the examination of contrast-enhanced ultrasonography and MRI conducted prior to the biopsy.

2.2. Contrast-Enhanced Ultrasonography Examination. Patients were maintained at a left lateral position. The transrectal conventional ultrasound was performed for each patient by LOGIQ E9 type ultrasound equipment (GE Company, USA). All the examination was conducted by two senior doctors who were blinded to this study. Then, the system of ultrasound was switched into the model of contrast-enhanced ultrasonography when the conventional ultrasound was finished. The contrast medium SonoVue (Bracco Suisse SA, Swiss) was injected into the peripheral vein of patients. Next, 5 ml normal saline was injected. The transducer was fixed over the suspicious lesions and regions of interest. The video was real-time dynamically observed for 3 min. Through reviewing the images, the prostate cancer was diagnosed according to the parameters reported by previous studies [10].

2.3. MRI Detection. The subjects were kept in the supine position with a proper distended bladder under the condition of steady breaths. The MRI examination was conducted using a 1.5 T Signa HDxt magnetic resonance scanner (GE Company, USA). The scanning scope involved in the whole prostate. T2WI sequence examination was used for analyzing the tumor of the prostate. T2 weighted fat saturation (T2WFS) scans were performed based on the following arguments: TE 100 ms, TR 5500 ms, FOV 230 mm × 230 mm, matrix 320 × 320, slice thickness 4.0 mm. Diffusion-weighted imaging (DWI) was conducted using spin echo-echo planar imaging. The parameters were as follows: b values were set as 0 s/mm^2, 500 s/mm^2, 1500 s/mm^2, 2000 s/mm^2, TR 4000 ms, TE 86 ms, Matrix 180 × 180, FOV 230 mm × 230 mm, slice thickness 4.0 mm. Apparent diffusion coefficient (ADC) imaging was constructed on basis of DWI. The original MRI image was transmitted to Picture Archiving and Communications Systems (PACS) workstation. The corresponding images from MRI were blindly assessed by two experienced radiologists together with prostate imaging report and data system version 2.1 (PI-RADS v2.1). The scoring criteria should refer to the latest version of PI-RADS V2.1 [11]. Three scores or more were considered as prostate cancer. The agreements should be reached by consensus when their views were different.

2.4. Prostate Biopsy Examination. After contrast-enhanced ultrasonography and MRI examination, all patients underwent prostate puncture under the guidance of ultrasound, and the standard puncture method was adopted. The puncture specimens from the patients were immediately embedded in paraffin and stained in sections. Two experienced pathologists blindly interpreted the pathological sections. Moreover, prostate cancer was pathologically confirmed by the Gleason scoring system from the International Association of Urological Pathology [12].

2.5. Statistical Methods. All the clinical data obtained in the research were analyzed through SPSS version 23.0. The measurement data were shown in the form of mean ± standard deviation. The count data were showed in the form of percentages/cases. The comparison among groups was conducted using χ^2 test. On the basis of the pathological results as the gold standard, the diagnostic value including specificity and sensitivity of CEUS, MRI, and the combined application for prostate cancer was analyzed. Diagnostic efficiency of CEUS, MRI and the combined application for prostatic malignant tumor was also evaluated through receiver operating characteristic (roc). $P < 0.05$ indicated significantly statistical differences.

3. Results

3.1. General Information. As seen in Table 1, the mean age of patients included in the research was 62.8 ± 6.5 years. The body mass index was 21.5 ± 0.7 kg/m^2. Disease periods of time were 2.5 ± 0.6 years. The serum PSA level was

Table 1: General data of patients included in the research.

Indicators	Values
Age (years)	62.8 ± 6.5
BMI (kg/m^2)	21.5 ± 0.7
PSA (ng/mL)	69.8 ± 10.4
Duration of diseases (years)	2.5 ± 0.6
BPH (*n*)	23
Intraepithelial neoplasia (*n*)	2
Prostatitis (*n*)	4
Prostate cancer (*n*)	43
Hyperlipidemia (*n*)	12
Hypertension (*n*)	15
Diabetes (*n*)	18

BPH: benign prostatic hyperplasia, PSA: prostate specific antigen, BMI: body mass index.

69.8 ± 10.4 ng/mL. It showed 23 cases with benign prostatic hyperplasia (BPH), 2 cases with intraepithelial neoplasia, 4 cases with prostatitis, and 43 cases with prostate cancer. Moreover, there were 15 patients with hypertension, 18 patients with diabetes, and 12 patients with hyperlipidemia.

3.2. Comparison of Diagnostic Efficiency of CEUS, MRI, and the Combined Application for Prostatic Cancer. The sensitivity of CEUS, MRI, and CEUS combined with MRI for prostate malignant tumor was 72.1%, 74.4%, and 90.7%, respectively. In contrast to CEUS or MRI, the sensitivity of CEUS combined with MRI in prostate cancer was significantly increased ($P < 0.05$). The specificity of CEUS, MRI, and CEUS combined with MRI in prostate malignant tumor was 79.3%, 82.8%, and 89.7%, respectively. The significant differences were not found regarding the specificity for examination of prostate cancer among different methods as shown in Table 2.

3.3. Comparison of ROC Results. The AUC of CEUS, MRI, and CEUS combined with MRI for prostate cancer was 0.608, 0.667, and 0.785, respectively. The AUC of CEUS plus MRI diagnosed for prostate cancer was significantly more than that of CEUS or MRI, and there was the obviously statistical difference ($P < 0.05$) as seen in Table 3 and Figure 1.

3.4. Diagnostic Efficiency of CEUS Combined with MRI among Different Levels of PSA. When PSA was in the range of 4 ng/mL to 10 ng/mL, the specificity and sensitivity of CEUS combined with MRI for diagnosis of prostate malignant tumor were 78.3% and 100%. When PSA was in the range of 10 ng/mL to 20 ng/mL, the sensitivity and specificity of CEUS combined with MRI for diagnosis of prostate cancer were 81.8% and 60.0%. When PSA was more than 20 ng/mL, the specificity and sensitivity of CEUS combined with MRI in diagnosis of prostate malignant tumor were 66.7% and 100% as seen in Table 4.

4. Discussion

In clinical practices, most of patients with early-stage prostate cancer do not have special clinical manifestations. When the clinical symptoms occur, it is usually diagnosed as the advanced stage. The differential diagnosis between prostate cancer and benign tumors was confirmed by the transrectal ultrasound guided biopsies. Many studies showed that the incidences of complications including bleeding and pain make a lot of patients to difficultly agree to the operation of needle biopsy [13]. Thus, the optimal examination technology for prostate malignant tumor is required to be less damage, noninvasive, and less adverse reactions and would be of benefit to a high proportion of patients.

The improvement of diagnostic pathways for prostate cancer is necessary and might be based on the progress of imaging detections. MRI, as a noninvasive examination, has the characteristic of good resolution for soft tissues and could show the invasion of seminal vesicle and extracapsular in prostate malignant tumor. The routine morphological examination of MRI is of great significance for evaluating the tumor size, location and stage, and guiding needle biopsy. This study showed the specificity and sensitivity of MRI for detecting prostate malignant tumor was 82.8% and 74.4%, which was basically similar with the results reported by previous studies [14]. CEUS, as an ultrasound imaging examination, makes an important progress in the diagnosis of malignant tumor. Microvascular imaging during CEUS could clearly display the images of blood flow perfusion and distribution in prostate cancer, which could improve the sensitivity and specificity in the prostate malignant tumor diagnosis. Some trials reported that the increased microvessel density in prostate malignant tumor was correlated with grading of tumors and metastasis and prognosis of patients [15]. In this study, it was showed that the specificity and sensitivity of MRI for detecting prostate malignant tumor were 79.3% and 72.1%. Huang et al. revealed the similar results [16]. However, there were few data regarding the diagnostic efficacy of MRI combined with CEUS in prostate cancer. Aiming at the features of MRI and CEUS, The strong points of both were obtained by the combined application technology. MRI combined with CEUS could not only evaluate the microvessel density in prostate tissues and observe the signal symmetry of the blood flow, but also offer the all-round vision for the physiological anatomy of prostate tissues and show the blood supply in the lesions and its peripheral tissue. The results of this study found that the specificity and sensitivity of CEUS combined with MRI for detecting prostate cancer were 89.7% and 90.7%, which were higher than those in MRI or CEUS. Moreover, the AUC of combined application was significantly higher than that in MRI or CEUS, and the obviously statistical differences were found. It was suggested that MRI combined with CEUS had obvious advantages in the term of prostate malignant tumor diagnosis.

PSA is considered as the commonly clinical indicator in the examination of prostate malignant tumor. PSA was also

Table 2: Comparison of diagnostic efficiency of CEUS, MRI, and the combined application for prostatic cancer.

Groups	*Pathological examination*		Sensitivity (%)	Specificity (%)
	Benign masses	Malignant masses		
Contrast-enhanced ultrasound			72.1	79.3
Benign masses	23	12		
Malignant masses	6	31		
MRI			74.4	82.8
Benign masses	24	11		
Malignant masses	5	32		
Contrast-enhanced ultrasound plus MRI			90.7	89.7
Benign masses	26	4		
Malignant masses	3	39		

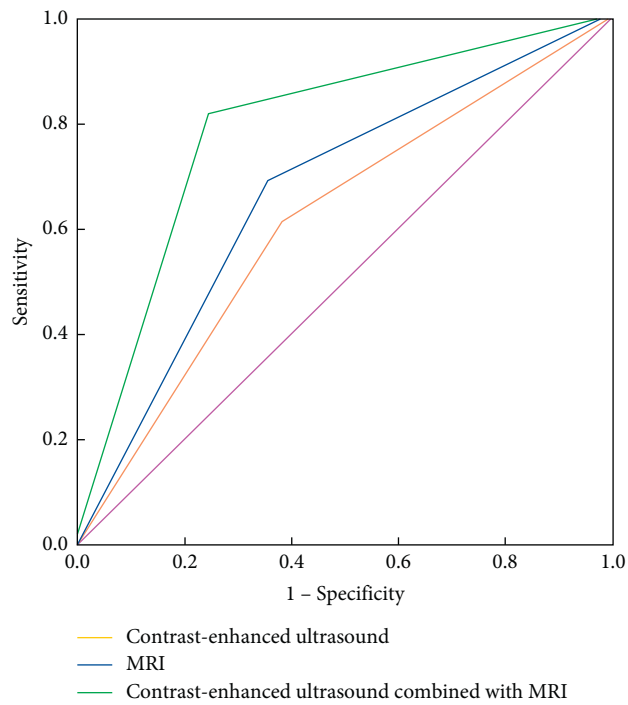

Figure 1: ROC curve of different examination methods for diagnosis of prostate cancer.

Table 3: Comparison of ROC results of CEUS, MRI, and the combined application for prostatic cancer.

Groups	AUC	Se	95%CI
Contrast-enhanced ultrasound	0.608	0.049	0.518~0.813
MRI	0.667	0.042	0.507~0.798
Contrast-enhanced ultrasound plus MRI	0.785	0.037	0.642~0.875

usually performed as a marker in the screening and assessment of treatment effect in prostate malignant tumor [6]. Previous research studies found that increased PSA levels were closely associated with the clinical phase of prostate malignant tumor and the higher PSA concentration indicated the worse damage of surrounding tissues and malignant degree [17]. This study revealed that MRI combined with CEUS showed a high specificity and sensitivity in patients with different increased PSA concentrations. It also indicated that this combined application technology could limit the number of biopsy cores and enhance the detection of prostate malignant tumor under the biopsy guidance. Some studies reported that the combined application was able to detect the prostate lesions which could not be

Table 4: Comparison of diagnostic efficiency of CEUS combined with MRI among different levels of PSA.

CEUS combined with MRI	4 ng/mL < PSA ≤ 10 ng/mL	10 ng/mL < PSA ≤ 20 ng/mL	PSA > 20 ng/mL
Sensitivity	100% (2/2)	81.8% (9/11)	100% (20/20)
Specificity	78.3% (18/23)	60.0% (6/10)	66.7% (4/6)

detected using systematic biopsy [18]. MRI combined with CEUS differentially diagnosed prostate malignant tumor from benign tumors and prostatitis based on various vascular enhancements. This technology strongly allowed features of vascular alterations in the areas of tumor, which was helpful to identify benign inflammatory nodules from neoplastic nodules. The distinguishment of suspected tissues with increased PSA concentration allowed guided biopsy, which would improve the probability of examining a possible malignant tumor.

The current study has several limitations that should be recognized. First, this was a retrospective study, which could not perform blind, randomization, and power calculation. Second, the sample size in this research was not large, which might influence the findings. Third, the clinical data of patients were obtained from single center, which may influence its generalization to other hospitals. In future studies, it was demanded to demonstrate this opinion by expanding the sample size and exploiting multi-center prospective study.

5. Conclusions

In summary, although CEUS or MRI revealed relatively high specificity and sensitivity in examining prostate malignant tumor, MRI combined with CEUS yields a higher detective rate of prostate cancer. A satisfactory finding seems to be achieved when the combined application is exploited for patients with different elevated PSA concentrations. If this combined application could be further development, it would be conductive to the prostate cancer monitoring following therapy and to the clearly distinguishment of malignant lesions when focal treatment is conducted. As a future application of CEUS combined with MRI, this technique has the potential to exert an important role in diagnosis and prognosis assessment for prostate cancer and must be further explored. The application of CEUS combined with MRI for diagnosis and treatment would develop a new field in prostate malignant tumor.

Data Availability

The experimental data used to support the findings of this study are available from the corresponding author upon request.

Conflicts of Interest

The authors declare that they have no conflicts of interest.

References

[1] Z. Chen, X. Chen, and R. Wang, "Application of SPECT and PET/CT with computer-aided diagnosis in bone metastasis of prostate cancer: a review," *Cancer Imaging*, vol. 22, no. 1, 2022.

[2] D. Nitusca, A. Marcu, E. Seclaman et al., "Diagnostic value of microRNA-375 as future biomarker for prostate cancer detection: a meta-analysis," *Medicina*, vol. 58, no. 4, p. 529, 2022.

[3] A. Gurwin, K. Kowalczyk, K. Knecht-Gurwin et al., "Alternatives for MRI in prostate cancer diagnostics-review of current ultrasound-based techniques," *Cancers*, vol. 14, no. 8, 2022.

[4] K. Beyer, L. Moris, M. Lardas et al., "Diagnostic and prognostic factors in patients with prostate cancer: a systematic review," *BMJ Open*, vol. 12, no. 4, Article ID e058267, 2022 Apr.

[5] K. A. Lindert, J. N. Kabalin, and M. K. Terris, "Bacteremia and bacteriuria after transrectal ultrasound guided prostate biopsy," *The Journal of Urology*, vol. 164, no. 1, pp. 76–80, 2000 Jul.

[6] L. Han, G. He, Y. Mei et al., "Combining magnetic resonance diffusion-weighted imaging with prostate-specific antigen to differentiate between malignant and benign prostate lesions," *Medical Science Monitor*, vol. 28, Article ID e935307, 2022.

[7] J. Morote, A. Borque-Fernando, M. Triquell et al., "Multiparametric magnetic resonance imaging grades the aggressiveness of prostate cancer," *Cancers*, vol. 14, no. 7, 2022.

[8] J. J. Mei, Y. X. Zhao, Y. Jiang, J. Wang, and J. S. Yu, "Association between contrast-enhanced ultrasound indicators and prostate cancer biochemical recurrence after treatment," *Cancer Management and Research*, vol. 12, pp. 4959–4968, 2020.

[9] G. Liu, S. Wu, and L. Huang, "Contrast-enhanced ultrasound evaluation of the prostate before transrectal ultrasound-guided biopsy can improve diagnostic sensitivity: a STARD-compliant article," *Medicine (Baltimore)*, vol. 99, no. 19, Article ID e19946, 2020 May.

[10] W. van den Bos, D. M. de Bruin, A. van Randen et al., "MRI and contrast-enhanced ultrasound imaging for evaluation of focal irreversible electroporation treatment: results from a phase I-II study in patients undergoing IRE followed by radical prostatectomy," *European Radiology*, vol. 26, no. 7, pp. 2252–2260, 2016.

[11] B. Turkbey, A. B. Rosenkrantz, M. A. Haider et al., "Prostate imaging reporting and data system version 2.1: 2019 update of prostate imaging reporting and data system version 2," *European Urology*, vol. 76, no. 3, pp. 340–351, 2019.

[12] S. Alqahtani, C. Wei, Y. Zhang et al., "Prediction of prostate cancer Gleason score upgrading from biopsy to radical prostatectomy using pre-biopsy multiparametric MRI PIRADS scoring system," *Scientific Reports*, vol. 10, no. 1, p. 7722, 2020.

[13] S. F. Brewster, N. Rooney, J. Kabala, and R. C. L. Feneley, "Fatal anaerobic infection following transrectal biopsy of a rare prostatic tumour," *British Journal of Urology*, vol. 72, no. 6, pp. 977-978, 1993.

[14] J. Morote, M. Campistol, A. Celma et al., "The efficacy of proclarix to select appropriate candidates for magnetic resonance imaging and derived prostate biopsies in men with suspected prostate cancer," *World Journal of Men's Health*, vol. 40, no. 2, pp. 270–279, 2022.

[15] F. Sano and H. Uemura, "The utility and limitations of contrast-enhanced ultrasound for the diagnosis and treatment of prostate cancer," *Sensors*, vol. 15, no. 3, pp. 4947–4957, 2015.

[16] R. Huang, L. Jiang, Y. Xu et al., "Comparative diagnostic accuracy of contrast-enhanced ultrasound and shear wave elastography in differentiating benign and malignant lesions: a network meta-analysis," *Frontiers in Oncology*, vol. 9, 2019.

[17] H. Cho, C. K. Oh, J. Cha et al., "Association of serum prostate-specific antigen (PSA) level and circulating tumor cell-based PSA mRNA in prostate cancer," *Prostate International*, vol. 10, no. 1, pp. 14–20, 2022.

[18] A. W. Postema, M. J. V. Scheltema, C. K. Mannaerts et al., "The prostate cancer detection rates of CEUS-targeted versus MRI-targeted versus systematic TRUS-guided biopsies in biopsy-naïve men: a prospective, comparative clinical trial using the same patients," *BMC Urology*, vol. 17, no. 1, p. 27, 2017.